1-1-2022

APPLICATIONS OF CORRELATED GAUSSIAN FUNCTIONS TO FEW-BODY IONS

William Earwood

APPLICATIONS OF CORRELATED GAUSSIAN FUNCTIONS TO FEW-BODY IONS

A Dissertation
presented in partial fulfillment of requirements
for the degree of Doctor of Philosophy
in the Department of Chemistry and Biochemistry
The University of Mississippi

by

William P. Earwood

May 2022

ABSTRACT

For few-body systems, the Schrödinger equation can be solved using the linear variational method, where the wavefunction is expanded in a set of parameterized, all-particle functions. However, it remains a challenging task to determine a quality set of nonlinear parameters that result in accurate wavefunctions when the Schrödinger equation is solved from the solution to an eigenvalue problem. In this work, a stochastic optimization algorithm has been implemented to drive the optimization of wavefunctions and first-order perturbed functions. For $Z \leq 10$ lithiumlike ions, variational wavefunctions are determined for the 2^2S, 2^2P, 3^2P, 4^2P, and 5^2P states. For the $Z \leq 10$ muonic heliumlike ions, comprised of a nucleus, electron, and muon, the ground-state (1^1S) wavefunctions have been optimized. Using these wavefunctions, relativistic/QED corrections to the ionization energies of the 2^2S lithiumlike states are determined, in order to assess the most recent experimental results. The n^2P $(n = 2\text{-}5)$ lithiumlike wavefunctions are used, in combination with multiple optimized first-order perturbed functions, to evaluate frequency-dependent dipole polarizabilities below the $2^2S \rightarrow 3^2P$ absorption frequency. Finally, the muonic heliumlike wavefunctions are used to determine the hyperfine splittings for the $Z \leq 5$ muonic heliumlike ions, while properties including radial integrals and their squares are considered as a function of nuclear charge.

DEDICATION

To Heather, Henry, and Leo

ACKNOWLEDGEMENTS

I would like to acknowledge my research advisor, Dr. Steven R. Davis, for his help throughout this process. As I was finishing up my master's degree with the School of Engineering, I chose to take his quantum chemistry course from the chemistry department, a critical decision in retrospect. His course stimulated my interest in quantum chemistry as a discipline, and following his course he kindly allowed me to work under him as a PhD student. In the years since then, I have had the luxury of being able to access his knowledge and experience whenever necessary. I am thankful for his support and patience with me, and for letting me work on things I was most interested in.

I would like to acknowledge Dr. Ryan Fortenberry and Dr. Nathan Hammer for their advice and encouragement during this time, and for supporting my endeavor to find a postdoctoral appointment, by taking time to kindly write reference letters on my behalf. I would like to acknowledge Dr. Gregory Tschumper and the University of Mississisippi Dept. of Chemistry and Biochemistry for supporting me over the years, and Dr. Luca Bombelli for serving as my outside of department committee member. I would also like to thank the Mississippi Center for Supercomputing Research (MCSR) for allowing me to use its computer resources.

TABLE OF CONTENTS

LIST OF TABLES

CHAPTER 1

INTRODUCTION

In non-relativistic quantum mechanics, the bound, stationary state energies of atoms and molecules are determined by solving the time-independent Schrödinger equation [1]:

$$\hat{H}\Psi = E_\Psi \Psi \tag{1.1}$$

The Schrödinger equation is an example of an eigenvalue equation; that is to say, it is an equation that can have multiple solutions. These solutions are known as wavefunctions, which together form a set $\{\Psi\}$, and corresponding to each wavefunction is a particular energy, E_Ψ. The only part of Eq. 1.1 which is known *a priori* is its Hamiltonian operator, $\hat{H}$, while E_Ψ/Ψ are unknown and must be solved for. $\hat{H}$ *operates* on the wavefunction, returning the wavefunction itself, but also its energy, and both the wavefunction and $\hat{H}$ depend on the coordinates of a collection of particles. Using the hydrogen atom as a simple example, the positions of the hydrogen nucleus (i.e., proton) and electron can be represented by the coordinates $\mathbf{r}_N$ and $\mathbf{r}_e$, respectively. Hence, $\Psi \equiv \Psi(\mathbf{r}_N, \mathbf{r}_e)$, and the Hamiltonian is explicitly:

$$\hat{H} = -\frac{1}{2m_N}\nabla_N^2 - \frac{1}{2}\nabla_e^2 - \frac{1}{|\mathbf{r}_e - \mathbf{r}_N|} \tag{1.2}$$

In Eq. 1.2, $\hbar = e = m_e = 1$ (i.e., Hartree atomic units), and this choice of units is used hereafter. The nuclear mass is meanwhile denoted m_N. Each of these coordinates can be represented in 3-D Cartesian space as $\mathbf{r}_i = (x_i\hat{x} + y_i\hat{y} + z_i\hat{z})$, where $\hat{x}, \hat{y}, \hat{z}$ are the Cartesian unit vectors. The distance $|\mathbf{r}_e - \mathbf{r}_N| = r_{eN} = \sqrt{(x_e - x_N)^2 + (y_e - y_N)^2 + (z_e - z_N)^2}$. The Laplacian part of the

kinetic energy operator for the ith particle, ∇_i^2, can also be expressed using Cartesian coordinates:

$$\nabla_i^2 = \frac{\partial^2}{\partial x_i^2} + \frac{\partial^2}{\partial y_i^2} + \frac{\partial^2}{\partial z_i^2} \tag{1.3}$$

For a more general system, Ψ will be a function of more particle coordinates, and $\hat{H}$ will consist of many more terms proportional to ∇_i^2, and many more interparticle interactions of the general form $1/r_{ij}$, where (i, j) label charged particles.

For the exact Hamiltonian, a closed-form solution to Eq. 1.1 is only possible for two-body wavefunctions. By two-body, one usually means consisting of two particles, examples of which are the hydrogen atom and its isotopes, but also hydrogenlike ions, or exotic two-body systems made up of particles such as the positron or muon. For a three-body or larger system, the lack of a closed-form solution means that a numerical solution to Eq. 1.1 is only possible. These solutions are best determined using computers, as repetitive, tedious mathematical operations are involved. Today, the idea of solving the Schrödinger equation for an atom, molecule, or solid is an extremely large subject spanning multiple disciplines and length scales.

The projects that make up this dissertation each require a numerical solution of Eq. 1.1, using an approach involving all-particle basis functions and the linear variational method. While this computational method is conceptually simple, it is quite restricted for the reason that all-particle basis sets for use in an arbitrary wavefunction expansion are not available. Hence, one needs to *create* a basis set for each wavefunction of interest. Although solving Eq. 1.1 using a basis set expansion is quite trivial using modern computers, in practice one needs to calculate its solution a very large number of times to determine the best basis set for minimizing E_Ψ and improving the wavefunction.

1.1 Summary of work

Now let us summarize the results of this work. In Chapter 3, wavefunctions, whose energies are accurate to within $\approx 1 \times 10^{-8}$ Hartree (a.u.), were optimized for the ground states (2^2S)

of the nuclear charge $3 \leq Z \leq 10$ lithiumlike ions. The leading-order relativistic and QED corrections were then determined using these wavefunctions. Higher-order QED corrections were also considered, but for the higher-order relativistic corrections, approximations were necessary. The total energies obtained by summing these contributions are then subtracted from the corresponding energies of the ground state (1^1S) heliumlike systems, in order to determine the ionization energies of the (2^2S) lithiumlike ions. Direct comparison with experiment is made for each ion, where in some cases the disagreements are quite notable, but at present unresolved.

In Chapter 4, we have considered the same three-electron ground states, providing an extensive tabulation of frequency-dependent dipole polarizabilities. In addition to the ground state wavefunctions, we determined wavefunctions for the 2^2P, 3^2P, 4^2P, and 5^2P states for each ion. The P-state wavefunctions were used to build a basis for calculating the dipole polarizability. It was important to maintain high-accuracy as a function of frequency, so frequency-dependent, first-order perturbed functions were constructed for each ion at select frequencies, and combined with the P-state wavefunctions to compute the final results. Prior to our work, frequency-dependent dipole polarizabilities had not been tabulated for the $Z > 6$ lithiumlike ions, while for $Z > 4$, our results are now the most accurate in the literature. For $Z = 3,4$, our results are in very good agreement with previously reported theoretical values of high-accuracy [2]. Using this data, analytic fits to the frequency-dependent dipole polarizabilities are provided.

In Chapter 5, we have considered the $2 \leq Z \leq 10$ muonic heliumlike ions. A muonic heliumlike ion is a three-body system comprised of a nucleus, an electron, and a muon. The primary purpose of this work was to calculate the hyperfine splittings for the $^9\mathrm{Be}\mu e$ and $^{11}\mathrm{B}\mu e$ ions, which were not available at the time this project was proposed and completed. During the course of preparing the manuscript detailing this work, however, we became aware of a study which did the same [3]. Our work has several distinguishing features, one being that we have used the variational method, whereas in Ref. [3] perturbation theory is used. In addition, we have reported variational wavefunction optimizations for the first time for $Z > 3$ muonic heliumlike ions. Overall, our results are in agreement with the results from Ref. [3]. Excellent agreement

with previous work [4, 5] for the $^4\mathrm{He}\mu e$ and $^7\mathrm{Li}\mu e$ hyperfine splittings is noted, as well. The primary task of this project was to optimize the basis sets used to calculate the wavefunctions from Eq. 1.1. As discussed in Chapter 5, compared to the electronic-only case (e.g., ordinary helium), this optimization was considerably more challenging.

1.2 Hierarchy of computational methods

Let us consider here the hierarchy of methods which have been developed over time to solve Eq. 1.1. While it is not possible to list and describe such an exhaustive amount of scientific development, one can point to a few representative examples of calculations and methods which provide a reasonable perspective. A basic point that should be emphasized is that as the number of particles decreases, the particle interactions can be treated with ever-increasing complexity.

An example of a very large calculation is found in Ref. [6], where linear scaling density functional theory (DFT) algorithms were used in order to solve Eq. 1.1 for over 2×10^6 silicon atoms. Another example of a large scale calculation may be found in Ref. [7], where the fragment molecular orbital (FMO) method in combination with 2nd-order Moller-Plesset theory (MP2) was used to consider over 4000 water molecules. The FMO approach relies on treating multiple atoms together as fragments. This is an example of an approximation; as the system of interest becomes smaller, one would ideally strip away each approximation in order to improve the accuracy of the solution.

DFT calculations are used to study matter at all length scales, and perform differently for different systems. One might argue that, for the largest molecules, DFT is the only methodology that can practically be used with success [8]. Normally, DFT calculations are reserved for very large molecular systems or bulk materials, but there are plenty of examples where DFT has been used with very good accuracy [9]. MP2 is one of the many "post-Hartree-Fock" methods. The idea of a post-Hartree-Fock method is to use the solution to the Hartree-Fock (HF) equations as a starting point, and to recover the electron-electron (Coulomb) correlation that is missing from the HF solution [10]. This missing correlation is due to HF theory assuming that the total wavefunction

is expressible in terms of an antisymmetrized Hartree product, known as a Slater determinant [10]. MP2 is one way to improve mitigate the HF approximation, while it is also possible to form a linear combination of many Slater determinants [10].

For medium-sized molecules, e.g., of order 10^2 atoms, a widely used and representative example of a post-HF theory is arguably the coupled-cluster (CC) family of methods [11]. Nearly 20 years ago, the benzene *dimer* was studied using the powerful CCSD(T) method, with a large (aug-cc-pVQZ) basis set [12], and even larger calculations are possible today. For a single benzene, a recent study has attempted to determine its full configuration-interaction (FCI) ground-state electronic energy, using a diverse set of methodologies [13]. However, it is notable that FCI was not able to be used for this molecule, even for small (cc-pVDZ) basis sets. This leads to the point that even for 6 small atoms with 6 hydrogens, the CC methods, as well as those discussed in Ref. [13], remain the most accurate methods which can be used in practice. While FCI is inaccessible currently for 36 electron systems, it can be used for a system about half that size, e.g., the N_2 molecule [14].

For the very smallest systems, however, it becomes possible to solve Eq. 1.1 using a direct variational approach. This method does not introduce single particle orbitals, but instead attempts to solve the full n-body problem without approximating the Hamiltonian, by expanding the wavefunction in a basis set of appropriate functions. For n-body problems where $n > 4$, the only functions which can be used are explicitly correlated Gaussians (ECGs) [15], as the Hamiltonian integrals can be calculated analytically for an arbitrary number of particles. For n-body problems where $n \leq 4$, one can alternatively use exponential [16] or Hylleraas [17] expansion functions, although ECG expansions are quite competitive [18].

The crossover point where ECG calculations can be performed is hard to identify, but, to the best of our knowledge, no more than 3 nuclei and/or 8 total particles have been considered previously. In principle, one could attempt to use the variational/ECG method for a much larger number of particles, but if the system becomes too large, the direct variational approach can not be utilized to its full power, so that the single particle orbital methods are superior. This sentiment is in

part inspired by recent FCI quantum Monte Carlo [19] and fixed-node diffusion Monte Carlo [20] calculations of the energies of small atoms. In Ref. [19], the ionization energy of the carbon atom, which includes estimates of both relativistic and QED corrections, was calculated within 1 cm^{-1} of experiment (magnitude ≈ 90000 cm^{-1}) using a large (aug-cc-pCV8Z) basis set. In Ref. [20], the variational upper bounds are slightly better, where the infinite nuclear mass ground state energy was estimated to have 2×10^{-5} a.u. accuracy. Compared to these results, a direct variational calculation [21] involving ECG functions was less accurate, although the ECG results could be further improved, and would eventually surpass the Monte Carlo results in terms of accuracy. A similar situation is observed for 8-body nitrogen, where ECG calculations [22] have not yet improved upon the Monte Carlo energies. While direct variational calculations are certainly more powerful overall, it can be argued that Monte Carlo methods, and presumably other methods, are competitive for 8-9 body systems, for the time being.

For small molecules, direct variational calculations have provided literature benchmarks for He_2^+, LiH^+, LiH, BeH^+, BeH, BH, and H_3^+ systems [23–28], to name a few. So the limit of what has been achieved is again about 8 particles, for no more than 3 nuclei. Finally, let us consider what is possible for small atomic systems. For six-body boron or ionized carbon (C^+) [29–31], the convergence of the non-relativistic energy is $\approx 1 \times 10^{-8}$ a.u. For five-body berylium, this energy is now known [32] to at least $\approx 1 \times 10^{-10}$ a.u. For four-body lithium, this energy is now known [33] with $\approx 1 \times 10^{-15}$ a.u. accuracy. For three-body helium, the non-relativistic energy has been converged to better than 1×10^{-30} a.u. [34]. As stated above, the calculations of interest herein are those involving either three-body and four-body systems.

CHAPTER 2

COMPUTATIONAL METHODS

2.1 Solving the time-independent Schrödinger equation

Let us consider a few-body atomic system consisting of n particles, labeling the nucleus as particle # 1. The remaining $n-1$ particles are assumed to have electric charge $q_i = -1$ and interact according to the pairwise Coulombic potential $\hat{V}$, denoting the electric charge of the nucleus as Z:

$$\hat{V} = -\sum_{i=2}^{n} \frac{Z}{|\mathbf{r}_i - \mathbf{r}_1|} + \sum_{\substack{j=2 \\ i>j}}^{n} \frac{1}{|\mathbf{r}_i - \mathbf{r}_j|} \tag{2.1}$$

For particles $i = (2,n)$, $\mathbf{r}_i$ is a position vector originating from the origin, while the position vector $\mathbf{r}_1$ relates the nucleus to the same origin. The kinetic energy operator takes on the same form as in Eq. 1.2:

$$\hat{T} = -\frac{1}{2m_N}\nabla_N^2 - \sum_{i=2}^{n} \frac{1}{2m_i}\nabla_i^2 \tag{2.2}$$

Here, the nuclear mass is denoted m_N, while the non-nuclear masses are collectively denoted $\{m_i\}$. As discussed in Chapter 1, we have worked to solve Eq. 1.1 using what has been called a direct variational method. In this method, an unknown Ψ is expanded using all-particle, parameterized basis functions:

$$\Psi = \sum_{k=1}^{m} c_k \phi_k \tag{2.3}$$

The first step of the variational method is to multiply Eq. 1.1 from the left by Ψ^*, the complex conjugate of the wavefunction, followed by an integration over all the coordinates of the wavefunction:

$$\int d\tau \Psi^* \hat{H} \Psi = \int d\tau \Psi^* E \Psi \tag{2.4}$$

$$E = \frac{\int d\tau \Psi^* \hat{H} \Psi}{\int \Psi^* \Psi} = \frac{\langle \Psi | \hat{H} | \Psi \rangle}{\langle \Psi | \Psi \rangle} \tag{2.5}$$

In the right-hand side of Eq. 2.5, we have used the Dirac bra-ket notation, as is customary. Eq. 2.5 defines the Rayleigh quotient. It can be shown, as is done in Ref. [1], that by expanding Ψ (Eq. 2.3), the energy E will be replaced by an approximate value, E', which will always be greater than the true energy E. In other words, E' is an *upper bound*. However, we will continue to use E, keeping in mind that E is strictly a variational upper bound to the *true* energy. As the linear coefficients are independent of the particle coordinates, following substitution of Eq. 2.3 into Eq. 2.5, these can be extracted from the integrals:

$$E = \frac{\sum_k \sum_l c_k^* c_l \langle \phi_k | \hat{H} | \phi_l \rangle}{\sum_k \sum_l c_k^* c_l \langle \phi_k | \phi_l \rangle} = \frac{\sum_k \sum_l c_k^* c_l H_{kl}}{\sum_k \sum_l c_k^* c_l S_{kl}} \tag{2.6}$$

Note that in the right-hand side of Eq. 2.6, the bra-ket notation has been suppressed, introducing H_{kl} and S_{kl} to denote these integrals, which are ordinarily known as the "Hamiltonian" and "overlap" integrals. From here, one uses the condition that an infinitesimal variation of the energy with respect to the linear coefficients should equal zero, for the coefficients to be optimal, i.e., the condition that $\partial E / \partial c_k^* = 0$. This results in the matrix equation:

$$H\mathbf{c} = ES\mathbf{c} \tag{2.7}$$

Here, H denotes the Hamiltonian matrix, while S denotes the overlap matrix. Both of these matrices are $m \times m$, while the coefficient vector, $\mathbf{c}$, is $m \times 1$, and should be understood as a generalized eigenvector. The entries for these matrices are simply the H_{kl} and S_{kl} integrals. In some cases, the basis functions used to expand Ψ may be orthogonal to one another, i.e., $\langle \phi_k | \phi_l \rangle = \delta_{kl}$. However, in the present work, this will not be the case, and therefore S is not reduced to the identity matrix. Solving Eq. 1.1 in this way is therefore reduced to the solution of a generalized eigenvalue problem (GEVP), which can be handled by computers.

To solve Eq. 2.7 for this work, various eigensolvers from the LAPACK distribution are

employed. We have used Fortran to write a program for calculating the H_{kl} and S_{kl} integrals, building these matrices, and using these matrices as inputs to the LAPACK libraries that solve the GEVP. The matrix H is symmetric, while the matrix S is symmetric and positive-definite, so we have used the LAPACK routines "dsygvx.f", "dsygvd.f", and "dsygv.f" at different times. For an expansion of Ψ using m functions, there are m eigenpairs that can be calculated, and dsygvx.f calculates only one of these at a time. In some cases, however, all eigenpairs are needed, as is the case when calculating the dipole polarizabilities. These linear algebra routines are easy to work with, but performance gains would be realized by implementing the inverse iteration algorithm (IIA) to solve Eq. 2.7 [35]. At present, an implementation of the IIA is being pursued, but has not been used in Chapters 3-5.

As stated in Chapter 1, this method is restricted by the need to construct a basis set for a particular wavefunction. Having now defined the Rayleigh quotient in Eq. 2.5, we can be a bit more specific about this task. What has been shown is that one can calculate E from the solution to a GEVP, but this energy, in turn, depends on the parameterization of the wavefunction, collectively denoted as $\{a\}$. For an arbitrary change to the set of parameters, one would find a different energy. Hence, one can attempt to minimize the energy with respect to the *nonlinear* parameters, applying the condition that $\partial E/\partial a_i = 0$. One can summarize this task as follows, where it is understood that the Rayleigh quotient can always be calculated from the solution to Eq. 2.7:

$$E = \min_{\{a\}} \frac{\langle \Psi_a | \hat{H} | \Psi_a \rangle}{\langle \Psi_a | \Psi_a \rangle} \tag{2.8}$$

2.2 Building the H and S matrices

The basis functions used in Chapters 3-5 are the explicitly correlated Gaussians (ECGs) [15, 36]. A Gaussian function, $f(r)$, is a function which decays with r^2:

$$f(r) = \exp(-\alpha r^2) \tag{2.9}$$

More generally, a Gaussian can have many arguments (for example, three), and may include products of these arguments. Letting $f(r) \to f(r_1, r_2, r_3)$,

$$f(r_1, r_2, r_3) = \exp(-\alpha_1 r_1^2 - \alpha_2 r_2^2 - \alpha_3 r_3^2 - 2\beta_{12} r_1 r_2 - 2\beta_{13} r_1 r_3 - 2\beta_{23} r_2 r_3) \tag{2.10}$$

In the context of basis sets, the appearance of the $r_i r_j$ factors is associated with the terminology "explicit correlation", where the idea is that the coordinates r_i and r_j are not separated for $\beta_{ij} \neq 0$. A spherical ECG function, which we will be denoted ϕ_k, can be expressed compactly in matrix form [36]:

$$\phi_k = \exp(-\mathbf{r}' \bar{A}_k \mathbf{r}) \tag{2.11}$$

The $3n \times 1$ vector $\mathbf{r} = (\mathbf{r}_1, \mathbf{r}_2, ..., \mathbf{r}_n)$ contains all the particle coordinates, while the $3n \times 3n$ matrix $\bar{A}_k$ contains the nonlinear parameters. The bar notation over a matrix denotes the Kronecker product operation, i.e., $\bar{M} = M \bigotimes I_3$, where M is a $n \times n$ matrix and I_3 is the 3×3 identity matrix. This bar notation will be used hereafter, following Ref. [37]. The prime notation, i.e., $\mathbf{r}'$, denotes the transpose operation.

The functions defined in Eq. 2.11 are spherical, and therefore appropriate for $L = 0$ angular momentum expansions, but cannot be used for the $L = 1$ expansions that are required to calculate dipole polarizabilities for an S-state. The $L = 1$ basis functions can be constructed using the pre-exponential multipliers z_{m_k}, the z coordinate of one of the n particles [15, 38]:

$$\phi_k = z_{m_k} \exp(-\mathbf{r}' \bar{A}_k \mathbf{r}) \tag{2.12}$$

The subscript m_k emphasizes that the coordinates $(z_1, z_2, ..., z_n)$ can be used for a particular ϕ_k. For both $L = 0$ and $L = 1$ functions, the matrix $\bar{A}_k$ is real-valued, and can be Cholesky decomposed as follows [37]:

$$\bar{A}_k = A_k \bigotimes I_3 = (L_k L_k') \bigotimes I_3 \tag{2.13}$$

The L_k matrix is a $n(n+1)/2$ lower triangular matrix, and L_k' is its transpose. Here, the

purpose of the Cholesky decomposition is to enforce the positive definiteness of the A_k matrix. Instead of optimizing the A_k parameters directly, one can optimize the L_k parameters, ensuring that A_k remains positive definite for any parameter values.

Whether one expands the wavefunction using single-particle orbitals [10], or uses all-particle basis functions, the wavefunction must be antisymmetric following the exchange of identical particles [39]:

$$\Psi(\mathbf{r}_1,...,\mathbf{r}_i,...,\mathbf{r}_j,...,\mathbf{r}_N) = -\Psi(\mathbf{r}_1,...,\mathbf{r}_j,...,\mathbf{r}_i,...,\mathbf{r}_N) \tag{2.14}$$

Here, it is assumed that particles i and j are identical, while Eq. 2.14 is true for any other permutation involving identical particles. If the wavefunction is assumed to be a product of one-electron wavefunctions, then the antisymmetrization can be enforced by constructing the Slater determinant, comprised of spin orbitals $\chi_i(\mathbf{r}_j)$ [10]:

$$\Psi(\mathbf{r}_1,...,\mathbf{r}_N) = \frac{1}{\sqrt{N!}} \begin{vmatrix} \chi_1(\mathbf{r}_1) & \chi_2(\mathbf{r}_1) & ... & \chi_N(\mathbf{r}_1) \\ \chi_1(\mathbf{r}_2) & \chi_2(\mathbf{r}_2) & ... & \chi_N(\mathbf{r}_2) \\ \vdots & \vdots & \ddots & \\ \chi_1(\mathbf{r}_N) & \chi_2(\mathbf{r}_N) & ... & \chi_N(\mathbf{r}_N) \end{vmatrix}$$

To enforce this symmetry when the wavefunction is expanded as in Eq. 2.3, provided the Hamiltonian is spin-independent [40], one can project this symmetry onto each ECG function. To reflect this symmetry projection, one can write Eq. 2.3 in a more general form:

$$\Psi = \sum_{k=1}^{m} c_k \mathscr{P} \phi_k \tag{2.15}$$

The operator $\mathscr{P}$ enforces the correct permutational symmetry for Ψ. One approach that can be used to define $\mathscr{P}$, discussed in Ref. [40], involves Young operators. If a state of interest is, for example, a two-electron singlet or triplet state,

$$\mathscr{P}_s = \frac{1}{\sqrt{2}}(1+\hat{P}_{12}) \tag{2.16}$$

$$\mathscr{P}_t = \frac{1}{\sqrt{2}}(1 - \hat{P}_{12}) \tag{2.17}$$

The permutation operator $\hat{P}_{12}$ permutes the coordinates of electrons 1 and 2, but for ECGs, one can equivalently apply the transformations $A_k \rightarrow P'_{12} A_k P_{12}$ and $z_{m_k} \rightarrow P'_{12} z_{m_k}$, where P_{12} is the 2×2 matrix that permutes the coordinates for electron 1 and 2 [21]. As this symmetry projection enters the integrals that define the H and S matrices for a finite basis set expansion, one needs to evaluate the matrix elements [40]:

$$\langle \mathscr{P}\phi_k | \hat{H} | \mathscr{P}\phi_l \rangle = \langle \phi_k | \mathscr{P}^\dagger \hat{H} \mathscr{P} | \phi_l \rangle = \langle \phi_k | \hat{H} (\mathscr{P}^\dagger \mathscr{P}) | \phi_l \rangle \tag{2.18}$$

$$\langle \mathscr{P}\phi_k | \mathscr{P}\phi_l \rangle = \langle \phi_k | (\mathscr{P}^\dagger \mathscr{P}) | \phi_l \rangle \tag{2.19}$$

The property that $\mathscr{P}$ commutes with $\hat{H}$ is used in Eq. 2.18, so that in both cases, it is necessary to calculate $(\mathscr{P}^\dagger \mathscr{P})$. For the permutational symmetry operator defined in Eq. 2.16, the product $\mathscr{P}^\dagger \mathscr{P} = (1 + \hat{P}_{12})$. Hence, for a two-electron singlet state, when building H and S, one must calculate:

$$H_{kl} = \langle \phi_k | \hat{H} | \phi_l \rangle + \langle \phi_k | \hat{H} | (\hat{P}_{12} \phi_l) \rangle \tag{2.20}$$

$$S_{kl} = \langle \phi_k | \phi_l \rangle + \langle \phi_k | (\hat{P}_{12} \phi_l) \rangle \tag{2.21}$$

As stated, $\hat{P}_{12}\phi_l$ only rearranges the elements of the A_k matrices for $L = 0$ basis functions, while for $L = 1$ basis functions the z_{m_k} factor is also subject to permutation. Hence, the permutational symmetry requirement for ECGs does not change how the matrix elements are calculated. These expressions can readily be generalized to systems with different numbers and types of particles using the Young operator formalism [21]. For three electrons, H_{kl} and S_{kl} each involve the calculation of six integrals, while Eqs. 2.18 and 2.19 remain valid. For the muon-electron-nucleus systems discussed in Chapter 5, there are no identical particles and therefore $\mathscr{P} = 1$.

Now, to define $\hat{H}$ explicitly, let us collect $\hat{V}$ and $\hat{T}$ from Eqs. 2.1 and 2.2, which for a

heliumlike ion is simply:

$$\hat{H} = -\frac{\nabla_N^2}{2m_N} - \frac{\nabla_1^2}{2} - \frac{\nabla_2^2}{2} - \frac{Z}{r_1} - \frac{Z}{r_2} + \frac{1}{r_{12}} \tag{2.22}$$

Very often, the approximation $m_N \to \infty$ is assumed. For atomic problems, the finite mass of the nucleus can be re-introduced by calculating perturbatively the so-called "normal" (NMS) and "specific" (SMS) mass shifts [1]:

$$E_{NMS} = -\frac{E}{m_N} \tag{2.23}$$

$$E_{SMS} = \sum_{i>j} \frac{\langle \Psi | \nabla_i \cdot \nabla_j | \Psi \rangle}{m_N} \tag{2.24}$$

However, in some cases it is desirable or perhaps even necessary to keep the nuclear mass finite. For the calculations in Chapters 3 and 4, the $m_N \to \infty$ limit is used. When calculating the ionization energies in Chapter 3, $m_N \to \infty$ and E_{NMS} and E_{SMS} are used, while in Chapter 4, the calculated dipole polarizabilities are valid for $m_N \to \infty$, and no finite nuclear mass correction is considered. Only in Chapter 5 is the fully non-adiabatic Hamiltonian ($m_N \neq \infty$) used.

Now, it will be shown how to calculate H_{kl} and S_{kl} for Eq. 2.22, for the $L = 0$ ECGs in Eq. 2.11. For $L = 1$ ECGs, the corresponding matrix elements can be derived similarly, but the reader is referred to Ref. [41] for derivations of those integrals, which are determined using a matrix calculus approach. In the implementation used for Chapters 3-5, normalized basis functions are employed. The normalization of the basis functions is enforced using [37]:

$$\langle \phi_k | \phi_l \rangle \to \frac{\langle \phi_k | \phi_l \rangle}{\sqrt{\langle \phi_k | \phi_k \rangle \langle \phi_l | \phi_l \rangle}} \tag{2.25}$$

If the basis functions are normalized, it is still only necessary to determine an integral of the general form $\langle \phi_k | \phi_l \rangle$, from which $\langle \phi_k | \phi_l \rangle$ and $\langle \phi_l | \phi_l \rangle$ are special cases. To determine $\langle \phi_k | \phi_l \rangle$, one first calculates the product of two ECGs, which in matrix form is simply:

$$\phi_k \phi_l = \exp[-\mathbf{r}' \bar{A}_k \mathbf{r}] \exp[-\mathbf{r}' \bar{A}_l \mathbf{r}] = \exp[-\mathbf{r}' (\bar{A}_k + \bar{A}_l) \mathbf{r}] \equiv \exp[-\mathbf{r}' \bar{A}_{kl} \mathbf{r}] \tag{2.26}$$

In the last step, the definition $\bar{A}_{kl} \equiv \bar{A}_k + \bar{A}_l$ is used. Integration over $\exp[-\mathbf{r}'\bar{A}_{kl}\mathbf{r}]$ is accomplished using the integral [37]:

$$\int_{-\infty}^{\infty} \exp[-\mathbf{x}'A\mathbf{x}]d\mathbf{x} = \frac{\pi^{n/2}}{|A|^{1/2}} \tag{2.27}$$

This expression is valid for a $n \times 1$ vector $\mathbf{x}$ and a $n \times n$ positive definite matrix A. Here, the vertical bar notation $|M|$ indicates a matrix determinant and $|M|^{1/2} \equiv (|M|)^{1/2}$. Using Eqs. 2.26 and 2.27, and the property $|A_{kl} \bigotimes I_3| = |A_{kl}|^3$ [37]:

$$S_{kl} = \frac{\langle \phi_k | \phi_l \rangle}{\sqrt{\langle \phi_k | \phi_k \rangle \langle \phi_l | \phi_l \rangle}} = \frac{\frac{\pi^{3n/2}}{|A_{kl}|^{3/2}}}{\sqrt{\frac{\pi^{3n/2}}{|2A_k|^{3/2}} \frac{\pi^{3n/2}}{|2A_l|^{3/2}}}} = 2^{3n/2} \left(\frac{|A_k|^{3/4} |A_l|^{3/4}}{|A_{kl}|^{3/2}} \right) \tag{2.28}$$

In the last step, $(|aM|)^{3/2} = (a^n|M|)^{3/2} = a^{3n/2}|M|^{3/2}$ has been used, for a constant a. This expression for S_{kl} is used to calculate the overlap integrals between $L = 0$ ECG functions. The $2^{3n/2}$ factor will of course depend on the number of particles. However, the quantity in parentheses on the RHS of Eq. 2.28 is valid for an arbitrary number of particles. This illustrates one of the main advantages of ECG basis functions, that the matrix elements are not complicated by increasing particle number, which is not generally true for other types of expansion functions. To calculate S_{kl}, the only requirement is to calculate the determinants of the matrices A_k, A_l, A_{kl}. It can be verified that for $k = l$, $S_{kl} = 1$, and is therefore normalized to unity.

To calculate the Hamiltonian matrix, H, one needs to determine $\langle \phi_k | \hat{T} | \phi_l \rangle$ and $\langle \phi_k | \hat{V} | \phi_l \rangle$. Here, a matrix-based derivation is also possible [37]. Instead, it will be shown how to derive T_{kl} by expanding $\mathbf{r}'\bar{A}_{kl}\mathbf{r}$. As the same derivation is possible for an arbitrary number of particles, albeit with more algebra, an explicit calculation for three-body systems will be considered, using:

$$\mathbf{r}'\bar{A}_{kl}\mathbf{r} = -A_{kl}^{11} r_1^2 - A_{kl}^{22} r_2^2 - 2A_{kl}^{21} r_1 r_2 \tag{2.29}$$

The superscript notation A^{ij} has been used to denote the (i, j) entry for matrix A. For a

heliumlike ion, where $m_N \to \infty$:

$$T_{kl} = \langle \phi_k | \hat{T} | \phi_l \rangle = \frac{1}{2} \sum_{i=1}^{2} \langle \nabla_i \phi_k | \nabla_i \phi_l \rangle \tag{2.30}$$

Again, it is understood that the T_{kl} matrix element is the same for different permutational symmetry terms. Allowing ∇_i to operator on both ϕ_k and ϕ_l:

$$\begin{aligned} \langle \phi_k | \hat{T} | \phi_l \rangle = 2 \Big[& A_k^{11} A_l^{11} \langle r_1^2 \rangle + A_k^{21} A_l^{21} \langle r_2^2 \rangle + [A_k^{11} A_l^{21} + A_k^{21} A_l^{11}] \langle r_1 r_2 \rangle + \\ & A_k^{22} A_l^{22} \langle r_2^2 \rangle + A_k^{21} A_l^{21} \langle r_1^2 \rangle + [A_k^{22} A_l^{21} + A_k^{21} A_l^{22}] \langle r_1 r_2 \rangle \Big] \end{aligned} \tag{2.31}$$

To simplify these expressions, the notation $\langle \phi_k | \mathscr{O} | \phi_l \rangle \equiv \langle \mathscr{O} \rangle$ has been used. Integrals of the forms $\langle r_i^2 \rangle$ and $\langle r_i r_j \rangle$ are therefore necessary to complete this derivation. For $L = 0$ ECG's, in Cartesian coordinates:

$$\begin{aligned} \langle \phi_k | r_i^2 | \phi_l \rangle &= 3 \langle \phi_k | x_i^2 | \phi_l \rangle \\ &= 3(\langle \phi_k | \phi_l \rangle)^{2/3} \int_{-\infty}^{\infty} \int_{-\infty}^{\infty} x_i^2 \exp(-A_{kl}^{ii} x_i^2 - A_{kl}^{jj} x_j^2 - 2A_{kl}^{ji} x_i x_j) dx_i dx_j \\ &= 3(\langle \phi_k | \phi_l \rangle)^{2/3} \left[\frac{\pi}{2(A_{kl}^{jj})^{1/2}} (A_{kl}^{ii} - \frac{(A_{kl}^{ji})^2}{A_{kl}^{jj}})^{-3/2} \right] \\ &= \frac{3}{2} \langle \phi_k | \phi_l \rangle \frac{A_{kl}^{jj}}{|A_{kl}|} = \frac{3}{2} \langle \phi_k | \phi_l \rangle (A_{kl}^{-1})^{ii} \end{aligned} \tag{2.32}$$

$$\begin{aligned} \langle \phi_k | r_i r_j | \phi_l \rangle &= 3 \langle \phi_k | x_i x_j | \phi_l \rangle \\ &= 3(\langle \phi_k | \phi_l \rangle)^{2/3} \int_{-\infty}^{\infty} \int_{-\infty}^{\infty} x_i x_j \exp(-A_{kl}^{ii} x_i^2 - A_{kl}^{jj} x_j^2 - 2A_{kl}^{ji} x_i x_j) dx_i dx_j \\ &= 3(\langle \phi_k | \phi_l \rangle)^{2/3} \left[\frac{-\pi A_{kl}^{ji}}{2(A_{kl}^{jj})^{1/2}} (A_{kl}^{jj})^{-3/2} (A_{kl}^{ii} - \frac{(A_{kl}^{ji})^2}{A_{kl}^{jj}})^{-3/2} \right] \\ &= \frac{3}{2} \langle \phi_k | \phi_l \rangle \frac{-A_{kl}^{ji}}{|A_{kl}|} = \frac{3}{2} \langle \phi_k | \phi_l \rangle (A_{kl}^{-1})^{ji} \end{aligned} \tag{2.33}$$

The normalization of the $\langle r_i^2 \rangle$ and $\langle r_i r_j \rangle$ integrals can be enforced once again, by using the

substitution in Eq. 2.28. For the rightmost term in both Eqs. 2.32 and 2.33, the notation A_{kl}^{-1} is used to represent the inverse of matrix A_{kl}. This notation will continue to be used throughout, so that for a matrix M, its inverse will be denoted M^{-1}, and the element (i, j) for M^{-1} will be denoted $(M^{-1})^{ij}$. Eqs. 2.32 and 2.33, modified according to Eq. 2.28, are then substituted into Eq. 2.31, leading to the normalized kinetic energy integral T_{kl}. For a three-body system, and for $m_N \to \infty$,

$$\begin{aligned} T_{kl} = 3S_{kl}\Big[&A_k^{11}A_l^{11}(A_{kl}^{-1})^{11} + A_k^{21}A_l^{21}(A_{kl}^{-1})^{22} + [A_k^{11}A_l^{21} + A_k^{21}A_l^{11}](A_{kl}^{-1})^{21} + \\ &A_k^{22}A_l^{22}(A_{kl}^{-1})^{22} + A_k^{21}A_l^{21}(A_{kl}^{-1})^{11} + [A_k^{22}A_l^{21} + A_k^{21}A_l^{22}](A_{kl}^{-1})^{21}\Big] \end{aligned} \tag{2.34}$$

It can be verified that this expression is equivalent to the matrix element T_{kl} in matrix form, where $Tr(M)$ denotes the trace of a matrix M, which may be a product of many matrices [37]:

$$T_{kl} = 3S_{kl}Tr(A_k A_{kl}^{-1} A_l) \tag{2.35}$$

To calculate the matrix elements $V_{kl} = \langle\phi_k|\hat{V}|\phi_l\rangle$, integrals of the forms $\langle\phi_k|1/r_{ij}|\phi_l\rangle$ are required, where r_{ij} is either r_1, r_2, or r_{12} for three-particle systems. Evaluation of these integral can be accomplished by integral transforming [37] the interparticle distance $1/r_{ij}$:

$$\frac{1}{r_{ij}} = \frac{2}{\sqrt{\pi}}\int_0^\infty \exp(-u^2 r_{ij}^2)du \tag{2.36}$$

$$V_{kl} = \frac{2}{\sqrt{\pi}}\int_0^\infty \Big[\langle\phi_k|\exp(-u^2 r_1^2)|\phi_l\rangle + \langle\phi_k|\exp(-u^2 r_2^2)|\phi_l\rangle + \langle\phi_k|\exp(-u^2 r_{12}^2)|\phi_l\rangle\Big]du \tag{2.37}$$

For integrals of the $1/r_{12}$ type:

$$\begin{aligned}\langle\phi_k|\exp(-u^2 r_{ij}^2)|\phi_l\rangle &= \langle\phi_k|\exp(-u^2(r_i^2+r_j^2-2r_i r_j)|\phi_l\rangle \\ &= \left[\int_{-\infty}^{\infty}\exp(-(A_{kl}^{ii}+u^2)x_i^2-(A_{kl}^{jj}+u^2)x_j^2-2(A_{kl}^{ji}-u^2)x_i x_j)dx_i dx_j\right]^3 \\ &= \frac{\pi^3}{((A_{kl}^{ii}+u^2)(A_{kl}^{jj}+u^2)-(A_{kl}^{ji}-u^2)^2)^{3/2}} = \frac{\pi^3}{(|A_{kl}|+(A_{kl}^{ii}+A_{kl}^{jj}+2A_{kl}^{ji})u^2)^{3/2}}\end{aligned} \tag{2.38}$$

$$V_{kl}^{ij} = \frac{2}{\sqrt{\pi}}\int_0^{\infty}\frac{\pi^3}{(|A_{kl}|+(A_{kl}^{ii}+A_{kl}^{jj}+2A_{kl}^{ji})u^2)^{3/2}}du = \frac{2}{\sqrt{\pi}}\frac{\pi^3}{|A_{kl}|\sqrt{A_{kl}^{ii}+A_{kl}^{jj}+2A_{kl}^{ji}}} \tag{2.39}$$

Verification of this matrix element with the results from Ref. [37] is provided by dividing the denominator of the RHS of Eq. 2.39 by $|A_{kl}|^{1/2}$, and once again using the substitution in Eq. 2.28,

$$\frac{2}{\sqrt{\pi}}\frac{\pi^3}{|A_{kl}|^{3/2}}\left(\frac{A_{kl}^{ii}+A_{kl}^{jj}+2A_{kl}^{ji}}{|A_{kl}|}\right)^{-1/2} = \frac{2}{\sqrt{\pi}}S_{kl}\frac{1}{\sqrt{(A_{kl}^{-1})^{jj}+(A_{kl}^{-1})^{ii}-2(A_{kl}^{-1})^{ji}}} \tag{2.40}$$

In matrix form, V_{kl}^{ij} is expressed as [37]:

$$V_{kl}^{ij} = \frac{2}{\sqrt{\pi}}S_{kl}\frac{1}{(Tr[A_{kl}^{-1}J_{ij}])^{1/2}} \tag{2.41}$$

In Eq. 2.41, J_{ij} is a $n\times n$ matrix with value 1 in the ii and jj positions, and value -1 in the ij and ji positions. For two electrons,

$$J_{ij} = \begin{bmatrix} 1 & -1 \\ -1 & 1 \end{bmatrix}$$

It can be verified by expanding $Tr[A_{kl}^{-1}J_{ij}]$ that Eq. 2.40 is identical to Eq. 2.41. For the

$1/r_i$ integrals,

$$\begin{aligned}\langle\phi_k|\exp(-u^2 r_i^2)|\phi_l\rangle &= \left[\int_{-\infty}^{\infty}\exp(-(A_{kl}^{ii}+u^2)x_i^2 - A_{kl}^{jj}x_j^2 - 2A_{kl}^{ji}x_i x_j)dx_i dx_j\right]^3 \\ &= \frac{\pi^3}{((A_{kl}^{ii}+u^2)(A_{kl}^{jj})-(A_{kl}^{ji})^2)^{3/2}} = \frac{\pi^3}{(|A_{kl}|+(A_{kl}^{jj})u^2)^{3/2}}\end{aligned} \tag{2.42}$$

The final expression for V_{kl}^i, i.e., for $1/r_1$ and $1/r_2$ is then:

$$V_{kl}^i = \frac{2}{\sqrt{\pi}}\int_0^{\infty}\frac{\pi^3}{(|A_{kl}|+(A_{kl}^{jj})u^2)^{3/2}}du = \frac{2}{\sqrt{\pi}}\frac{\pi^3}{|A_{kl}|\sqrt{A_{kl}^{jj}}} \tag{2.43}$$

Again, dividing the denominator of the RHS of Eq. 2.43 by $|A_{kl}|^{1/2}$,

$$\frac{2}{\sqrt{\pi}}\frac{\pi^3}{|A_{kl}|^{3/2}}\left(\frac{A_{kl}^{jj}}{|A_{kl}|}\right)^{-1/2} = \frac{2}{\sqrt{\pi}}S_{kl}\frac{1}{\sqrt{(A_{kl}^{-1})^{ii}}} \tag{2.44}$$

In matrix form, for V_{kl}^i [37],

$$V_{kl}^i = \frac{2}{\sqrt{\pi}}S_{kl}\frac{1}{(Tr[A_{kl}^{-1}J_{ii}])^{1/2}} \tag{2.45}$$

$$J_{ii} = \begin{bmatrix}\delta_{i1} & 0\\ 0 & \delta_{i2}\end{bmatrix}$$

In defining J_{ii}, the Kronecker delta function $\delta_{ab} = 1, a = b, \delta_{ab} = 0, a \neq b$ has been used. It can again be verified that Eq. 2.45 expands to give Eq. 2.44.

2.3 Optimization of the nonlinear parameters of Ψ

According to Eq. 2.8, the optimal solution to Eq. 1.1 is determined by minimizing the Rayleigh quotient with respect to the nonlinear parameters, which were denoted $\{a\}$, but have since been defined using the L_k matrices. For, convenience, the matrix L_k is written explicitly for a

three-body system:

$$L_k = \begin{bmatrix} L_k^{11} & 0 \\ L_k^{21} & L_k^{22} \end{bmatrix}$$

Hence, there are three parameters per function. To minimize the energy with respect to these parameters, a stochastic selection algorithm has been implemented, that is inspired by the work in Ref. [42]. The basic idea of this algorithm is to successively lower the bound state energy, in this case calculated from the Rayleigh quotient, by *guessing* new parameters. As outlined in Section 2.1, the eigenvectors $\{c\}$ that enter the Rayleigh quotient are determined from the solution of a generalized eigenvalue problem (GEVP). Thus, one has to store the initial energy, and continuously solve the GEVP, hoping that the randomly selected parameters will over time provide a lower energy in an efficient manner. In practice, the energy can be lowered very quickly. However, the gradients are not minimized in this approach, so there are many functions that are far from optimal, which makes the resulting wavefunctions less compact. Eventually, this slows down the optimization process, as nonlinear parameters which have large gradients begin to accumulate.

A function parameter is *guessed* by selecting real values from some domain. The domain could be a normal or uniform distribution, and can depend on the current value of the parameter prior to stochastic selection. During the initial optimization, it has been advantageous to use a fixed, uniform domain for sampling. As convergence ensues, however, the process speeds up by sampling semi-locally around the parameter value. For instance, it is typical to use as a domain, $[p_0 - \frac{1}{2}p_0, p_0 + \frac{1}{2}p_0]$, where p_0 is the parameter value prior to optimization. To make this description more concrete, let us assume a $m = 4$ function basis is used to calculate the Rayleigh quotient. The first step will be to take parameter 1, for function 1 ($i.e., L_1^{11}$), and replace the initial value with a new random value. The Rayleigh quotient is then calculated, and if the energy is lowered, then the new parameter replaces the old parameter, provided no linear dependencies are introduced. By linear dependency, it is meant that the overlap integral, S_{kl}, between two functions ϕ_k and ϕ_l does not exceed a predetermined threshold (i.e., 0.99). It is typical for this step to be repeated many times for a single parameter value. After a fixed number of attempts to lower the Rayleigh quotient

by perturbing L_1^{11}, the algorithm moves to parameters L_1^{21} and L_1^{22}. Then the process is repeated for functions 2, 3, and 4. At this point, the whole process is repeated until convergence slows.

As the linear coefficients $\{c_k\}$ are available during the course of optimization, it is sometimes helpful to differentiate between those with large magnitude contributions, from those with small magnitude contributions. Hence, the specific strategy tailored to a particular optimization can depend on these coefficients. Generating an initial basis set has mostly followed a random selection of parameters based on values which have been tested and shown to provide a reasonable distribution. The first few optimizations with very small basis sets ($m < 100$) are repeated until it is decided that the sampling has stalled. New basis functions are then added to the expansion set. First, these functions are optimized separately, then the whole basis is re-optimized. The cost of these optimizations grows dramatically, and is limited by the $\mathcal{O}(N^3)$ scaling of the eigenvalue problem. In practice, this means that fewer optimization cycles can be completed as the basis set begins to grow.

Within our implementation, for three-body systems, it has been found that beyond ≈ 1500 functions, the convergence slows dramatically. This appears to be true for four-body systems near ≈ 2500 functions. The issue, in the author's view, appears to be that many functions begin to accumulate in the expansion set that do not contribute much to the wavefunction, as evidenced by small ($\approx 1 \times 10^{-10}$) linear coefficients. Despite these shortcomings, the stochastic-based optimizations are capable of providing wavefunctions with fairly accurate energies, and these wavefunctions can be used for the calculation of various properties. This minimization algorithm is identical for both $L = 0$ and $L = 1$ optimizations, and is applied similarly to both three- and four-body systems.

2.4 Dipole Polarizabilities

For an operator $\hat{H}_0$ and a perturbing operator $\hat{H}_1$, one defines $\hat{H}$, the total Hamiltonian:

$$\hat{H} = \hat{H}_0 + \lambda \hat{H}_1 \tag{2.46}$$

The parameter λ is assumed to be small, such that the field-dependent energy/wavefunction (E/Ψ) is close to the field-independent energy/wavefunction (E_0/Ψ_0). Hence, these changes should be expressible as power series:

$$E = E_0 + \lambda E_1 + \lambda^2 E_2 + ... \tag{2.47}$$

$$\Psi = \Psi_0 + \lambda \Psi_1 + \lambda^2 \Psi_2 + ... \tag{2.48}$$

These expansions when substituted into Eq. 1.1 result in infinitely many, coupled linear equations [1]:

$$H_0\Psi_0 = E_0\Psi_0 \tag{2.49}$$

$$H_0\Psi_1 + H_1\Psi_0 = E_0\Psi_1 + E_1\Psi_0 \tag{2.50}$$

$$H_0\Psi_2 + H_1\Psi_1 = E_0\Psi_2 + E_1\Psi_1 + E_2\Psi_0 \tag{2.51}$$

$$\vdots$$

From Eqs. 2.49 and 2.50,

$$E_1 = \langle \Psi_0 | H_1 | \Psi_0 \rangle \tag{2.52}$$

As $E_1 = 0$ for the dipole polarizabilities considered in Chapter 4, our interest is to consider the E_2 and/or Ψ_1 corrections. One could determine each of the eigenpairs of H_0, in order to use the well-known expression for E_2 in terms of the spectrum of H_0 [43]:

$$E_2 = -\sum_n \frac{|\langle \Psi_0 | H_1 | \Psi_n \rangle|^2}{E_n - E_0} \tag{2.53}$$

Instead, one could left multiply Eq. 2.49 by Ψ_2, Eq. 2.51 by Ψ_0 [1]. Subtracting the two resulting equations, and integrating over the coordinates, one finds:

$$E_2 = \langle \Psi_0 | H_1 | \Psi_1 \rangle \tag{2.54}$$

The calculation of E_2 therefore is possible provided Ψ_1 is known, instead of enumerating the spectrum of H_0, as in Eq. 2.53. One can collect Eq. 2.50 as follows, where we assume $E_1 = 0$, defining Ψ_1:

$$(H_0 - E_0)\Psi_1 = -H_1\Psi_0 \tag{2.55}$$

From here, it is possible to write down the following expression [1]:

$$E_2[\Psi_1] = 2\langle\Psi_1|H_1|\Psi_0\rangle + \langle\Psi_1|H_0 - E_0|\Psi_1\rangle \tag{2.56}$$

It is not necessary to derive this equation, as it can be demonstrated that the stationary variation of E_2 with respect to Ψ_1 recovers exactly Eq. 2.55, provided the exact Ψ_1 is known. Hence, one can perform a variational optimization of Ψ_1, just as is done for Ψ_0. Eq. 2.56 is often known as a first-order Hylleraas functional.

Now, let us consider an electric field as the perturbation [43]:

$$H_1 = -F\hat{\mathbf{F}} \cdot \mathbf{d} = -\mathbf{F} \cdot \mathbf{d} \tag{2.57}$$

Here, the parameter F is the field strength and $\mathbf{F}$ is the electric field, while $\mathbf{d}$ is the dipole moment operator:

$$\mathbf{d} = \sum_{i=1}^{n} q_i \mathbf{r}_i \tag{2.58}$$

For this operator, the parameter λ is the electric field strength, which defines the field dependent energy $E_F = E_0 + F^2 E_2 + ...$ in place of Eq. 2.47. Then, one can express E_2 in terms of α, the dipole polarizability [38, 44]:

$$\alpha = -\left(\frac{\partial^2 E_F}{\partial F^2}\right)_{F\to 0} = -2E_2 \tag{2.59}$$

Hence, the determination of the second-order energy, in this context, is equivalent to determining the dipole polarizability. Generalized versions of Eqs. 2.53 and 2.56 which depend on

the electric field frequency ω are used to determine the final, frequency-dependent dipole polarizabilities for the lithiumlike ions in Chapter 4. Both Ψ_0 and Ψ_1 are optimized using the method described in the previous section.

2.5 Non-relativistic quantum electrodynamics (NRQED)

In Chapter 3, calculations of three-electron ionization energies are discussed, which include *relativistic and QED* corrections to the non-relativistic energy obtained from the Schrödinger equation. In the computational methods section for that project, one will see the following excerpt: "The $(Z\alpha)$ expansion used here is based on non-relativistic quantum electrodynamics (NRQED) theory". The goal of this section is therefore to provide some additional background relating to this topic.

First, it should be pointed out that the systems considered in Chapter 3, where the nuclear charge does not exceed $Z = 10$, are considered as *light* atoms. For light atoms, a very good first approximation to the energy levels comes from Eq. 1.1. This is not generally true for more massive atoms, and it may be preferable to avoid the Schrödinger equation altogether, an example of which may be found in Ref. [45]. When considering light atoms, however, the most accurate calculational approach is to treat the non-relativistic solution as the lowest order in perturbation theory [46].

Much of the theory for treating relativistic and QED corrections using perturbation theory is a very old subject. For instance, the leading-order relativistic correction is defined by the expectation value of the non-relativistic wavefunction with the Breit-Pauli Hamiltonian [1]. The non-relativistic energy is of order α^2, where α is the QED fine structure constant, while the leading-order relativistic energy is of order α^4. Hence, this energy is often termed the α^4 correction. The leading-order QED correction for a multielectron system has likewise been known for over half a century [47–49]. This correction is of order α^5.

There are difficulties, however, when going beyond order α^5, which include the appearance of divergences in perturbation theory [50]. For this reason, among others, the effective field theory known as non-relativistic quantum electrodynamics (NRQED) has emerged as a power-

ful theoretical formalism for enumerating higher orders in perturbation theory [51, 52]. NRQED was introduced in the 1980s [53] well after the expressions for the leading-order relativistic and QED corrections were known. However, NRQED has since provided a rigorous framework for determining the operators ultimately used in perturbation theory.

The present acknowledgment of NRQED has to do, exclusively, with the fact that it is used to define a perturbation theory starting from the non-relativistic energies obtained from Eq. 1.1. In other words, we are not concerned with the quantum field theory aspects of NRQED and other effective field theories. What is most important, is that NRQED defines the system energy of a bound state as a power series in the QED fine structure constant, $\alpha \approx 1/137$:

$$E = E^{(2)} + E^{(4)} + E^{(5)} + E^{(6)} + \mathscr{O}(\alpha^7) \tag{2.60}$$

Each of the expansion coefficients is proportional to $\alpha^{(x)}$. The leading term, $E^{(2)}$, turns out to be [50] the energy obtained from the solution of Eq. 1.1. Hence, the $E^{(x)}$ terms, where $x \geq 4$, are the correction energies. While $E^{(4)}$ and $E^{(5)}$ are straightforward to calculate using all-particle wavefunctions, the $E^{(6)}$ correction has never been implemented completely for a four-body system. Although the Hamiltonian is now known [54], numerical results are only available for the more simple three-body system [55]. There are parts of the $E^{(6)}$ correction, however, which can be calculated using the results from the $E^{(4)}$ correction. For instance, $E^{(4)}$ is determined using the first-order correction [1]:

$$E^{(4)} = \langle \Psi | H^{(4)} | \Psi \rangle \tag{2.61}$$

$$H^{(4)} = -\alpha^2 \left(\sum_i \frac{\nabla_i^4}{8} + \frac{Z\pi}{2} \sum_i \delta(r_i) + \pi \sum_{i>j} \delta(r_{ij}) + \frac{1}{2} \sum_{i>j} \left[\frac{1}{r_{ij}} \nabla_i \cdot \nabla_j + \frac{1}{r_{ij}^3} \mathbf{r}_{ij} \cdot (\mathbf{r}_{ij} \cdot \nabla_i) \nabla_j \right] \right) \tag{2.62}$$

Note that $H^{(4)}$ has been defined for the restricted case where the state of interest is a doublet state, and where fine-structure contributions vanish (i.e., for ^2S states). This definition is appropriate for the present purposes, as $E^{(4)}$ is determined only for ^2S states in Chapter 3. For a more general $H^{(4)}$, one may consult Ref. [56]. The matrix elements used to compute these corrections

with ECG functions have been derived in Refs. [40, 57–59]. Meanwhile, $E^{(6)}$ is calculated using the expression [54]:

$$E^{(6)} = E_{R1} + E_{R2} + E'_H + E_{log} + E_Q + E_{sec} \tag{2.63}$$

The first four terms $(E_{R1}, E_{R2}, E'_H, E_{log})$ can be readily evaluated using the calculated inter-particle delta function integrals that are necessary to determine $E^{(4)}$:

$$E_{R1} + E_{R2} + E'_H + E_{log} = \langle \Psi | H_{R1} + H_{R2} + H'_H + H_{log} | \Psi \rangle \tag{2.64}$$

$$H_{R1} = \left(\frac{427}{96} - 2\ln(2) \right) \sum_i \pi \delta(r_i) + \left(\frac{6\zeta(3)}{\pi^2} - \frac{697}{27\pi^2} - 8\ln(2) + \frac{1099}{72} \right) \sum_{i>j} \pi \delta(r_{ij}) \tag{2.65}$$

$$\begin{aligned} H_{R2} = &\left(-\frac{9\zeta(3)}{4\pi^2} - \frac{2179}{648\pi^2} + \frac{3\ln(2)}{2} - \frac{10}{27} \right) \sum_i \pi \delta(r_i) + \\ &\left(\frac{15\zeta(3)}{2\pi^2} + \frac{631}{54\pi^2} - 5\ln(2) + \frac{29}{27} \right) \sum_{i>j} \pi \delta(r_{ij}) \end{aligned} \tag{2.66}$$

$$H'_H = \left(-\frac{39\zeta(3)}{\pi^2} + \frac{32}{\pi^2} - 6\ln(2) + \frac{7}{3} \right) \sum_{i>j} \frac{\pi}{4} \delta(r_{ij}) \tag{2.67}$$

$$H_{log} = -\ln(\alpha) \sum_{i>j} \pi \delta(r_{ij}) \tag{2.68}$$

In these expressions, $\zeta(3) \approx 1.202056....$ However, the expressions for H_Q and H_{sec}, which may be found in Ref. [54], require additional calculation. It is these terms which incorporate the higher-order relativistic corrections, which become more important with increasing Z.

Summarizing, NRQED is an effective field theory that defines a perturbation theory suitable for light, atomic systems. For four-body atoms, the dominating relativistic and QED corrections can be calculated and used to correct the eigenvalues obtained from the Schrödinger equation. However, we have not found it possible to evaluate the complete $E^{(6)}$ correction. Therefore, the results in Chapter 3 reflect an application of NRQED that incorporates these dominating correction energies, and attempts to consider what is anticipated to be the largest source of uncertainty, namely the contribution to $E^{(6)}$ which is not calculated.

CHAPTER 3

RELATIVISTIC AND QED CORRECTIONS FOR THE GROUND STATE LITHIUMLIKE IONIZATION ENERGIES

ABSTRACT

The ground state ionization energies of $Z \leq 10$ lithiumlike ions are calculated using fully correlated Gaussian wavefunctions. Leading-order relativistic corrections are evaluated, while QED corrections are established with small uncertainties by directly calculating the Araki-Sucher energy and expanding the three-electron Bethe logarithm in $1/Z$. The non-relativistic α^6 level shifts have also been calculated, and we have used these energies to recommend ionization energies, which include estimates of the influence of the relativistic portion of the α^6 energy. The results emphasize the importance of the direct computation of the complete α^6 correction, but also the need for new, higher accuracy experimental ionization limits.

3.1 Introduction

The ionization limit of Li I has been determined [60] with much higher precision (1.8×10^{-4} cm^{-1}) compared to the results for the lithiumlike ions [61]. Experimentally, uncertainties are observed to grow rapidly with Z, and already for B^{2+} the uncertainty is 0.6 cm^{-1} [62]. On the

theoretical side, there are difficulties treating simultaneously, to all orders, the nuclear binding and electron-electron interactions [63]. For the low Z ions, for example those where $Z \leq 10$, the most accurate state energies are those resulting from a wavefunction-based non-relativistic perturbation theory [33, 46, 56]. The idea here is to revisit the ionization energies of the $Z \leq 10$ lithiumlike ions using correlated Gaussian wavefunctions and perturbative relativistic and QED corrections. This endeavor constitutes a considerable improvement of previous theory [64, 65] for the ions not including Li, Be^+, and O^{5+} [33, 46, 56]. Beyond $Z = 10$, the lithiumlike ionization energies have been calculated up to $Z = 100$ [66]. Hence, the efforts here can be viewed as an attempt to fill in the gaps between the latest low Z [33, 46, 56] and high Z [66, 67] calculations. Furthermore, previous calculations for Be^+ [46, 68] and O^{5+} [56] suggest it may be possible in some of these cases to recommend ionization energies which are determined with higher accuracy compared to previous experimental work [61].

In what follows, let us refer to the results for which accurate theory is available (Li, Be^+, and O^{5+}) as "subset 1", while "subset 2" refers to B^{2+}, C^{3+}, N^{4+}, F^{6+}, and Ne^{7+}. For subset 2, it is notable that the leading-order (α^4) relativistic corrections to the non-relativistic $2^2S_{1/2}$ energies have not been reported using Hylleraas, exponential, or correlated Gaussian wavefunctions while the leading-order (α^5) QED energies [65] are subject to improvement. These considerations have motivated us to calculate the α^4 energies and the α^5 Araki-Sucher energies using accurately determined correlated Gaussian wavefunctions, while for the Bethe logarithms which enter the electron-nucleus part of the α^5 energies, we have used an established approximation method [69]. Considering now the previous experimental work, there are a number of ionization limits whose relationships with theory are interesting to examine. For Be^+, a 0.06 cm^{-1} difference between experiment [70] and theory [46, 68] has been identified. These calculated ionization energies both involve very accurate wavefunctions which are used to determine the α^4 and α^5 corrections, and have used high numerical accuracy Bethe logarithms. In these studies, an approximation wherein the α^6 correction is defined by the dominating one-loop radiative correction (E_6^{R1}) is used, and the other α^6 contributions including higher-order relativistic corrections are not considered. This

discrepancy is large compared to the theoretical uncertainties (0.005 cm^{-1} [46] and 0.007 cm^{-1} [68]) but is not inconsistent with the 0.35 cm^{-1} experimental [70] uncertainty. In both cases the theoretical uncertainty is mostly due to the incomplete treatment of the order α^6 correction energy.

For B^{2+}, a full-core plus correlation (FCPC) calculation with screened QED corrections [64] might be considered as the best result, although more accurate QED energies were shortly thereafter calculated, deteriorating the agreement with experiment [62, 65]. To the best of our knowledge, there are no high-accuracy calculations in agreement with the experimental value of 305 930.8(6) cm^{-1}. For C^{3+}, a recent relativistic configuration-interaction (RCI) calculation [67] is within the experimental uncertainty bounds [71]. In Ref. [67], the model operator method was used to evaluate the leading-order QED corrections, following Ref. [72]. However, the total uncertainty of that calculation is larger than 10 cm^{-1}, to be compared with the 1.5 cm^{-1} experimental uncertainty. In this case, it is of interest to see how the present level of theory compares to the RCI and experimental results and to independently confirm these values but with smaller uncertainties. For F^{6+}, the situation is similar to B^{2+}, as the ionization energy [73] has not been confirmed by high-accuracy calculations. There is a semi-empirical result [74], which is 10 cm^{-1} smaller, and it is of interest to see how these compare with non-relativistic perturbation theory. For Ne^{7+}, the uncertainty shown in the Atomic Spectra Database (ASD) of the National Institute of Standards and Technology [75] is large and might be reduced by improving the existing leading-order relativistic and QED energies. For N^{4+}, a small discrepancy between RCI [67] and experimental [76] energies is noted.

3.2 Method

The $(Z\alpha)$ expansion used here is based on non-relativistic quantum electrodynamics (NRQED) theory [53]. This approach solves the Schrödinger equation for the non-relativistic energy, and the correction energies are defined by a power series in the QED fine-structure constant, α. First, the non-relativistic energy is minimized variationally using a large set of correlated Gaussians, and the finite-mass corrections are included perturbatively to leading order in $\frac{m_e}{M_N}$, where

m_e and M_N are the electron and nuclear mass, respectively. To this non-relativistic energy are added the leading-order relativistic correction energy, the one-electron Lamb shift involving an expansion of the Bethe logarithm, and the (directly calculated) two-electron Lamb shift. The one- and two-loop radiative corrections at order α^6 are calculated, as well as the complete logarithmic contribution and the correction associated with the forward three-photon scattering amplitude [54].

The n-electron wavefunctions used to evaluate these corrections have been expanded using explicitly correlated Gaussian (ECG) functions [36]. Although for each ion a different wavefunction is constructed, hereafter Ψ is understood to be any particular wavefunction. Likewise, we generically refer to any particular ECG function as ϕ_k:

$$\phi_k = e^{-\mathbf{r}' A_k \mathbf{r}} \tag{3.1}$$

As defined here, ϕ_k is a scalar-valued matrix function of A_k [37]. These basis functions have been used extensively by Adamowicz and co-workers (see the review articles [21, 40] and references therein). In (3.1), the $3n$-component position vector, $\mathbf{r} = (\mathbf{r}_1, \mathbf{r}_2, ..., \mathbf{r}_n)$, contains the coordinates of each electron, where $\mathbf{r}_i$ is defined with respect to the position of the nucleus fixed at the origin, while the positive-definite A_k matrices host the nonlinear parameters. The Cholesky decomposition of A_k into the product of a lower triangular matrix L_k and its transpose $L_k^{'}$ is used to maintain positive-definiteness for A_k for changes in the components of A_k occurring during the optimization of the nonlinear parameters (i.e., $A_k = L_k L_k^{'}$). Each ϕ_k used to expand Ψ then contains $(n^2 + n)/2$ unique nonlinear parameters, the non-zero components of L_k.

The nonlinear parameters contained in A_k for each expansion function (3.1) must be optimized to efficiently determine Ψ and the non-relativistic energy, which is denoted E_2 hereafter. The optimization procedure we have used is based on the stochastic selection of the components of L_k using the variational method [42]. A disadvantage of our implementation is that it optimizes Ψ with respect to the energy E_2 without minimizing the gradients associated with $\{L_k\}$. As a result, E_2 can lower even if "bad" basis functions remain in the expansion. This makes our Ψ less

compact compared to other work that uses either more sophisticated basis functions [16] or more powerful nonlinear optimization routines [41]. In any case, the stochastic selection is effective for an ECG wavefunction expansion where the total number of ECGs is not too large.

Next, the relativistic corrections are included to first order by calculating the expectation value of the infinite nuclear mass limit Breit-Pauli Hamiltonian [1] with the non-relativistic wavefunction; this correction energy is denoted E_4. These individual Hamiltonians are proportional to α^4, and for $L = 0$ states include the orbit-orbit interaction, terms proportional to the Dirac delta functions $\delta(r_i)$ and $\delta(r_{ij})$, resulting from the Darwin and spin-spin interaction, and also a term proportional to ∇_i^4 (mass-velocity correction). For further details, see [1]. It is well known that the Darwin and mass-velocity integrals with Gaussian functions are slowly-converging. To circumvent this problem, we have adopted the Drachmanization approach [77, 78], which replaces the delta function and ∇_i^4 integrals which enter the Breit-Pauli Hamiltonian [1] with equivalent expressions that converge faster in finite basis set calculations. The two types of delta function integrals $\langle\Psi|\delta(r_i)|\Psi\rangle$ and $\langle\Psi|\delta(r_{ij})|\Psi\rangle$ are replaced by:

$$\pi\,\langle\Psi|\delta(r_i)|\Psi\rangle = \langle\Psi|\frac{1}{r_i}(E_2-\hat{V})|\Psi\rangle - \frac{1}{2}\sum_{k=1}^{n}\langle\nabla_k\Psi|\frac{1}{r_i}|\nabla_k\Psi\rangle \tag{3.2}$$

$$\pi\,\langle\Psi|\delta(r_{ij})|\Psi\rangle = \frac{1}{2}\,\langle\Psi|\frac{1}{r_{ij}}(E_2-\hat{V})|\Psi\rangle - \frac{1}{4}\sum_{k=1}^{n}\langle\nabla_k\Psi|\frac{1}{r_{ij}}|\nabla_k\Psi\rangle \tag{3.3}$$

The potential energy operator, $\hat{V}$, associated with the non-relativistic Hamiltonian enters each of these expressions, while r_i denotes the distance between the ith electron and the nucleus, while r_{ij} is the distance between the ith and jth electrons. These integrals have to be evaluated for the distances r_1, r_2, r_3, and for r_{12}, r_{13}, r_{23}. Likewise, the mass-velocity operator is replaced by:

$$\langle\Psi|\sum_{i=1}^{n}\nabla_i^4|\Psi\rangle = 4\,\langle\Psi|(E_2-\hat{V})^2|\Psi\rangle - 2\sum_{i=1}^{n}\sum_{j>i}^{n}\langle\nabla_i^2\Psi|\nabla_j^2\Psi\rangle \tag{3.4}$$

The orbit-orbit interaction exhibits better convergence compared to these operators. The reader is referred to [57] for a derivation of this matrix element with ECG functions.

The α^5 energy, E_5, is expressed in terms of E_{L1} and E_{L2}, the one- and two-electron Lamb shifts [47–49, 79]:

$$E_5 = E_{L1} + E_{L2} \tag{3.5}$$

$$\frac{E_{L1}}{\alpha^3} = \left(\frac{19}{30} - 2\ln(\alpha) - \ln(k_0)\right)\frac{4Z}{3}\sum_{i=1}^{n}\langle\Psi|\delta(r_i)|\Psi\rangle \tag{3.6}$$

$$\frac{E_{L2}}{\alpha^3} = \sum_{i=1}^{n}\sum_{j>i}^{n}\left[\left(\frac{164}{15} + \frac{14}{3}\ln(\alpha)\right)\langle\Psi|\delta(r_{ij})|\Psi\rangle - \frac{7}{6\pi}\langle\Psi|P(r_{ij}^{-3})|\Psi\rangle\right] \tag{3.7}$$

Provided (3.2) and (3.3) are available from the α^4 correction, the only new computational tasks are the Bethe logarithm, $\ln(k_0)$, and the Araki-Sucher integral, $\langle\Psi|P(r_{ij}^{-3})|\Psi\rangle$. The latter is defined by the distribution [80]:

$$P(r_{ij}^{-3}) = \lim_{\varepsilon\to 0}\left[r_{ij}^{-3} + 4\pi(\gamma + \ln(\varepsilon))\delta(r_{ij})\right] \tag{3.8}$$

Matrix elements of (3.8), where $\gamma = 0.577...$ is the Euler-Mascheroni constant, with ECG functions have been derived by Stanke et al. [81] and are used in these calculations:

$$\langle\phi_k|P(r_{ij}^{-3})|\phi_l\rangle = \frac{2}{\sqrt{\pi}}\frac{\langle\phi_k|\phi_l\rangle}{(\mathrm{tr}[A_{kl}^{-1}J_{ij}])^{3/2}}[\gamma + \ln(\mathrm{tr}[A_{kl}^{-1}J_{ij}])] \tag{3.9}$$

In (3.9), ϕ_k and ϕ_l are any two ECG functions that are used to expand a particular Ψ. We have adopted the notation from [81], where J_{ij} and A_{kl}^{-1} are $n\times n$ matrices that appear in the matrix-function derivation of (3.9). To the best of our knowledge, E_{L2} has not been directly evaluated for any of the ions of subset 2.

In (3.6), $\ln(k_0)$ is defined following Ref. [82]:

$$\ln(k_0) = \frac{\sum_n |\langle\Psi|\mathbf{p}|\Psi_n\rangle|^2(E_n - E_2)\ln|E_n - E_2|}{\sum_n |\langle\Psi|\mathbf{p}|\Psi_n\rangle|^2(E_n - E_2)} \tag{3.10}$$

The intermediate states, Ψ_n, couple to Ψ by the linear momentum operator $\mathbf{p}$, and the summations in (3.10) span both bound and continuum states, where E_n are the intermediate state

energies. Hence, the calculation of $\ln(k_0)$ presents a different challenge, as there is no simple matrix element in terms of Ψ only, unlike the corrections presented thus far. Calculations of $\ln(k_0)$ are mostly based on two approaches, namely the pseudostate [82, 83] and integral [84–86] representations. For three-electron ground states, these have only been calculated for subset 1 [33, 46, 56]. There are also reports of Bethe logarithms calculated for the four-electron Be atom, B^+ and C^{2+} [84, 87, 88].

For the present ionization energy calculations, however, it is not necessary to evaluate $\ln(k_0)$ directly for each three-electron ground state. This is true for two reasons. First, the desired uncertainty of our calculations is for each ion just less than its corresponding NIST ASD uncertainty. As discussed above, for $Z > 3$, the ionization limit uncertainties are greater than 0.35 cm^{-1} and grow quickly with Z. Second, there is a $\ln(k_0)$ approximation method that we have found capable of reproducing directly calculated $\ln(k_0)$ for Be^+ and O^{5+}, to the extent that the E_5 errors are much less than the NIST ASD uncertainties. This method works by expanding the three-electron Bethe logarithm in $1/Z$, using two-electron Bethe logarithms and the resulting fractional parentage coefficients [65]. To first-order in the $1/Z$ expansion [69]:

$$\ln(k_0/Z^2) = \beta_0 + 2\ln[(Z-\sigma)/Z] \tag{3.11}$$

The leading-order term, β_0, is determined [69] by the hydrogen [89] Bethe logarithms:

$$\beta_0(n^2S) = \frac{2\beta(1S) + \beta(nS)/n^3}{2 + 1/n^3} \tag{3.12}$$

The state-dependent constant σ we have used is -0.00842 which has been calculated previously [65] using the two-electron $1/Z$ expansion coefficients from [90]. Although there are more accurate $1/Z$ coefficients [91] that have since been determined, these have not used these to reevaluate σ. This method has been used in [69] to calculate $\ln(k_0)$ for Li, prior to its direct calculation [83, 92]. Considering that the goal here is to produce high-accuracy ionization energies for subset 2, the question is then whether for the subset 2 ions this approximation method results in E_5 cor-

rections whose uncertainties are much smaller than the NIST ASD uncertainties. This assessment is provided in Section III.C.

The order α^6 correction energy E_6 can be represented as follows (see Eq. (20) of Ref. [54]):

$$E_6 = E_6^Q + E_6^{H'} + E_6^{sec} + E_6^{R1} + E_6^{R2} - \ln(\alpha)\,\langle\Psi|\sum_{i=1}^{n}\sum_{j>i}^{n}\pi\delta^3(r_{ij})|\Psi\rangle \tag{3.13}$$

The one-loop radiative energy E_6^{R1} is often used as an approximate E_6 and is defined by the effective Hamiltonian (see Ref. [93], Eq. 14):

$$H_{R1} = Z^2\pi\left(\frac{427}{96} - 2\ln 2\right)\sum_{i=1}^{n}\delta^3(r_i) + \pi\left(\frac{6\zeta(3)}{\pi^2} - \frac{697}{27\pi^2} - 8\ln 2 + \frac{1099}{72}\right)\sum_{i=1}^{n}\sum_{j>i}^{n}\delta^3(r_{ij}) \tag{3.14}$$

Note that the fraction 427/96 in the first term of Eq. (14) was misprinted as 472/96 in Eq. (18) of Ref. [54]. The two-loop radiative energy E_6^{R2}, the forward three-photon scattering energy $E_6^{H'}$, and that from the logarithmic term all contribute very little to the final ionization energies, but they can be included after having calculated (3.2) and (3.3) to further isolate E_6^Q and E_6^{sec}, which have not been calculated here.

Finally, the leading-order, perturbative finite mass corrections are considered [1]:

$$E_{FM} = -\frac{E_2}{M_N} + \frac{1}{M_N}\sum_{i=1}^{n}\sum_{j>i}^{n}\langle\Psi|\nabla_i\nabla_j|\Psi\rangle \tag{3.15}$$

The use of E_{FM} as the sole finite mass correction is justified, since for Li and Be^+ the remaining mass-dependent terms contribute less than 0.001 cm^{-1} to the ionization energy [68].

3.3 Results

3.3.1 Non-relativistic Calculation

The non-relativistic ground state energies E_2 are approximately minimized by optimization of the nonlinear parameters $\{L_k\}$. In Table 3.1 these are compared with highly accurate reference

energies using Hylleraas wavefunctions [17]. It is observed that the convergence using m = 3000 functions is better than 88 nano-Hartree (nE_H) in each case (i.e., less than 0.02 cm^{-1}). When calculating the ionization energy, this error, ΔE_2, can ultimately be eliminated by using the established non-relativistic benchmark energies [17, 94]. In practice, these are sufficiently accurate, because the α^4 and α^5 level shifts can be calculated accurately enough (see below), so that the α^6 level shifts quickly become the dominant sources of error. The effect of E_{FM} on the ionization energy is assigned no uncertainty. Our mass-polarization corrections are essentially identical to those previously calculated [95, 96].

3.3.2 α^4 Corrections

The values of E_4 for subset 1 are given in Table 3.2 alongside the exact energies [33, 56, 68] whose errors are negligible for our purposes. In Table 3.3, E_4 for the $2^2S_{1/2}$ states are provided alongside ΔE_4, which gives an estimate of the errors in E_4. In arriving at error estimates for the subset 2 ions, we have used a quadratic polynomial interpolation. While not strictly justified, it should be accurate enough for our purposes. Although these errors are for the $2^2S_{1/2}$ states only, in computing each ionization energy we have used the "exact" two-electron E_4 values from [91], so that the ionization energy errors at order α^4 are just ΔE_4. From these results, it is clear that improvements to the three-electron wavefunctions would result in a more negative E_4 for the $2^2S_{1/2}$ states, so that the ionization energies would become larger.

Table 3.1. $2^2S_{1/2}$ non-relativistic energies, E_2 (a.u.), 3000 ECGs

Z	$-E_2$	$-E_2$ [17]	$\Delta E_2(nE_H)$
3	7.478 060 288	7.478 060 323	35.0
4	14.324 763 137	14.324 763 176	38.7
5	23.424 605 665	23.424 605 720	55.7
6	34.775 511 238	34.775 511 275	37.6
7	48.376 898 245	48.376 898 319	73.5
8	64.228 542 016	64.228 542 082	66.0
9	82.330 338 020	82.330 338 097	77.1
10	102.682 231 394	102.682 231 482	87.6

Table 3.2. Subset 1 $2^2S_{1/2}$ α^4 energies, E_4 (cm^{-1})

Z	$-E_4$	$-E_4$ [33, 56, 68]
3	140.8211	140.8311
4	510.5630	510.5959
8	10444.9420	10445.1024

3.3.3 α^5 Corrections

The α^5 energy E_5 is defined by (3.5-3.7). First, the one-electron Lamb shift (3.6) is discussed. Here, there are two quantities that depend on the quality of the underlying wavefunction. The first is the one-electron Dirac delta integral, and the second is the Bethe logarithm, $\ln(k_0)$. The error associated with (3.6) then reflects the errors associated with (3.2) and $\ln(k_0)$. Table 3.4 assembles our E_{L1} values using (3.2) and (3.11) for subset 1. For the reference values of E_{L1}, we have used the most recent $\ln(k_0)$ data from [33, 46, 56] and the corresponding $\langle\Psi|\delta(r_{ij})|\Psi\rangle$ integrals from [33, 56, 68]. The errors in (3.2) are non-trivial for the relativistic corrections, but here act as a multiplicative constant only, and the errors associated with $\ln(k_0)$ dominate. The deviation of $\ln(k_0)$ using (3.11) from those computed directly is denoted $\Delta\ln(k_0)$ in Table 3.4. In order to estimate the E_{L1} errors for subset 2, a quadratic polynomial interpolation has been used as was the case for ΔE_4. Table 3.5 gives the $\ln(k_0)$ used here, E_{L1}, and the estimated E_{L1} errors, ΔE_{L1}. It is observed that although $\Delta\ln(k_0)$ becomes smaller with increasing Z, the errors in E_{L1} nonetheless grow quickly owing to the growth of the delta function integral. We can remark that the interpolated ΔE_{L1} are much smaller than the NIST ASD ionization energy uncertainties [61].

Table 3.3. $2^2S_{1/2}$ α^4 energies, E_4, and associated errors, ΔE_4 (cm^{-1}), Z=5-7, 9, 10 ΔE_4 interpolated (see text)

Z	$-E_4$	ΔE_4
3	140.82	0.01
4	510.56	0.03
5	1368.17	0.06
6	3030.71	0.09
7	5896.60	0.12
8	10444.94	0.16
9	17236.33	0.20
10	26911.99	0.25

Table 3.4. Subset 1 $2^2S_{1/2}$ E_{L1} energies (cm^{-1})

Z	$\Delta\ln(k_0)$	E_{L1}	E_{L1} [33, 46, 56, 68]
3	0.00134	25.014	25.008
4	0.00106	75.416	75.400
8	0.00027	946.667	946.594

The two-electron Lamb shift (3.7) is in terms of two quantities whose accuracies depend on the quality of the underlying wavefunctions. These are the two-particle Dirac delta integral (3.3) and the Araki-Sucher integral. The latter dominates the E_{L2} error, which is unsurprising considering the nature of the $1/r^3$ integral combined with Gaussian wavefunctions that are not entirely converged. It should be emphasized that the Araki-Sucher integrals reported here are not regularized, as discussed in Ref. [77]. Table 3.6 gives the errors for the Araki-Sucher energies for subset 1, denoted ΔE^P_{L2}. The errors for the Dirac delta term are small and of opposite sign compared to ΔE^P_{L2}. The total E_{L2} are also provided and compared to references [33, 56, 68]. Here, E_{L2} is again for the $2^2S_{1/2}$ state only, since the exact 1^1S_0 E_{L2} [91] values are used to evaluate the correction to the ionization energy.

In Table 3.7 are assembled the values of E_{L2} with the associated errors determined again using a quadratic interpolation for subset 2, denoted ΔE_{L2}, while the Araki-Sucher integrals are reported as $P/(4\pi)$. Having evaluated the QED energies with relatively high accuracy compared to previous theory [64, 65], it is interesting to examine in particular the B^{2+} QED energy. It was suggested by Kramida et al. [62] that the QED corrections of [65] should be used instead of those from [64], but that without a measure of accuracy of these energies, an experimental ionization energy is necessary. Our B^{2+} leading-order QED correction is estimated to be in error by $\Delta E_{L1} + \Delta E_{L2}$, which amount to 0.028 and 0.005 cm^{-1}, respectively, from our interpolations. Comparing then to the results of McKenzie and Drake [65] and of Chung [64], the E_5 contribution to the B^{2+} ionization energy calculated here is -4.78 cm^{-1}, while theirs are -4.96 and -2.95 cm^{-1}, respectively. The resulting ionization energy using our updated E_4 and E_5 energies (including E_{FM}) is 305 928.93 cm^{-1}, to be compared with the 305 930.8(6) cm^{-1} experimental limit.

Table 3.5. $2^2S_{1/2}$ E_{L1} energies and associated errors, ΔE_{L1} (cm^{-1}), Z=5-7,9,10 ΔE_{L1} interpolated (see text)

Z	$\ln(k_0)$	E_{L1}	ΔE_{L1}
3	5.1768	25.014	0.006
4	5.7508	75.416	0.016
5	6.1962	173.802	0.028
6	6.5603	339.023	0.041
7	6.8682	590.331	0.056
8	7.1350	946.667	0.073
9	7.3703	1426.067	0.091
10	7.5808	2045.153	0.110

Table 3.6. Subset 1 $2^2S_{1/2}$ E_{L2} energies (cm^{-1}). ΔE_{L2}^P, error associated with Araki-Sucher energies

Z	ΔE_{L2}^P	E_{L2}	E_{L2} [33, 56, 68]
3	0.0008	-0.566	-0.567
4	0.0025	-1.381	-1.383
8	0.0329	-8.918	-8.946

3.3.4 α^6 Corrections

The complete three-electron α^6 energies E_6 have not been calculated other than for the Li and Be^+ fine structure intervals [97]. However, E_6 has been evaluated for the helium-like ions and for H_2 [55, 91, 93, 98]. In discussing the complete E_6 correction defined in (3.13), we refer to the logarithmic contribution as E_6^{log}, while $E_6^{log} + E_6^{R1} + E_6^{R2} + E_6^{H'} \equiv E_6^{nrel}$. Here, E_6^{nrel} is meant to emphasize that this part of E_6 is not associated with the corrections derived from the Foldy-Wouthuysen Hamiltonian (see Ref. [54], Appendix A), or from the second-order Breit-Pauli contributions (see Ref. [54], Appendix B). We will refer to the remaining part of E_6 as $E_6^{rel} \equiv E_6^{sec} + E_6^{Q}$. For the $Z \leq 10$ heliumlike ground states, E_6^{nrel} dominates E_6^{rel} for both the 1^1S_0 term energy and its ionization interval with the hydrogenlike ground states [91]. This has been determined by extracting E_6^{rel} from the total E_6 energies of Ref. [91], by calculating the E_6^{nrel} contribution. In evaluating E_6^{nrel} for the 1^1S_0 states, we have generated accurate ECG wavefunctions (ΔE_2 ¡ 1 nE_H) and calculated the delta function integrals defined within the Drachmanization scheme discussed above. It can also be verified that E_6^{nrel} dominates E_6^{rel} for the hydrogenlike ground state energies. Based on these results, the complete E_6 contributions to the $2^2S_{1/2}$ ionization energies are to a first approximation provided by E_6^{nrel}. Both E_6^{R1} and E_6^{nrel} are provided in Table 3.8 as *ionization energy* corrections for the $2^2S_{1/2} \rightarrow 1^1S_0$ interval. Here, it is the case that E_6^{R1} dominates E_6^{nrel}, which decreases each ionization energy. The numerical uncertainty of E_6^{nrel} is insignificant compared to the anticipated magnitudes of $\left|E_6^{Q} + E_6^{sec}\right|$ (see below).

Table 3.7. $2^2S_{1/2}$ Araki-Sucher integrals, P (a.u.), E_{L2} energies and associated errors, ΔE_{L2} (cm^{-1}), Z=5-7,9,10 ΔE_{L2} interpolated (see text)

Z	$(4\pi)^{-1}P$	E_{L2}	ΔE_{L2}
3	0.0197	-0.566	0.0006
4	-0.6042	-1.381	0.0018
5	-2.3737	-2.623	0.0052
6	-5.9071	-4.314	0.0106
7	-11.9755	-6.416	0.0182
8	-21.2861	-8.918	0.0278
9	-34.6681	-11.756	0.0396
10	-52.9315	-14.881	0.0534

Table 3.8. E_6 contributions to the ionization energies. E_6^{R1}, the one-loop radiative energy. $E_6^{nrel} \equiv E_6^{R1+R2+H'-log}$ (cm^{-1})

Z	E_6^{R1}	E_6^{nrel}
3	-0.0076	-0.0077
4	-0.0687	-0.0695
5	-0.2933	-0.2956
6	-0.8848	-0.8900
7	-2.1685	-2.1789
8	-4.6204	-4.6387
9	-8.8957	-8.9256
10	-15.8572	-15.9034

3.3.5 Theoretical $2^2S_{1/2}$ Ionization Energies

The total ionization energies are collected alongside those from the NIST ASD in Table 3.9. In the first column, $\tilde{E}_5 \equiv E_2 + E_{FM} + E_4 + E_5$, while for the second column, $\tilde{E}_6^{nrel} \equiv \tilde{E}_5 + E_6^{nrel}$. The corrections E_i that determine $\tilde{E}_5$ and $\tilde{E}_6^{nrel}$ are to be understood as differences between the $2^2S_{1/2}$ and 1^1S_0 level shifts. The atomic masses of the isotopes used to calculate E_{FM} are taken from Ref. [99] and are provided in Table 3.10. The corresponding nuclear masses, $M_N(A,Z)$, are obtained from the formula [99]:

$$M_N(A,Z) = M_A(A,Z) - Z \times m_E + B_E(Z) \tag{3.16}$$

In this expression, $M_A(A,Z)$ is the isotope-dependent atomic mass, m_E is the electron mass, and $B_E(Z)$ is the total electron binding energy. Following [100], we have calculated $B_E(Z)$ using:

$$B_E(Z) = 14.4381Z^{2.39} + 1.55468 \times 10^{-6}Z^{5.35}eV \tag{3.17}$$

Each of the errors in our calculations has the effect of reducing the ionization energies by the amounts of Tables 3.3, 3.5, and 3.7. These errors range from 0.017 to 0.409 cm^{-1}, but only reflect the (estimated) internal numerical accuracy of our model, and do not include the anticipated contribution of E_6^{rel}.

Table 3.9. Total ionization energies. $\tilde{E}_5 \equiv E_2 + E_{FM} + E_4 + E_5$. $\tilde{E}_6^{nrel} \equiv \tilde{E}_5 + E_6^{nrel}$ (cm^{-1}). Literature sources compiled by NIST ASD are provided below in order of nuclear charge

Z	$\tilde{E}_5$	$\tilde{E}_6^{nrel}$	NIST ASD [60–62, 70, 71, 73–76]	Uncertainty [60–62, 70, 71, 73–76]
3	43 487.148	43 487.141	43 487.15940	0.00018
4	146 882.93	146 882.86	146 882.86	0.35
5	305 928.93	305 928.64	305 930.8	0.6
6	520 176.20	520 175.31	520 175.3	1.5
7	789 534.22	789 532.04	789 537.0	3
8	1 114 001.8	1 113 997.1	1 114 004	17
9	1 493 622.1	1 493 613.1	1 493 632	5
10	1 928 451.3	1 928 435.4	1 928 447	15

Table 3.10. Isotopes and their atomic masses

Z	Isotope	Mass (u) [99]
3	^{7}Li	7.016 003 436
4	^{9}Be	9.012 183 066
5	^{11}B	11.009 305 166
6	^{12}C	12.000 000 000
7	^{14}N	14.003 074 004
8	^{16}O	15.994 914 619
9	^{19}F	18.998 403 162
10	^{20}Ne	19.992 440 176

For the purposes of recommending new ionization energies based on the available data, an estimate of E_6^{rel} is necessary. Let us first assume that E_6^{rel} would increase each ionization energy, as is the case for the internal errors. Second, we assume that for the ionization energies, $\left|E_6^{rel}\right| \leq \left|E_6^{nrel}\right|$. Each of these assumptions is supported by the heliumlike data [91] as discussed above. In effect, this defines an interval containing the assumed ionization energy, which is between $\tilde{E}_5$ and $\tilde{E}_6^{nrel}$.

It is unfortunately not obvious how to further refine this interval using the available heliumlike data, since we are considering $2^2S_{1/2}$ states, which may result in a different balance between E_6^{nrel} and E_6^{rel} compared to that for the 1^1S_0 heliumlike ground states. As a result, we use as the uncertainty of E_6^{rel} the magnitude of E_6^{nrel}. Since this addition to E_6^{nrel} is assumed to be of positive sign, we have added half the magnitude of E_6^{nrel} to $\tilde{E}_5$ and introduced a two-sided *uncertainty*, which is also half E_6^{nrel}. More precisely, by uncertainty, following Drake [101] we really mean estimated bounds for the reported energies. It is also sensible to add the quadratically interpolated errors to this uncertainty. To do this, and because the total internal errors, δE_{int}, demonstrate that $\tilde{E}_6^{nrel}$ is underestimated, we have added δE_{int} to the modified ECG energies that contain the E_6^{rel} estimates, adding an uncertainty that is taken to be δE_{int}. The total uncertainty, δ_{tot}, is defined in terms of δE_{int} and δE_6^{rel} (the uncertainty associated with the assumption that $|E_6^{nrel}| > E_6^{rel} > 0$):

$$\delta_{tot} = \delta E_{int} + \delta E_6^{rel} \equiv \delta E_{int} + \frac{1}{2}|E_6^{nrel}| \tag{3.18}$$

In Table 3.11, ECG^{mod} denotes this "modified" ionization energy and its associated error bounds. It is worth reemphasizing that the recommended ionization energies are not as a whole determined from the non-relativistic perturbation theory results of Table 3.9. Instead, we have used these results with the knowledge that the ionization energies are internally underestimated, and the assumptions regarding E_6^{rel} described above.

For $Z > 5$, there are RCI ionization energies available for comparison [67]. These are collected in Table 3.12, alongside data columns labeled $\delta E^{DCB}, \delta E^{FM}$, and δE^{QED}. We have de-

fined the difference between $E_2 + E_4$ and the Dirac-Coulomb-Breit (ionization) energies as δE^{DCB}, while the difference between E_{FM} and those of Ref. [67] are denoted δE^{FM}. Finally, δE^{QED} gives the difference between E_5 and the QED energies from the model operator approach. Compared to Ref. [67], our QED correction should be considered more accurate. For the ionization energies from Ref. [67], if the QED energies calculated using the model operator method [72] are replaced by the sum of our E_5 ionization energy correction and E_6^{nrel}, then it can be observed that the new ionization energies agree very well with our "recommended" ones. These modified RCI energies, RCI^{mod}, are also provided in Table 3.11.

Following these compilations, let us consider $\tilde{E}_5$, $\tilde{E}_6^{nrel}$, and ECG^{mod}, and how these compare with the NIST ASD results, denoted IE_{NIST}. It is difficult to compare ECG^{mod} with IE_{NIST} because of the addition of E_6^{rel} as discussed above. However, the rather conservative error estimates that result from this addition might approximately be considered as 1σ uncertainties. If we make this assumption, then the difference between ECG^{mod} and IE_{NIST} can be calculated and assigned an uncertainty, which is determined by combining in quadrature the two uncertainties. This may also be done for $\tilde{E}_5$ and $\tilde{E}_6^{nrel}$. Figure 3.1 provides a visualization of this analysis for $5 \leq Z \leq 10$. For $Z = 3$ and $Z = 4$, our results provide no information building on previous works [33, 46, 68], so we have not included our results for Li and Be^+ in Figure 3.1. For O^{5+}, our perturbation theory energies do not improve upon previous results [56], however, these have not been used to assess the $2^2S_{1/2}$ ionization energy, including the potential magnitude of the E_6 correction.

In Figure 3.1, we have considered the difference $IE_{calc} - IE_{NIST}$, where IE_{calc} is either $\tilde{E}_5$, $\tilde{E}_6^{nrel}$, or ECG^{mod}. The difference between IE_{calc} and IE_{NIST} and the corresponding error bars have been plotted and are scaled by $(1/Z^7) \times 10^6$ cm^{-1}, so that the relative discrepancies are apparent. It is immediately clear from Figure 3.1 that the statistical differences between the calculated and experimental results are not very sensitive to the treatment of the α^6 corrections. These treatments are, as discussed, neglecting E_6 altogether, calculating E_6^{nrel} and neglecting E_6^{rel}, or calculating E_6^{nrel} and estimating E_6^{rel}. It is also clear that the primary outlier in Figure 3.1 is for $Z = 5$. The difference $(IE_{calc} - IE_{NIST})$ is for each level of theory approximately three times

the magnitude of the combined uncertainties as represented by the error bars. Another notable discrepancy evidenced in Figure 3.1 is for $Z = 9$. Here the results depend more strongly on the E_6 treatment compared to the results for $Z = 5$. For instance, neglecting E_6 altogether results in a 1.91 ratio of the difference $IE_{calc} - IE_{NIST}$ to the combined uncertainty, whereas by including E_6^{nrel} the ratio grows to 3.70. For ECG^{mod}, the ratio is 2.03. However, as alluded to previously, Edlén's [74] semiempirical result (1 493 622 cm^{-1}) is much smaller than the experimental [73] value, and happens to be in good agreement with the present calculations. Unless future E_6 corrections indicate that $|E_6^{rel}| > |E_6^{nrel}|$, it does not appear possible to reconcile the NIST ASD results with non-relativistic perturbation theory calculations for $Z = 5$ and $Z = 9$. Figure 3.1 also indicates that at the level of accuracy of our calculations, IE_{NIST} for $Z = 6, 8$, and 10 does not conflict with our results. For $Z = 7$, a minor disagreement is evident upon considering E_6, but this discrepancy is not statistically significant. To conclude this discussion, we should reemphasize that Figure 3.1 should be interpreted as a qualitative visualization of our results, but it is not possible to emphatically state which results are incorrect. Instead, Figure 3.1 should promote the view that there are apparently discrepancies between the NIST ASD results and non-relativistic perturbation theory, and as a result both experimental and theoretical work should be refined to make any definitive conclusions.

While these results encourage the point of view that non-relativistic perturbation theory calculations are valuable in this intermediate range of nuclear field strength, direct E_6^{rel} calculations should be the next step in this analysis. On the other hand, the complexity of this calculation presents a serious obstacle to the utility of the $(Z\alpha)$ expansion method. Recently, a procedure for evaluating variationally the no-pair Dirac-Coulomb-Breit energy has been reported [102]. It might be that calculations of this type are more successful in assessing the NIST ASD results we have considered. Regardless, it would be interesting to see how these results compare to the present calculations. Alternatively, calculations that combine all-orders in $(Z\alpha)$ calculations with $1/Z$ expansions, as discussed in [63], might be more fruitful. Having examined the various numerical errors, we can remark that the E_4 contributions reported are not as converged as is possible with more advanced wavefunction optimization methods. However, any further optimization of the

wavefunctions becomes less useful with increasing Z. For example, for Ne^{7+}, E_6^{nrel} is nearly 16 cm^{-1} while the error in the leading-order relativistic correction is estimated to be less than 1 cm^{-1}. A more accurate computation of the Bethe logarithms and Araki-Sucher intergrals can be characterized similarly. For states with increasing Z it appears more important to establish the scaling and anticipated magnitudes of the higher-order perturbation theory corrections. To this end, while the correlated Gaussian wavefunctions used here are better than what has been used previously, it would be more useful in the future to have exponential, Hylleraas, or LECG [103] wavefunctions, which can be used to evaluate E_6 directly. The present calculations suggest there is much work remaining to be done on the lithiumlike ionization energies both experimentally and within the context of the $(Z\alpha)$ expansion approach.

Table 3.11. Recommended ionization energies (cm^{-1}). Literature sources compiled by NIST ASD are provided below in order of nuclear charge

Z	ECG^{mod}	RCI^{mod}	NIST [60–62, 70, 71, 73–76]
3	43 487.161(4)	-	43 487.15940(18)
4	146 882.95(3)	-	146 882.86(35)
5	305 928.88(24)	-	305 930.8(6)
6	520 175.90(59)	520 175.80	520 175.3(15)
7	789 533.3(13)	789 532.83	789 537(3)
8	1 113 999.7(23)	1 113 999.9	1 114 004(17)
9	1 493 617.9(48)	1 493 618.0	1 493 632(5)
10	1 928 443.8(84)	1 928 444.4	1 928 447(15)

Table 3.12. RCI ionization energies (cm^{-1})

Z	RCI [67]	δE^{DCB}	δE^{FM}	δE^{QED}
6	520 175.73	-0.10	0.71	0.96
7	789 533.65	-1.96	0.07	1.36
8	1 114 001.65	-2.14	0.42	2.92
9	1 493 620.34	-4.82	-0.09	6.63
10	1 928 448.96	-8.95	-0.07	11.37

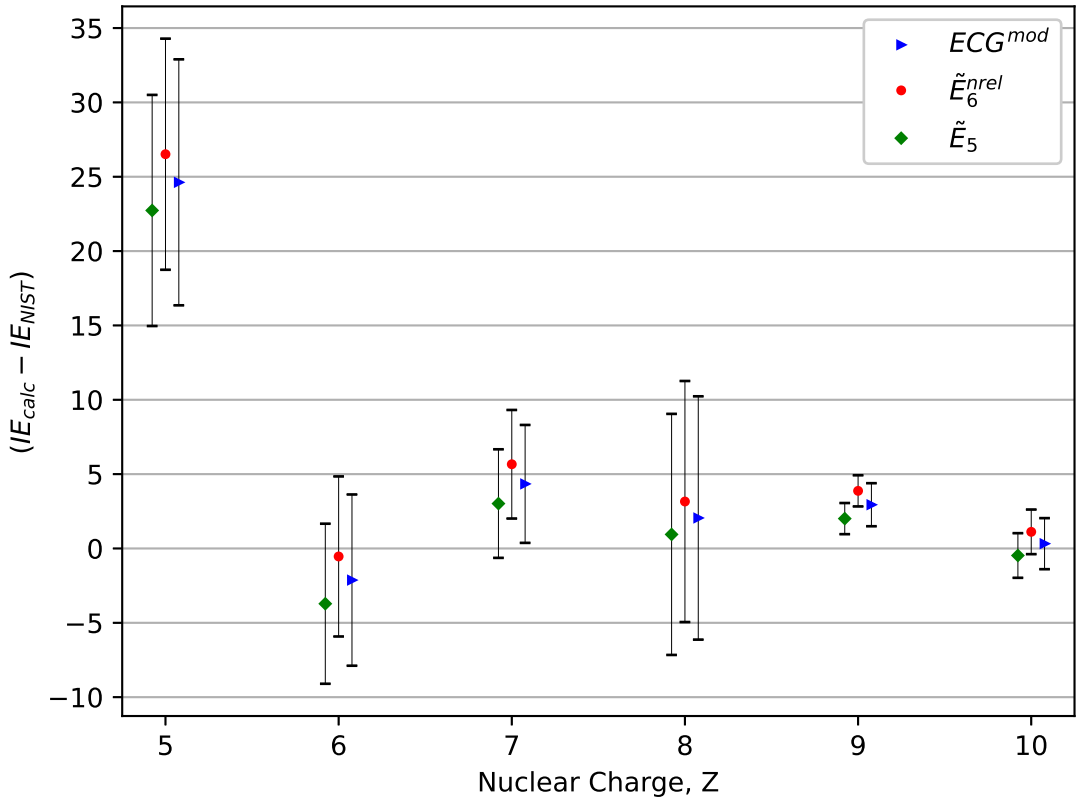

Figure 3.1. Calculated vs. NIST ASD ionization energies. IE_{calc}, either $\tilde{E}_5$, $\tilde{E}_6^{nrel}$, or ECG^{mod}. The difference $(IE_{calc} - IE_{NIST})$ and error bars have been scaled according to $Z^{-7} \times 10^6$ cm^{-1} for better visualization

CHAPTER 4

GROUND STATE FREQUENCY-DEPENDENT DIPOLE POLARIZABILITIES OF $3 \leq Z \leq 10$ THREE-ELECTRON IONS

This article was published in Atomic Data and Nuclear Data Tables, 144, William P. Earwood and Steven R. Davis, Ground-state frequency-dependent dipole polarizabilities of $3 \leq Z \leq 10$ three-electron ions, 101490, Copyright Elsevier (2022).

Abstract

Frequency-dependent dipole polarizabilities of 2^2S lithiumlike states for $3 \leq Z \leq 10$ are tabulated for frequencies up to the 3^2P absorption frequency using fully correlated Gaussian expansions. To account for the frequency-dependence between and near the poles at the 2^2P and 3^2P absorption frequencies, the Schrödinger-Coulomb Hamiltonian is diagonalized in a composite basis of $L = 1$ angular momentum Gaussians containing subsets of partially optimized n^2P ($n = 2 - 5$) wavefunctions and both frequency-independent and frequency-dependent first-order perturbed functions. The tabulated results are well-converged and should be considered as benchmark dipole polarizabilities in the non-relativistic limit. The calculated dipole polarizabilities are used to determine a fit to the Cauchy expansion. The 3^2P and 4^2P energies calculated using the composite basis set are new upper bounds to the exact non-relativistic energies, as are many of the 5^2P energies.

4.1 Introduction

The application of an external electric field of angular frequency ω has the effect of modifying the system energy of a bound state. If this field is weaker than the internal binding strength,

then the response of the bound state can be quantified according to its polarizabilities, the most important of which is usually the dipole polarizability, $\alpha(\omega)$. Other than its role in determining this energy response, the importance of $\alpha(\omega)$ can be argued from a variety of perspectives, including the determination of magic wavelengths [104], long-range interaction coefficients [105], refractive indices/dielectric constants [43], and Stark shifts [2], to name a few. The objective here is somewhat different, to simply catalog non-relativistic $\alpha(\omega)$ for the lowest nuclear charge Z lithiumlike ions in their ground states, for real frequencies and for the infinite nuclear mass limit. Because experimental work is limited for these ions, and because previous high-accuracy $\alpha(\omega)$ are only available for Li and Be^+ [2], it is of interest to extend these results beyond $Z > 4$ for a wide range of ω. In order to meet the goal of supplying high-accuracy $\alpha(\omega)$ in the non-relativistic limit, it is essential to include electron-electron correlations explicitly in the computational framework. Specifically used here are all-electron Gaussians, for the three-electron case depending explicitly on r_1, r_2, r_3, r_{12}, r_{13}, and r_{23}, where r_i and r_{ij} are interparticle coordinates.

Regarding the frequency-independent dipole polarizabilities, $\alpha(0)$, a compilation of $3 \leq Z \leq 10$ data is available [106]. The method used in Ref. [106] involved the variation-perturbation theory approach [1], where both zeroth- and first-order wavefunctions are determined using the full-core plus correlation (FCPC) ansatz. Evidenced by the improvement over the FCPC-calculated $\alpha(0)$ by those from Refs. [107] and [2], which have used expansions in Hylleraas functions, a recalculation of $\alpha(0)$ for $Z > 4$ is justifiable in its own right. In Ref. [2], high-accuracy $\alpha(\omega)$ have been tabulated for Li and Be^+. For Li, the calculated $\alpha(\omega)$ improved upon previous work which used the Hylleraas configuration interaction (Hy-CI) method [108]. For Be^+, the calculated $\alpha(\omega)$ improved upon those calculated using a time-dependent gauge invariant (TDGI) method [109]. A generalized configuration-interaction method known as the superposition of correlated configurations (SCC) has also been used for Be^+ [110]. There is for each frequency considered in Ref. [2] a much larger improvement for Be^+ over the TDGI and SCC results than what is observed for Li over the Hy-CI results. This is significant because the TDGI and SCC methods have afforded the most accurate $\alpha(\omega)$ to date for B^{2+} and C^{3+}. This observation provides an

impetus for reevaluation of $\alpha(\omega)$ for B^{2+} and C^{3+}. Meanwhile, for the $7 \leq Z \leq 10$ lithiumlike ground states, there is no $\alpha(\omega)$ data of either moderate or high-accuracy.

4.2 Theory

In this section, two approaches for calculating $\alpha(\omega)$ are discussed. The first [43] is the sum-over-states expression resulting from Rayleigh-Schrödinger perturbation theory:

$$\alpha(\omega) = \sum_m \frac{\langle \Psi_0 | H_d | \Psi_m \rangle \langle \Psi_m | H_d | \Psi_0 \rangle (E_m - E_0)}{(E_m - E_0)^2 - \omega^2} \tag{4.1}$$

In Eq. (4.1), for the state of interest (in our case 2^2S), Ψ_0 and E_0 denote the Z-dependent non-relativistic wavefunction and energy. Ψ_m and E_m meanwhile denote the mth intermediate state wavefunction and energy obtained from a diagonalization of the non-relativistic Hamiltonian in a basis set expansion of $L = 1$ angular momentum functions, while $H_d = \sum_{i=1}^{n_e} z_i$ is the dipole operator, where n_e is the number of electrons. From Eq. (4.1), the static limit $\alpha(0)$ reduces to an expression [43] in terms of oscillator strengths, f_{0m}:

$$\alpha(0) = \sum_m \frac{f_{0m}}{(E_m - E_0)^2} \tag{4.2}$$

An equivalent expression for $\alpha(\omega)$ in terms of the frequency-dependent first-order perturbed function, $\Psi_1^{\pm\omega}$, may also be used to calculate $\alpha(\omega)$ [38]:

$$\alpha(\omega) = -2\left[\langle \Psi_1^{+\omega} | H_d | \Psi_0 \rangle + \langle \Psi_1^{-\omega} | H_d | \Psi_0 \rangle \right] \tag{4.3}$$

In this alternative definition, $\Psi_1^{\pm\omega}$ is defined by the perturbation-theory equation:

$$(H_0 - E_0 \pm \omega)\Psi_1^{\pm\omega} = -H_d \Psi_0 \tag{4.4}$$

In Eq. (4.4), H_0 is the non-relativistic Hamiltonian operator, which assumes the infinite nuclear mass limit for each ion. The solution to Eq. (4.4) is determined by a variational minimization

of the corresponding Hylleraas functional, $J[\Psi_1^{\pm\omega}]$, provided the exact Ψ_0 is available:

$$J[\Psi_1^{\pm\omega}] = \langle \Psi_1^{\pm\omega} | H - E_0 \pm \omega | \Psi_1^{\pm\omega} \rangle + 2 \langle \Psi_1^{\pm\omega} | H_d | \Psi_0 \rangle \tag{4.5}$$

Eqs. (4.3)−(4.5) constitute what is often referred to as variation-perturbation theory.

The frequency-dependence of α for small frequencies can be used [38] to determine the Cauchy moments, $S(-2k-2)$, related to the various oscillator strength sums [2, 108, 111]:

$$\alpha(\omega) = \sum_{k=0}^{\infty} S(-2k-2)\omega^{2k} \tag{4.6}$$

This analytic representation for $\alpha(\omega)$ determines various properties, including the frequency dependent index of refraction [38, 43].

4.3 Calculations

The computational/numerical procedure used to calculate $\alpha(\omega)$ using Eqs. (4.1)−(4.5) is now described. The basic idea is to ultimately use Eq. (4.1) to determine $\alpha(\omega)$, but to construct $\{\Psi_m\}$ using a combined basis set approach that is built to supplement an approximate $\Psi_1^{\pm\omega}$, for $\omega = 0$, denoted Ψ_1^0 hereafter. The first step of this method employs Eq. (4.5) to find Ψ_1^0. As stated in Section 2, Ψ_0 should in principle be an exact eigenfunction of H_0, so that the variational property can be exploited. As such, the accuracy of the Ψ_0 for each ion is very important so that the variational property of $J[\Psi_1^0]$ is approximately preserved. The approach used to find an approximation for all state functions and first-order perturbed functions involves the minimization of the Rayleigh-Ritz or Hylleraas functionals using a set of all-electron Gaussian functions of the form:

$$\Psi_L = \sum_k \mathscr{P} c_k \phi_k = \sum_k \mathscr{P} c_k f_L e^{-\vec{r}' A_k \vec{r}} \tag{4.7}$$

In this expression, $\mathscr{P}$ is the three-particle antisymmetrizer, f_L is a function of the electronic coordinates determined by the angular momentum, c_k are the linear coefficients of the expansion,

and ϕ_k is the spatial Gaussian defined in the R.H.S. of Eq. (4.7). When calculating $\alpha(\omega)$ for a n^2S spherical state, as is the case here, both the intermediate spectrum Ψ_m and the first-order perturbed function $\Psi_1^{\pm\omega}$ should be expanded using $L = 1$ angular momentum functions. For S-symmetry and P-symmetry functions, respectively, f_L is then 1 and z_i, where z_i is the Cartesian z-coordinate of the ith electron. The coordinate vector $\vec{r} \equiv (\vec{r}_1, \vec{r}_2, \vec{r}_3)$, where r_i is the position vector of the ith electron, has $3n$ components, so that A_k has $3n \times 3n$ components, which can be expressed in terms of the Kronecker product of an $n \times n$ lower triangular matrix L_k with the 3×3 identity matrix [37]:

$$A_k = (L_k L_k^T) \bigotimes I_3 \tag{4.8}$$

Each spatial function ϕ_k, for a fixed f_L, then contains $n(n+1)/2$ nonlinear parameters, the non-zero values of L_k. Indeed, in all calculations involving $L = 1$ angular momentum functions, the z_i prefactors are chosen to maintain a uniform distribution. In this representation, Ψ_L is an expansion in correlated Gaussians which are functions of the matrices $\{A_k\}$ and the vectors $\{\vec{r}\}$ [37]. For further details concerning the matrix-based correlated Gaussian method, see [21, 40] and references therein.

The selection of the nonlinear parameters $\{L_k\}$ is the main obstacle when using this type of expansion. The procedure we have used is a simple implementation of the stochastic variational method [42] that refines each trial function by generating random parameters which successively lower the value of the objective function. The essence of our algorithm is to try to improve a single nonlinear parameter at a time using a stochastic selection from a predetermined range of real values which are neither too small nor large to cause problems when using double precision arithmetic. When this procedure becomes less capable of lowering the energy efficiently, a semi-local sampling around the value of each parameter is carried out. This procedure is repeated continuously until suitable convergence is achieved. Linear dependencies are controlled during this optimization by rejecting changes which lead to functions whose overlap integrals with other functions become near unity. Using this strategy as applied to the minimization of Eq. (4.5), Ψ_0 is constructed for

each ion, and is then held fixed during the subsequent stochastic determination of Ψ_1^0.

Once Ψ_1^0 is determined which results in high-accuracy $\alpha(0)$ values, the next step is to build in the frequency dependence to $\{\Psi_m\}$ so that $\alpha(\omega)$ is of high-accuracy for $\omega > 0$. The idea we have used for this purpose is to find approximations to the n^2P $(n = 2-5)$ states for each ion, and to perform additional $\alpha(\omega)$ optimizations using Eq. (4.5) for $\pm\omega$, where ω is just below $\Delta E_{2s\rightarrow 2p}$, and where ω is just below 1/2 $\Delta E_{2s\rightarrow 2p}$, where $\Delta E_{a\rightarrow b}$ denotes the frequency $E(a) \rightarrow E(b)$ for states a and b. Hereafter, the two frequencies near 1/2 $\Delta E_{2s\rightarrow 2p}$ and near $\Delta E_{2s\rightarrow 2p}$ are denoted ω_1 and ω_2. These separate optimizations constitute a merged basis set approach employed to calculate $\alpha(\omega)$, borrowing from a previous calculation of $\alpha(\omega)$ for He, Li, and Be atoms [38]. In the approach used in Ref. [38], the n^2P $(n = 2-4)$ optimized functions are added to Ψ_1^0, and are used in Eq. (4.3). Our approach is similar, but instead forms a composite basis that is then used in Eq. (4.1).

Following the construction of this set of expansion functions, a diagonalization of H_0 is used to determine $\{\Psi_m\}$ for each ion. The number of 2^2S functions used to build Ψ_0 for each ion is 3000, while the number of $\{\Psi_m\}$ functions for each ion is 4450. The breakdown of $\{\Psi_m\}$ into separate basis sets is as follows: 1500 from Ψ_1^0, 500 from each of the n^2P $(n = 2-4)$ states, 250 from the 5^2P state, and 600 from each of the $\alpha(\omega_1)$ and $\alpha(\omega_2)$ optimizations. Specifically, 300 Gaussians are used to determine $\Psi_1^{+\omega_1}$, $\Psi_1^{-\omega_1}$, $\Psi_1^{+\omega_2}$, $\Psi_1^{-\omega_2}$. Different subsets of basis functions are denoted "Basis 1", ..., "Basis 7". Basis 1 is the 1500 Gaussian function set optimized to minimize $J[\Psi_1^0]$. Bases $2-5$ consecutively add the 2^2P, 3^2P, 4^2P, and 5^2P optimized function sets and are, respectively, comprised of 2000, 2500, 3000, and 3250 Gaussian functions total. Basis 6 contains Basis 5, with the addition of the $\Psi_1^{\pm\omega_1}$ bases (3850 Gaussians), and Basis 7 contains Basis 6 with the addition of the $\Psi_1^{\pm\omega_2}$ bases (4450 Gaussians).

The calculated $\alpha(\omega)$ are then fit to Eq. (4.6). To determine the optimal fit parameters for each ion, three domains of equally spaced frequencies beginning at $\omega = 0$ and extending to 50%, 60%, and 70% of $\Delta E_{2s\rightarrow 2p}$ in increments of $\Delta E_{2s\rightarrow 2p}/500$ are used. The simultaneous convergence of $S(-2k-2)$ with respect to both the change in frequency domain and polynomial order

determines the final fit parameters.

4.4 Results

4.4.1 Non-relativistic state energies

Table 4.1 reports the infinite nuclear mass, non-relativistic energies, $E(2^2S)$, resulting from the 3000 Gaussian expansions for each 2^2S state. Compared to a previous compilation [80] which determined $E(2^2S)$ for each lithiumlike ground state to ≈ 12 decimals, $E(2^2S)$ in Table 4.1 are in agreement to $19-65$ nanoHartree (nE_H). For the n^2P states, there are two sets of energies to report. The first are those that result from the subset optimizations using 500 Gaussian functions for each ion for the $n = 2-5$ states. The labels $E(n^2P)$ denote these energies in Table 4.1. For Li, high-accuracy $E(n^2P)$ for $n \leq 12$ are available [18], and the $E(n^2P)$ in Table 4.1 are in agreement to 3.4, 16.7, 33.1, and 164.2 μE_H, respectively, for the $n = 2-5$ states. For the other ions, there are high-accuracy energies available for the 2^2P states also from Ref. [80]; for $Z > 3$, the $E(2^2P)$ errors with respect to these values are between $6-22$ μE_H. For the 3^2P, 4^2P, and 5^2P states for $Z > 3$, the FCPC method provides upper bounds for each of these state energies for each ion [112]. Compared to these upper bounds, $E(n^2P)$ are lower for the 3^2P and 4^2P states, while for the 5^2P states $E(5^2P)$ is slightly higher for each ion.

Also reported in Table 4.1 are the first four roots for each ion resulting from the diagonalization of H_0 in the 4450 function composite basis, which are much lower than the 500 function state energies. These energies are denoted "Root 1", ..., "Root 4". Comparisons with Refs. [18, 80, 112] are as follows. For $E(n^2P)$ for Li, the errors with respect to Ref. [18] become 0.1, 3.1, 19.7, and 117.0 μE_H, respectively, for the $n = 2-5$ states. For the 2^2P states for $Z > 3$ with respect to Ref. [80], the range of errors becomes $0.2-0.6$ μE_H. Also, for Be^+ and B^{2+}, Roots $2-4$ are lower than the upper bounds of previous work [112–114]. For $Z > 5$, this appears to be true as well, except for Root 4 for $Z = 7, 8, 10$, where there exist lower upper bounds [112].

4.4.2 Convergence of $\alpha(\omega)$ within the composite basis

Tables 4.2 and 4.3 illustrate the convergence of $\alpha(\omega)$ with respect to enlargement of the composite basis for Li and Be^+, for frequencies corresponding to those reported in Ref. [2] up to $\Delta E_{2s\to 3p}$. In the rightmost column of Tables 4.2 and 4.3, the heading "|% Diff.|" refers to the % difference between our results from Basis 7 and those from Ref. [2], denoted in Tables 4.2 and 4.3 as "Hyll.[2]". Examining first the results for Li, the differences are less than 0.001% for frequencies below $\omega = 0.057$, which is approximately 85 % of $\Delta E_{2s\to 2p}$. The largest differences are on either side of $\Delta E_{2s\to 2p}$, namely 0.004 % and 0.007 % before and after $\Delta E_{2s\to 2p}$. For the remaining frequencies between $\Delta E_{2s\to 2p}$ and $\Delta E_{2s\to 3p}$, the differences are no greater than 0.0023%. A similar analysis applied to Table 4.3 for Be^+ sees that between $\omega = 0$ and $\Delta E_{2s\to 2p}$, the differences are no greater than 0.0007 %, while five of these eight frequencies are identical to the number of reported significant figures. Between $\Delta E_{2s\to 2p}$ and $\Delta E_{2s\to 3p}$ the largest difference is for $\omega = 0.4$, which is approximately 93 % of $\Delta E_{2s\to 3p}$. The absolute difference in this case is, however, only 0.0001 a.u., which is within the uncertainty of $\alpha(\omega = 0.40)$ from Ref. [2]. Comparing finally Table 4.2 and Table 4.3, both the absolute and % differences for Be^+ are proportionally smaller. An additional conclusion from this assessment of Tables 4.2 and 4.3 is that for frequencies considered herein the errors are essentially negligible except near the poles, where the errors may be larger. The convergence with respect to the addition of basis subsets indicates that these additions are essential for high accuracy, especially near the poles.

4.4.3 Comparison with previous B^{2+} and C^{3+} calculations

In Table 4.4 we have evaluated $\alpha(\omega)$ for the previously reported frequencies [109, 110]. For B^{2+} and C^{3+}, respectively, ω extends up to 86 % and 68 % of $\Delta E_{2s\to 2p}$. The agreement between our $\alpha(\omega)$ and those from Refs. [109, 110] is clearly worse compared to the agreement with Hylleraas calculations for Li and Be^+ as demonstrated in Tables 4.2 and 4.3. For the largest frequencies in Table 4.4, $\alpha(\omega)$ improves upon the SCC and TDGI results by approximately 3 % for B^{2+}, and approximately 1 % for C^{3+}.

4.4.4 $\alpha(\omega)$, $3 \leq Z \leq 10$

Tables 4.5 and 4.6 report $\alpha(\omega)$ for each of the lithiumlike ions for frequencies between zero and $\Delta E_{2s\rightarrow 3p}$. In an attempt to recommend uncertainties for these values, a first observation is that for Table 4.3, the Basis 7 $\alpha(\omega)$ are in agreement to four decimal places with those from Ref. [2] below $\omega = 0.08$, which is 56 % of $\Delta E_{2s\rightarrow 2p}$. As Z increases, the absolute accuracy of our calculations should increase since the polarizabilities become smaller, as evidenced by the comparison between Tables 4.2 and 4.3, but also because the Ψ_1^0 optimization stabilizes much more quickly as Z increases. This would suggest that for $Z > 4$, the $\alpha(\omega)$ for ω below $\approx 50\%$ of $\Delta E_{2s\rightarrow 2p}$ are accurate to the number of decimals reported. For $\alpha(\omega)$ above this threshold but below $\approx 90\%$ of $\Delta E_{2s\rightarrow 2p}$, the errors are likely no greater than 0.001 a.u. for $Z > 4$. For $\omega > \Delta E_{2s\rightarrow 2p}$, but not too close to the pole, the errors should likewise be no greater than 0.001 a.u. Near the $\Delta E_{2s\rightarrow 3p}$ poles, we have not attempted to estimate the uncertainty of $\alpha(\omega)$.

4.4.5 Cauchy moments

Table 4.7 reports the Cauchy moments, $S(-2k-2)$, for $k = \{1,2,3,4,5\}$ for each ion. The frequency domains described in Section 3 produce largely invariant fit parameters at large polynomial order, whereas the order of the polynomial fit changes the results appreciably. For the largest two polynomial fits employed, the values in Table 4.7 are significant within the accuracy of our calculated $\alpha(\omega)$. We are not aware of any reported $S(-2k-2)$ in the literature, except for Li, although a similar fit has been used for both Li and Be^+ in Ref. [2]. In Ref. [108], the S(-4) value of 35170 is very close to the value from Table 4.7. In Ref. [111], the oscillator strength sums corresponding to $S(-4)$, $S(-6)$, $S(-8)$, and $S(-10)$, 35040, 7.590E+06, 1.646E+09, and 3.569E+11, respectively, agree well with Table 4.7.

4.4.6 Additional considerations

The calculated $\alpha(\omega)$ all assume an infinite nuclear mass and do not account for physics beyond the Schrödinger equation. One way to incorporate these corrections is to use the non-

relativistic quantum electrodynamics (NRQED) formalism for a bound state in an external electric field [115]. The calculation of the finite mass corrections can be included by using a finite nuclear mass non-relativistic Hamiltonian, while the relativistic/QED corrections require next-order perturbed functions or third-order perturbation theory, depending on the choice of methodology. One thing to mention is that the finite mass and relativistic corrections are usually of opposite magnitudes, with the relativistic corrections becoming progressively more dominating with Z. From the experimental perspective, infinite nuclear mass $\alpha(\omega)$ in the non-relativistic limit should be closer to the true values compared to those which include the finite nuclear mass contributions without relativistic corrections [107]. The calculation of these relativistic corrections is more challenging and at present is being pursued by the authors. Once these contributions are determined, these can be combined with the finite mass corrections and an estimate of QED corrections to determine ultra high-accuracy $\alpha(\omega)$ which incorporate all the important physics affecting experiments.

Table 4.1. Non-relativistic energies, $E(n^2L)$, from subset optimizations and corresponding roots of H_0 from diagonalization in composite basis.

Z	$E(2^2S)$	$E(2^2P)$	$E(3^2P)$	$E(4^2P)$	$E(5^2P)$
3	-7.47806030	-7.4101531	-7.337135	-7.311856	-7.300124
4	-14.32476315	-14.1793267	-13.885133	-13.783663	-13.736991
5	-23.42460568	-23.2044340	-22.545692	-22.318422	-22.213911
6	-34.77551124	-34.4820919	-33.317926	-32.915831	-32.730898
7	-48.37689827	-48.0110432	-46.201548	-45.575819	-45.287806
8	-64.22854204	-63.7907240	-61.196437	-60.298320	-59.884802
9	-82.33033804	-81.8208613	-78.302515	-77.083358	-76.521675
10	-102.68223142	-102.1013020	-97.519753	-95.930885	-95.198365

	Root 1	Root 2	Root 3	Root 4
3	-7.4101563	-7.3371489	-7.3118718	-7.3001737
4	-14.1793330	-13.8851472	-13.7836881	-13.7370563
5	-23.2044409	-22.5457050	-22.3184479	-22.2140084
6	-34.4821028	-33.3179452	-32.9158670	-32.7310198
7	-48.0110539	-46.2015700	-45.5758515	-45.2879634
8	-63.7907392	-61.1964554	-60.2983686	-59.8849768
9	-81.8208804	-78.3025408	-77.0834001	-76.5218939
10	-102.1013237	-97.5197947	-95.9309430	-95.1987498

Table 4.2. Comparison of calculated $\alpha(\omega)$ with literature for Li

ω	Basis 1	Basis 2	Basis 3	Basis 4	Basis 5	Basis 6	Basis 7	Hyll.[2]	|% Diff.|
0.0000	164.1116	164.1118	164.1119	164.1119	164.1120	164.1120	164.1122	164.112(1)	0.00012
0.0050	164.9957	164.9959	164.9960	164.9961	164.9961	164.9962	164.9963	164.996(1)	0.00018
0.0100	167.7068	167.7070	167.7071	167.7072	167.7072	167.7073	167.7074	167.707(1)	0.00024
0.0200	179.5159	179.5162	179.5163	179.5164	179.5164	179.5165	179.5166	179.517(1)	0.00022
0.0293	201.2395	201.2400	201.2401	201.2402	201.2403	201.2404	201.2406	201.242(2)	0.00070
0.0300	203.4368	203.4373	203.4374	203.4375	203.4376	203.4377	203.4379	203.438(1)	0.00005
0.0342	219.2196	219.2202	219.2204	219.2206	219.2206	219.2208	219.2210	219.221(1)	0.00000
0.0400	250.2622	250.2632	250.2635	250.2637	250.2638	250.2640	250.2644	250.265(1)	0.00024
0.0462	304.2731	304.2749	304.2754	304.2757	304.2759	304.2762	304.2768	304.278(1)	0.00039
0.0500	356.0696	356.0723	356.0730	356.0736	356.0738	356.0743	356.0752	356.077(1)	0.00051
0.0570	550.2366	550.2445	550.2471	550.2487	550.2492	550.2506	550.2530	550.259(1)	0.00109
0.0600	741.1189	741.1348	741.1400	741.1431	741.1442	741.1470	741.1514	741.165(2)	0.00183
0.0651	1984.2085	1984.3441	1984.3913	1984.4165	1984.4252	1984.4471	1984.4816	1984.577(1)	0.00481
$\Delta E_{2s\to 2p}$									
0.0700	-2582.3281	-2582.0544	-2581.9546	-2581.9061	-2581.8897	-2581.8485	-2581.7851	-2581.603(2)	0.00705
0.0759	-645.5339	-645.5127	-645.5045	-645.5010	-645.4999	-645.4969	-645.4925	-645.478(2)	0.00225
0.0800	-415.0929	-415.0828	-415.0787	-415.0771	-415.0766	-415.0752	-415.0733	-415.067(1)	0.00152
0.0900	-211.5287	-211.5251	-211.5235	-211.5229	-211.5228	-211.5223	-211.5217	-211.518(2)	0.00175
0.0911	-199.9492	-199.9458	-199.9444	-199.9439	-199.9437	-199.9433	-199.9428	-199.941(1)	0.00090
0.1000	-135.8786	-135.8767	-135.8758	-135.8756	-135.8755	-135.8752	-135.8749	-135.872(2)	0.00213
0.1139	-86.2682	-86.2676	-86.2673	-86.2671	-86.2671	-86.2669	-86.2668	-86.266(1)	0.00093
$\Delta E_{2s\to 3p}$									

Table 4.3. Comparison of calculated $\alpha(\omega)$ with literature for Be^{+}

ω	Basis 1	Basis 2	Basis 3	Basis 4	Basis 5	Basis 6	Basis 7	Hyll. [2]	|% Diff.|.
0.0000	24.4965	24.4966	24.4966	24.4966	24.4966	24.4966	24.4966	24.4966(1)	0.00000
0.0100	24.6087	24.6088	24.6088	24.6088	24.6088	24.6088	24.6088	24.6088(1)	0.00000
0.0200	24.9518	24.9518	24.9518	24.9518	24.9518	24.9519	24.9519	24.9518(1)	0.00040
0.0400	26.4290	26.4290	26.4291	26.4291	26.4291	26.4291	26.4291	26.4291(1)	0.00000
0.0600	29.3388	29.3389	29.3389	29.3390	29.3390	29.3390	29.3390	29.3390(1)	0.00000
0.0800	34.7355	34.7357	34.7357	34.7357	34.7357	34.7358	34.7358	34.7358(1)	0.00000
0.1000	45.6502	45.6506	45.6506	45.6507	45.6507	45.6507	45.6508	45.6509(1)	0.00022
0.1200	74.7833	74.7844	74.7846	74.7848	74.7848	74.7850	74.7852	74.7857(1)	0.00067
$\Delta E_{2s\rightarrow 2p}$									
0.1500	-367.9523	-367.9158	-367.9095	-367.9031	-367.9013	-367.8952	-367.8882	-367.8708(2)	0.00473
0.1800	-43.2054	-43.2046	-43.2045	-43.2044	-43.2043	-43.2042	-43.2041	-43.2038(1)	0.00069
0.2000	-25.3202	-25.3199	-25.3198	-25.3198	-25.3198	-25.3197	-25.3196	-25.3195(1)	0.00039
0.3000	-5.7972	-5.7970	-5.7968	-5.7968	-5.7967	-5.7967	-5.7967	-5.7967(1)	0.00000
0.4000	-0.3285	-0.3129	-0.2917	-0.2915	-0.2915	-0.2914	-0.2913	-0.2912(1)	0.03433
$\Delta E_{2s\rightarrow 3p}$									

Table 4.4. Calculated $\alpha(\omega)$ for B^{2+} and C^{3+} vs. SCC and TDGI

ω	$\alpha_{Z=5}$	SCC [110]	TDGI [109]	ω	$\alpha_{Z=6}$	SCC [110]	TDGI [109]
0.00	7.8591	7.81	7.86	0.00	3.4645	3.44	3.47
0.01	7.8746	7.82	7.87	0.02	3.4799	3.46	3.48
0.03	8.0011	7.95	8.00	0.04	3.5271	3.51	3.53
0.05	8.2674	8.21	8.26	0.06	3.6088	3.59	3.61
0.07	8.7034	8.64	8.69	0.08	3.7300	3.71	3.73
0.09	9.3653	9.29	9.34	0.10	3.8989	3.87	3.90
0.11	10.3561	10.31	10.31	0.12	4.1284	4.10	4.12
0.13	11.8761	11.80	11.80	0.14	4.4388	4.40	4.42
0.15	14.3587	14.20	14.21	0.16	4.8631	4.82	4.84
0.17	18.9341	18.60	18.61	0.18	5.4586	5.40	5.41
0.19	29.7368	28.80	28.76	0.20	6.3320	6.29	6.26
$\Delta E_{2s\to 2p}$				$\Delta E_{2s\to 2p}$			

Table 4.5. $Z = 3 - 6$ $\alpha(\omega)$

ω	$\alpha_{Z=3}$	ω	$\alpha_{Z=4}$	ω	$\alpha_{Z=5}$	ω	$\alpha_{Z=6}$
0.0000	164.1122	0.0000	24.4966	0.0000	7.8591	0.0000	3.4645
0.0014	164.1771	0.0029	24.5061	0.0044	7.8621	0.0059	3.4658
0.0027	164.3721	0.0058	24.5345	0.0088	7.8711	0.0117	3.4698
0.0041	164.6982	0.0087	24.5820	0.0132	7.8862	0.0176	3.4764
0.0054	165.1570	0.0116	24.6488	0.0176	7.9074	0.0235	3.4858
0.0068	165.7506	0.0145	24.7352	0.0220	7.9349	0.0293	3.4979
0.0081	166.4821	0.0175	24.8417	0.0264	7.9688	0.0352	3.5128
0.0095	167.3550	0.0204	24.9688	0.0308	8.0092	0.0411	3.5306
0.0109	168.3738	0.0233	25.1171	0.0352	8.0564	0.0469	3.5513
0.0122	169.5437	0.0262	25.2875	0.0396	8.1105	0.0528	3.5752
0.0136	170.8708	0.0291	25.4807	0.0440	8.1720	0.0587	3.6022
0.0149	172.3622	0.0320	25.6978	0.0484	8.2410	0.0646	3.6326
0.0163	174.0262	0.0349	25.9401	0.0528	8.3180	0.0704	3.6665
0.0177	175.8720	0.0378	26.2088	0.0572	8.4035	0.0763	3.7042
0.0190	177.9105	0.0407	26.5056	0.0616	8.4979	0.0822	3.7457
0.0204	180.1539	0.0436	26.8322	0.0661	8.6017	0.0880	3.7914
0.0217	182.6161	0.0465	27.1906	0.0705	8.7157	0.0939	3.8416
0.0231	185.3129	0.0494	27.5832	0.0749	8.8405	0.0998	3.8966
0.0244	188.2625	0.0524	28.0125	0.0793	8.9770	0.1056	3.9567
0.0258	191.4856	0.0553	28.4816	0.0837	9.1262	0.1115	4.0224
0.0272	195.0057	0.0582	28.9939	0.0881	9.2892	0.1174	4.0941
0.0285	198.8501	0.0611	29.5534	0.0925	9.4671	0.1232	4.1725
0.0299	203.0499	0.0640	30.1646	0.0969	9.6615	0.1291	4.2581

Table 4.5. continued

ω	$\alpha_{Z=3}$	ω	$\alpha_{Z=4}$	ω	$\alpha_{Z=5}$	ω	$\alpha_{Z=6}$
0.0312	207.6412	0.0669	30.8328	0.1013	9.8739	0.1350	4.3516
0.0326	212.6657	0.0698	31.5639	0.1057	10.1065	0.1408	4.4540
0.0340	218.1722	0.0727	32.3652	0.1101	10.3613	0.1467	4.5662
0.0353	224.2175	0.0756	33.2448	0.1145	10.6410	0.1526	4.6894
0.0367	230.8686	0.0785	34.2125	0.1189	10.9488	0.1584	4.8250
0.0380	238.2051	0.0814	35.2798	0.1233	11.2882	0.1643	4.9745
0.0394	246.3214	0.0844	36.4605	0.1277	11.6638	0.1702	5.1399
0.0407	255.3315	0.0873	37.7712	0.1321	12.0806	0.1761	5.3235
0.0421	265.3732	0.0902	39.2319	0.1365	12.5452	0.1819	5.5281
0.0435	276.6152	0.0931	40.8670	0.1409	13.0652	0.1878	5.7571
0.0448	289.2663	0.0960	42.7070	0.1453	13.6505	0.1937	6.0149
0.0462	303.5873	0.0989	44.7898	0.1497	14.3129	0.1995	6.3067
0.0475	319.9089	0.1018	47.1633	0.1541	15.0679	0.2054	6.6392
0.0489	338.6565	0.1047	49.8895	0.1585	15.9350	0.2113	7.0212
0.0503	360.3867	0.1076	53.0493	0.1629	16.9400	0.2171	7.4639
0.0516	385.8417	0.1105	56.7504	0.1673	18.1171	0.2230	7.9825
0.0530	416.0338	0.1134	61.1400	0.1717	19.5133	0.2289	8.5975
0.0543	452.3809	0.1164	66.4242	0.1761	21.1939	0.2347	9.3379
0.0557	496.9314	0.1193	72.9005	0.1805	23.2537	0.2406	10.2454
0.0570	552.7586	0.1222	81.0157	0.1849	25.8346	0.2465	11.3825
0.0584	624.6933	0.1251	91.4715	0.1893	29.1598	0.2523	12.8476
0.0598	720.7898	0.1280	105.4382	0.1937	33.6011	0.2582	14.8045
0.0611	855.5515	0.1309	125.0228	0.1982	39.8282	0.2641	17.5484

Table 4.5. continued

ω	$\alpha_{Z=3}$	ω	$\alpha_{Z=4}$	ω	$\alpha_{Z=5}$	ω	$\alpha_{Z=6}$
0.0625	1058.0018	0.1338	154.4410	0.2026	49.1804	0.2699	21.6697
0.0638	1395.9202	0.1367	203.5363	0.2070	64.7835	0.2758	28.5465
0.0652	2072.9492	0.1396	301.8721	0.2114	96.0191	0.2817	42.3156
0.0666	4110.9556	0.1425	597.6707	0.2158	189.8391	0.2876	83.6950
$\Delta E_{2s\to 2p}$		$\Delta E_{2s\to 2p}$		$\Delta E_{2s\to 2p}$		$\Delta E_{2s\to 2p}$	
0.0694	-3708.1812	0.1513	-283.7480	0.2333	-60.3850	0.3167	-19.8277
0.0708	-1837.1807	0.1572	-138.7015	0.2465	-29.1458	0.3400	-9.4632
0.0723	-1212.0532	0.1631	-90.3636	0.2597	-18.7596	0.3633	-6.0239
0.0738	-899.3564	0.1690	-66.2301	0.2729	-13.5861	0.3866	-4.3152
0.0752	-711.7824	0.1749	-51.7808	0.2860	-10.4966	0.4098	-3.2977
0.0767	-586.8088	0.1807	-42.1730	0.2992	-8.4479	0.4331	-2.6253
0.0781	-497.6194	0.1866	-35.3306	0.3124	-6.9932	0.4564	-2.1494
0.0796	-430.7991	0.1925	-30.2155	0.3256	-5.9090	0.4797	-1.7960
0.0811	-378.8925	0.1984	-26.2509	0.3387	-5.0712	0.5030	-1.5238
0.0825	-337.4252	0.2043	-23.0908	0.3519	-4.4054	0.5263	-1.3083
0.0840	-303.5491	0.2102	-20.5149	0.3651	-3.8643	0.5495	-1.1337
0.0854	-275.3655	0.2160	-18.3764	0.3783	-3.4164	0.5728	-0.9896
0.0869	-251.5595	0.2219	-16.5737	0.3914	-3.0398	0.5961	-0.8688
0.0884	-231.1919	0.2278	-15.0343	0.4046	-2.7189	0.6194	-0.7661
0.0898	-213.5739	0.2337	-13.7048	0.4178	-2.4424	0.6427	-0.6779
0.0913	-198.1889	0.2396	-12.5454	0.4310	-2.2017	0.6660	-0.6012

Table 4.5. continued

ω	$\alpha_{Z=3}$	ω	$\alpha_{Z=4}$	ω	$\alpha_{Z=5}$	ω	$\alpha_{Z=6}$
0.0927	-184.6419	0.2455	-11.5256	0.4441	-1.9902	0.6892	-0.5339
0.0942	-172.6254	0.2513	-10.6215	0.4573	-1.8029	0.7125	-0.4744
0.0957	-161.8969	0.2572	-9.8144	0.4705	-1.6357	0.7358	-0.4213
0.0971	-152.2623	0.2631	-9.0893	0.4837	-1.4854	0.7591	-0.3736
0.0986	-143.5645	0.2690	-8.4340	0.4968	-1.3494	0.7824	-0.3303
0.1000	-135.6748	0.2749	-7.8385	0.5100	-1.2256	0.8057	-0.2909
0.1015	-128.4871	0.2808	-7.2944	0.5232	-1.1122	0.8289	-0.2547
0.1030	-121.9127	0.2867	-6.7948	0.5364	-1.0075	0.8522	-0.2212
0.1044	-115.8773	0.2925	-6.3338	0.5495	-0.9105	0.8755	-0.1900
0.1059	-110.3177	0.2984	-5.9064	0.5627	-0.8199	0.8988	-0.1607
0.1073	-105.1804	0.3043	-5.5082	0.5759	-0.7348	0.9221	-0.1329
0.1088	-100.4191	0.3102	-5.1353	0.5891	-0.6543	0.9454	-0.1065
0.1103	-95.9941	0.3161	-4.7844	0.6022	-0.5776	0.9686	-0.0811
0.1117	-91.8708	0.3220	-4.4523	0.6154	-0.5039	0.9919	-0.0564
0.1132	-88.0188	0.3278	-4.1363	0.6286	-0.4327	1.0152	-0.0322
0.1146	-84.4117	0.3337	-3.8336	0.6418	-0.3630	1.0385	-0.0082
0.1161	-81.0258	0.3396	-3.5416	0.6549	-0.2944	1.0618	0.0158
0.1176	-77.8402	0.3455	-3.2578	0.6681	-0.2259	1.0851	0.0401
0.1190	-74.8359	0.3514	-2.9795	0.6813	-0.1568	1.1083	0.0651
0.1205	-71.9958	0.3573	-2.7037	0.6945	-0.0861	1.1316	0.0912
0.1219	-69.3040	0.3631	-2.4271	0.7076	-0.0127	1.1549	0.1189
0.1234	-66.7457	0.3690	-2.1457	0.7208	0.0649	1.1782	0.1487
0.1249	-64.3064	0.3749	-1.8547	0.7340	0.1486	1.2015	0.1815

Table 4.5. continued

ω	$\alpha_{Z=3}$	ω	$\alpha_{Z=4}$	ω	$\alpha_{Z=5}$	ω	$\alpha_{Z=6}$
0.1263	-61.9718	0.3808	-1.5476	0.7472	0.2407	1.2248	0.2185
0.1278	-59.7268	0.3867	-1.2155	0.7603	0.3449	1.2480	0.2611
0.1292	-57.5540	0.3926	-0.8455	0.7735	0.4664	1.2713	0.3117
0.1307	-55.4320	0.3984	-0.4178	0.7867	0.6131	1.2946	0.3738
0.1322	-53.3308	0.4043	0.1002	0.7999	0.7984	1.3179	0.4536
0.1336	-51.2023	0.4102	0.7665	0.8130	1.0462	1.3412	0.5618
0.1351	-48.9578	0.4161	1.6967	0.8262	1.4041	1.3645	0.7198
0.1365	-46.3977	0.4220	3.1601	0.8394	1.9831	1.3877	0.9777
0.1380	-42.9326	0.4279	5.9634	0.8526	3.1159	1.4110	1.4856
0.1395	-35.6060	0.4337	14.1465	0.8657	6.4678	1.4343	2.9945
$\Delta E_{2s\to3p}$		$\Delta E_{2s\to3p}$		$\Delta E_{2s\to3p}$		$\Delta E_{2s\to3p}$	

Table 4.6. $Z = 7 - 10$ $\alpha(\omega)$

ω	$\alpha_{Z=7}$	ω	$\alpha_{Z=8}$	ω	$\alpha_{Z=9}$	ω	$\alpha_{Z=10}$
0.0000	1.8233	0.0000	1.0750	0.0000	0.6862	0.0000	0.4643
0.0073	1.8240	0.0088	1.0754	0.0102	0.6864	0.0116	0.4645
0.0146	1.8261	0.0175	1.0767	0.0204	0.6872	0.0232	0.4651
0.0220	1.8296	0.0263	1.0788	0.0306	0.6885	0.0349	0.4660
0.0293	1.8345	0.0350	1.0817	0.0408	0.6904	0.0465	0.4672
0.0366	1.8409	0.0438	1.0854	0.0509	0.6928	0.0581	0.4689
0.0439	1.8487	0.0525	1.0901	0.0611	0.6958	0.0697	0.4709
0.0512	1.8581	0.0613	1.0956	0.0713	0.6993	0.0813	0.4733
0.0585	1.8690	0.0701	1.1021	0.0815	0.7035	0.0929	0.4761
0.0659	1.8816	0.0788	1.1095	0.0917	0.7082	0.1046	0.4793
0.0732	1.8959	0.0876	1.1179	0.1019	0.7136	0.1162	0.4830
0.0805	1.9119	0.0963	1.1274	0.1121	0.7197	0.1278	0.4871
0.0878	1.9298	0.1051	1.1380	0.1223	0.7264	0.1394	0.4917
0.0951	1.9496	0.1138	1.1497	0.1325	0.7339	0.1510	0.4968
0.1024	1.9715	0.1226	1.1626	0.1427	0.7422	0.1627	0.5024
0.1098	1.9956	0.1313	1.1769	0.1528	0.7513	0.1743	0.5086
0.1171	2.0220	0.1401	1.1925	0.1630	0.7613	0.1859	0.5153
0.1244	2.0510	0.1489	1.2096	0.1732	0.7723	0.1975	0.5228
0.1317	2.0827	0.1576	1.2284	0.1834	0.7843	0.2091	0.5309
0.1390	2.1173	0.1664	1.2488	0.1936	0.7974	0.2208	0.5398
0.1463	2.1551	0.1751	1.2712	0.2038	0.8117	0.2324	0.5495
0.1537	2.1964	0.1839	1.2956	0.2140	0.8273	0.2440	0.5601
0.1610	2.2415	0.1926	1.3222	0.2242	0.8443	0.2556	0.5717

Table 4.6. continued

ω	$\alpha_{Z=7}$	ω	$\alpha_{Z=8}$	ω	$\alpha_{Z=9}$	ω	$\alpha_{Z=10}$
0.1683	2.2909	0.2014	1.3514	0.2344	0.8630	0.2672	0.5843
0.1756	2.3448	0.2102	1.3833	0.2446	0.8834	0.2788	0.5982
0.1829	2.4040	0.2189	1.4182	0.2547	0.9058	0.2905	0.6133
0.1902	2.4689	0.2277	1.4566	0.2649	0.9303	0.3021	0.6300
0.1976	2.5404	0.2364	1.4989	0.2751	0.9574	0.3137	0.6483
0.2049	2.6192	0.2452	1.5454	0.2853	0.9872	0.3253	0.6686
0.2122	2.7064	0.2539	1.5970	0.2955	1.0202	0.3369	0.6909
0.2195	2.8031	0.2627	1.6542	0.3057	1.0568	0.3486	0.7158
0.2268	2.9110	0.2714	1.7179	0.3159	1.0976	0.3602	0.7435
0.2342	3.0318	0.2802	1.7893	0.3261	1.1433	0.3718	0.7745
0.2415	3.1677	0.2890	1.8696	0.3363	1.1947	0.3834	0.8093
0.2488	3.3215	0.2977	1.9606	0.3464	1.2528	0.3950	0.8488
0.2561	3.4968	0.3065	2.0642	0.3566	1.3192	0.4067	0.8938
0.2634	3.6982	0.3152	2.1832	0.3668	1.3953	0.4183	0.9455
0.2707	3.9316	0.3240	2.3212	0.3770	1.4836	0.4299	1.0054
0.2781	4.2050	0.3327	2.4828	0.3872	1.5871	0.4415	1.0756
0.2854	4.5292	0.3415	2.6745	0.3974	1.7098	0.4531	1.1588
0.2927	4.9196	0.3503	2.9052	0.4076	1.8574	0.4647	1.2590
0.3000	5.3981	0.3590	3.1880	0.4178	2.0385	0.4764	1.3818
0.3073	5.9976	0.3678	3.5424	0.4280	2.2653	0.4880	1.5357
0.3146	6.7700	0.3765	3.9991	0.4382	2.5575	0.4996	1.7340
0.3220	7.8019	0.3853	4.6090	0.4483	2.9479	0.5112	1.9988
0.3293	9.2487	0.3940	5.4642	0.4585	3.4953	0.5228	2.3702

Table 4.6. continued

ω	$\alpha_{Z=7}$	ω	$\alpha_{Z=8}$	ω	$\alpha_{Z=9}$	ω	$\alpha_{Z=10}$
0.3366	11.4218	0.4028	6.7487	0.4687	4.3175	0.5345	2.9279
0.3439	15.0479	0.4116	8.8921	0.4789	5.6894	0.5461	3.8587
0.3512	22.3087	0.4203	13.1838	0.4891	8.4366	0.5577	5.7222
0.3585	44.1314	0.4291	26.0810	0.4993	16.6938	0.5693	11.3223
$\Delta E_{2s\to 2p}$		$\Delta E_{2s\to 2p}$		$\Delta E_{2s\to 2p}$		$\Delta E_{2s\to 2p}$	
0.4020	-8.2948	0.4897	-4.0500	0.5798	-2.2012	0.6726	-1.2947
0.4382	-3.9169	0.5416	-1.8931	0.6502	-1.0190	0.7642	-0.5938
0.4744	-2.4676	0.5935	-1.1811	0.7206	-0.6299	0.8558	-0.3639
0.5106	-1.7498	0.6454	-0.8296	0.7909	-0.4385	0.9475	-0.2512
0.5468	-1.3238	0.6972	-0.6218	0.8613	-0.3258	1.0391	-0.1851
0.5830	-1.0433	0.7491	-0.4854	0.9317	-0.2521	1.1307	-0.1420
0.6192	-0.8455	0.8010	-0.3897	1.0020	-0.2006	1.2223	-0.1121
0.6554	-0.6992	0.8529	-0.3191	1.0724	-0.1628	1.3140	-0.0901
0.6916	-0.5869	0.9048	-0.2652	1.1428	-0.1339	1.4056	-0.0735
0.7278	-0.4983	0.9567	-0.2227	1.2132	-0.1113	1.4972	-0.0604
0.7639	-0.4268	1.0086	-0.1886	1.2835	-0.0932	1.5889	-0.0500
0.8001	-0.3679	1.0604	-0.1606	1.3539	-0.0784	1.6805	-0.0416
0.8363	-0.3187	1.1123	-0.1373	1.4243	-0.0661	1.7721	-0.0345
0.8725	-0.2770	1.1642	-0.1175	1.4946	-0.0557	1.8638	-0.0286
0.9087	-0.2413	1.2161	-0.1006	1.5650	-0.0468	1.9554	-0.0235
0.9449	-0.2102	1.2680	-0.0860	1.6354	-0.0391	2.0470	-0.0192

Table 4.6. continued

ω	$\alpha_{Z=7}$	ω	$\alpha_{Z=8}$	ω	$\alpha_{Z=9}$	ω	$\alpha_{Z=10}$
0.9811	-0.1831	1.3199	-0.0732	1.7057	-0.0324	2.1387	-0.0153
1.0173	-0.1591	1.3718	-0.0619	1.7761	-0.0265	2.2303	-0.0120
1.0535	-0.1376	1.4237	-0.0518	1.8465	-0.0212	2.3219	-0.0090
1.0897	-0.1184	1.4755	-0.0428	1.9168	-0.0164	2.4135	-0.0063
1.1258	-0.1009	1.5274	-0.0345	1.9872	-0.0121	2.5052	-0.0038
1.1620	-0.0850	1.5793	-0.0270	2.0576	-0.0082	2.5968	-0.0016
1.1982	-0.0703	1.6312	-0.0201	2.1279	-0.0045	2.6884	0.0005
1.2344	-0.0567	1.6831	-0.0136	2.1983	-0.0011	2.7801	0.0024
1.2706	-0.0440	1.7350	-0.0076	2.2687	0.0021	2.8717	0.0043
1.3068	-0.0320	1.7869	-0.0019	2.3390	0.0051	2.9633	0.0060
1.3430	-0.0205	1.8387	0.0036	2.4094	0.0080	3.0550	0.0077
1.3792	-0.0096	1.8906	0.0089	2.4798	0.0109	3.1466	0.0094
1.4154	0.0011	1.9425	0.0141	2.5501	0.0137	3.2382	0.0110
1.4516	0.0115	1.9944	0.0192	2.6205	0.0164	3.3299	0.0126
1.4877	0.0218	2.0463	0.0243	2.6909	0.0192	3.4215	0.0143
1.5239	0.0321	2.0982	0.0294	2.7612	0.0221	3.5131	0.0160
1.5601	0.0426	2.1501	0.0347	2.8316	0.0250	3.6048	0.0177
1.5963	0.0533	2.2019	0.0401	2.9020	0.0280	3.6964	0.0195
1.6325	0.0645	2.2538	0.0458	2.9723	0.0312	3.7880	0.0215
1.6687	0.0763	2.3057	0.0519	3.0427	0.0347	3.8796	0.0236
1.7049	0.0889	2.3576	0.0585	3.1131	0.0384	3.9713	0.0259
1.7411	0.1028	2.4095	0.0658	3.1834	0.0426	4.0629	0.0284
1.7773	0.1182	2.4614	0.0740	3.2538	0.0474	4.1545	0.0314

Table 4.6. continued

ω	$\alpha_{Z=7}$	ω	$\alpha_{Z=8}$	ω	$\alpha_{Z=9}$	ω	$\alpha_{Z=10}$
1.8135	0.1358	2.5133	0.0833	3.3242	0.0528	4.2462	0.0348
1.8496	0.1563	2.5651	0.0944	3.3945	0.0593	4.3378	0.0388
1.8858	0.1808	2.6170	0.1077	3.4649	0.0671	4.4294	0.0437
1.9220	0.2113	2.6689	0.1243	3.5353	0.0769	4.5211	0.0498
1.9582	0.2508	2.7208	0.1459	3.6056	0.0897	4.6127	0.0578
1.9944	0.3047	2.7727	0.1755	3.6760	0.1073	4.7043	0.0689
2.0306	0.3838	2.8246	0.2192	3.7464	0.1332	4.7960	0.0853
2.0668	0.5135	2.8765	0.2910	3.8167	0.1760	4.8876	0.1123
2.1030	0.7697	2.9283	0.4331	3.8871	0.2608	4.9792	0.1659
2.1392	1.5324	2.9802	0.8564	3.9575	0.5136	5.0708	0.3258
$\Delta E_{2s\to3p}$		$\Delta E_{2s\to3p}$		$\Delta E_{2s\to3p}$		$\Delta E_{2s\to3p}$	

Table 4.7. Cauchy Moments from $\alpha(\omega) = \sum_{k=0}^{\infty} S(-2k-2)\omega^{2k}$ fit.

Z	$S(-2)$	$S(-4)$	$S(-6)$	$S(-8)$	$S(-10)$
3	164.112152	35173.41368	7.620771E+06	1.65253E+09	3.5838E+11
4	24.496622	1116.65143	5.265975E+04	2.48923E+06	1.1769E+08
5	7.859058	154.93349	3.189800E+03	6.57989E+04	1.3574E+06
6	3.464469	38.40426	4.454716E+02	5.17431E+03	6.010E+04
7	1.823265	13.01819	9.717041E+01	7.25989E+02	5.424E+03
8	1.075030	5.37232	2.800946E+01	1.46130E+02	7.624E+02
9	0.686155	2.53865	0.997617E+01	3.76660E+01	1.451E+02
10	0.464343	1.32462	0.392389E+01	1.16278E+01	3.445E+01

CHAPTER 5

CORRELATED GAUSSIAN CALCULATIONS OF HYPERFINE SPLITTINGS FOR MUONIC HELIUMLIKE IONS

Below is a pre-print of a manuscript submitted to Chemical Physics Letters: *Correlated Gaussian calculations of hyperfine splittings for muonic heliumlike ions*, William P. Earwood, Steven R. Davis (2022)

Abstract

Muon-electron-nucleus systems for nuclear charge $2 \leq Z \leq 10$ have been studied using all-particle Gaussian wavefunctions. The nonadiabatic, nonrelativistic Hamiltonian is used to solve the Schrödinger equation, and the nonlinear parameters of the basis functions are optimized using a stochastic approach. Using these wavefunctions, integrals with the interparticle delta functions are calculated and used to determine the hyperfine splittings for the $^{9}\mathrm{Be}\mu e$ and $^{11}\mathrm{B}\mu e$ ions. For $Z > 3$, these are the first variational calculations where each interparticle correlation is treated explicitly.

5.1 Introduction

Exotic atoms containing muons have gained considerable attention in recent years. The muonic hydrogen ($^{1}\mathrm{H}\mu$) system has been important due to the interest in the proton radius puzzle [116–118], while $^{4}\mathrm{He}\mu$ has been used to determine the alpha particle radius experimentally [119]. For two-body muon ions with nuclear charge $Z > 2$, a number of high-accuracy calculations of energy levels and hyperfine splittings have recently been reported [120–122]. Three-body muonic helium ($^{4}\mathrm{He}\mu e$) has also been studied both theoretically [123, 124] and experimentally [125] for many years now. Since then, the focus has remained mostly on muonic helium on the theoretical side [4, 126, 127]. Less studied are the ”muonic heliumlike” ions, comprised of a muon, electron,

and a nucleus with $Z > 2$, such that the three-body system obtains a net positive charge. For muonic heliumlike ^{6}Liμe and ^{7}Liμe, high-accuracy calculations of term energies, properties, and hyperfine splittings have been reported [4, 5, 128, 129].

More recently, energy levels of ^{9}Beμe and ^{11}Bμe were calculated using perturbation theory, and both relativistic and quantum electrodynamics corrections were included to determine the $2S-2P$ and $1S-2S$ intervals [130]. Motivated by these results, our interest became to study, using the variational method, the ground states of the $4 \leq Z \leq 10$ muonic heliumlike ions. Specifically, we hoped to calculate non-adiabatic wavefunctions for these systems, in order to evaluate the integrals with interparticle delta functions, which are important as they can be used to determine hyperfine splittings. In [131], formulas for calculating the hyperfine splittings for the ^{7}Liμe ions (with nuclear spin $3/2$) were reported. Because the ^{9}Beμe and ^{11}Bμe systems have nuclear spins which are also $3/2$, our intent was to use the formulas in [131] to report the first hyperfine splittings for these two systems.

Having completed these calculations, which are the subject of the present work, we became aware of perturbation theory calculations of three-body hyperfine splittings for these same ions [3], which included vacuum polarization, nuclear structure, and α^6 relativistic and radiative corrections. In any case, one purpose of this letter is to report energies, expectation values, and hyperfine splittings for the ^{9}Be and ^{11}B muonic ions. It will be shown that our calculations are consistent with the results in [3]. Although we have not calculated the hyperfine splittings for the $Z > 5$ muonic heliumlike ions, we report energies and integrals with these wavefunctions. For the $Z > 3$ isotopes, our results constitute the first direct variational calculations of energies and integrals for the muonic heliumlike ions. There are, however, calculations of muonic heliumlike ions, which were reported for $2 \leq Z \leq 18$, using single-particle orbitals [132, 133]. A full configuration-interaction treatment results in accurate binding energies.

Recently, we have begun studying various few-body problems using correlated Gaussian wavefunctions, relying on a stochastic selection of nonlinear parameters. Although this procedure does not generate highly compact wavefunctions, we have found it possible to determine non-

relativistic energies with accuracy 1×10^{-12} a.u. for the three-body heliumlike ions, and 1×10^{-8} a.u. for the four-body lithiumlike ions. Whether this implementation was adaptable to three-body muon ions was initially unknown, but we found that for $^4\mathrm{He}\mu e$ and $^7\mathrm{Li}\mu e$, the calculated hyperfine splittings agreed well with previous work [4, 5]. Other than the interparticle delta function integrals, we have considered in this study the integrals with the interparticle distances r_{eN}, $r_{\mu N}$, and $r_{e\mu}$, and their squares.

5.2 Methods

For the calculation of each wavefunction, we have used the non-adiabatic Hamiltonian (in atomic units):

$$\hat{H} = -\frac{\nabla_e^2}{2} - \frac{1}{m_\mu}\frac{\nabla_\mu^2}{2} - \frac{1}{m_N}\frac{\nabla_N^2}{2} - \frac{Z}{r_{eN}} - \frac{Z}{r_{\mu N}} + \frac{1}{r_{e\mu}} \tag{5.1}$$

Following [29], one can write the kinetic energy portion in compact form using the 6×6 mass matrix, $\bar{M}$, and the vector of gradients $\nabla_r = (\nabla_{e_x}, \nabla_{e_y}, \nabla_{e_z}, \nabla_{\mu_x}, \nabla_{\mu_y}, \nabla_{\mu_z})$:

$$-\frac{\nabla_e^2}{2} - \frac{1}{m_\mu}\frac{\nabla_\mu^2}{2} - \frac{1}{m_N}\frac{\nabla_N^2}{2} = -\nabla_r' \bar{M} \nabla_r \tag{5.2}$$

$$\bar{M} = M \bigotimes I_3 \tag{5.3}$$

$$M = \tfrac{1}{2}\begin{pmatrix} m_{eN}^{-1} & m_N^{-1} \\ m_N^{-1} & m_{\mu N}^{-1} \end{pmatrix}$$

The matrix $\bar{M}$ is defined by the Kronecker product of a 2×2 matrix M with the 3×3 identity matrix I_3 [37]. The variable m_N is used to denote the nuclear masses, which are collected in Section 5.3, while m_{eN} and $m_{\mu N}$ are the electron-nucleus and muon-nucleus reduced masses. For the muon mass, we adopt the CODATA [134] value $m_\mu = 206.7682830(46)$, while $m_e = 1$. Each wavefunction Ψ is expanded using explicitly correlated Gaussians [15]:

$$\Psi = \sum_k c_k \phi_k = \sum_k c_k \exp(-A_k^{11} r_{eN}^2 - A_k^{22} r_{\mu N}^2 - 2A_k^{21} r_{e\mu}) \tag{5.4}$$

Defining the 6×1 vector $\mathbf{r} = (\mathbf{r}_{eN}, \mathbf{r}_{\mu N})$, where $\mathbf{r}_{eN}$ and $\mathbf{r}_{\mu N}$ are the 3×1 position vectors of the electron and muon originating from the nucleus, the basis functions can be expressed in matrix form [36, 40]:

$$\phi_k = \exp(-\mathbf{r}' \bar{A}_k \mathbf{r}) \tag{5.5}$$

The 6×6 matrix $\bar{A}_k$ is defined by the Kronecker product of a 2×2 positive definite matrix A_k with the 3×3 identity matrix I_3, while the matrix A_k can be Cholesky decomposed using the lower triangular matrix L_k and its transpose L_k' [37]:

$$\bar{A}_k = A_k \bigotimes I_3 = (L_k L_k') \bigotimes I_3 \tag{5.6}$$

For the optimization of the nonlinear parameters stored in L_k, we have used a stochastic selection method that lowers the value of the Rayleigh quotient by sampling from an unrestricted domain of real numbers. In other words, the energy is determined repeatedly for different parameter values, and the parameter set is updated each time the energy is lowered, provided the parameter changes do not introduce linear dependencies within Ψ.

The parameters in L_k are allowed to take on any (both positive and negative) values, since the Cholesky decomposition automatically enforces A_k to remain positive definite during optimization [40]. To develop an optimization strategy for these ions, we performed trial optimizations of small ($m < 100$) basis sets for each ion, where the initial L_k matrices were populated from uniform distributions. These optimizations involved sampling a single parameter, from a single function, a number of times (e.g., 10). This procedure was repeated for each parameter, for each function, an indefinite number of times, up to which point convergence slowed.

During sampling, we observed a tendency for the L_k^{22} parameters to grow quite large, compared to the L_k^{11} and L_k^{21} parameters. This behavior is observed for nearly every function in the trial optimization sets. The L_k^{22} parameters additionally become larger with increasing Z. For large L_k^{22}, the argument A_k^{22} in Eq. 5.4 becomes large and positive, so that the Gaussians decay especially quickly for the $r_{\mu N}$ component.

While the growth of these parameters is controlled, it became clear that the optimization has to *find* functions that have these large parameters in order to describe the wavefunction with accuracy. As the overall parameter domain becomes much larger than for the electronic-only case, it eventually became more practical to sample uniformly from a semi-local domain around each parameter, as opposed to sampling from a large, fixed uniform domain. Different semi-local domains were tested, which each depend on the current value of the parameter, which we will call p_0. An interval (p_{min}, p_{max}), centered at p_0 is then constructed for sampling. The values p_{min} and p_{max} can vary, but we have found $p_{min} = p_0/2$, $p_{max} = 3p_0/2$, for positive p_0, and $p_{min} = 3p_0/2$, $p_{max} = p_0/2$, for negative p_0, to be effective.

Using this sampling method, 300 Gaussians were extensively optimized for each ion. Once this convergence slowed, we added to the 300 term bases, for each ion, two different 300 term bases from the other ions. During this merging, the functions added to the original bases that introduce linear dependencies are replaced by randomly selected new function parameters. Having many different combinations of bases to merge for each ion, the choice of which bases to add to the original 300 term bases was determined according to which combinations lowered the energy most upon merging. The total number of Gaussians for each ion was then 900 after this merging.

Subsequently, the 900 Gaussian bases for each ion were optimized again, rather extensively, but using fewer cycles than before. At which point this convergence slowed, a second merging of bases was used. This time, the 900 Gaussian bases were combined with a second 900 Gaussian basis, which is determined for each ion as stated above, resulting in 1800 total functions for each ion. After a much smaller number of optimization cycles for the 1800 term basis sets, each basis set was "pruned" to remove functions with small linear coefficients. This resulted in the energy becoming temporarily larger, but the calculated integrals were largely unaffected. Finally, the pruned basis sets were optimized until convergence slows, re-pruning as necessary in between optimization cycles. During this pruning process, around 100-300 functions are removed for each ion. These final wavefunctions are used when reporting the energies and integrals in the Results section.

As pointed out in Section 5.1, the hyperfine splitting is often a quantity of interest. The hyperfine splitting is determined by treating perturbatively the Hamiltonian [5, 124]:

$$\hat{H}_{HF} = -\frac{8\pi}{3}(\vec{\mu}_\mu \cdot \vec{\mu}_N)\delta(\mathbf{r}_{\mu N}) - \frac{8\pi}{3}(\vec{\mu}_e \cdot \vec{\mu}_\mu)\delta(\mathbf{r}_{e\mu}) - \frac{8\pi}{3}(\vec{\mu}_e \cdot \vec{\mu}_N)\delta(\mathbf{r}_{eN}) \tag{5.7}$$

Here, the quantities $\vec{\mu}_e$, $\vec{\mu}_\mu$, and $\vec{\mu}_N$ are the magnetic moment vectors of each particle. The shift due to this perturbation can be factorized into coordinate and spin components, introducing the spin vectors $\vec{s}_e$, $\vec{s}_\mu$, and $\vec{I}_N$ of each particle [5, 124]:

$$\langle \hat{H}_{HF} \rangle = -a \langle \vec{s}_\mu \cdot \vec{I}_N \rangle - b \langle \vec{s}_e \cdot \vec{s}_\mu \rangle - c \langle \vec{s}_e \cdot \vec{I}_N \rangle \tag{5.8}$$

$$a = A \langle \delta(\mathbf{r}_{\mu N}) \rangle = \frac{2\pi}{3}\alpha^2 \frac{g_\mu g_N}{m_\mu m_p} \langle \delta(\mathbf{r}_{\mu N}) \rangle \tag{5.9}$$

$$b = B \langle \delta(\mathbf{r}_{e\mu}) \rangle = \frac{2\pi}{3}\alpha^2 \frac{g_e g_\mu}{m_e m_\mu} \langle \delta(\mathbf{r}_{e\mu}) \rangle \tag{5.10}$$

$$c = C \langle \delta(\mathbf{r}_{eN}) \rangle = \frac{2\pi}{3}\alpha^2 \frac{g_e g_N}{m_e m_p} \langle \delta(\mathbf{r}_{eN}) \rangle \tag{5.11}$$

In Eqs. (5.9-5.11), the integrals with the interparticle delta functions are calculated for each (ground state) wavefunction Ψ. The QED fine structure constant α enters these expressions, as do the g-factors of each particle, and the proton mass, m_p. To actually calculate the hyperfine splitting, however, it is necessary to diagonalize $\langle \hat{H}_{HF} \rangle$ in the space of all spin states, but it is possible to make simplifying assumptions based on the magnitudes of a, b, and c.

Without modification, for our wavefunctions, the delta function integrals unfortunately cannot be computed with high accuracy. Therefore, we have adopted the Drachman regularization [77, 78] to define these integrals. For the interparticle distances r_{ab}, we have used the formula from [135], which is valid when the nuclear mass is finite:

$$\frac{\pi \langle \Psi | \delta(r_{ab}) | \Psi \rangle}{m_{ab}} = \langle \Psi | \frac{E - \hat{V}}{r_{ab}} | \Psi \rangle - \langle \nabla_r \Psi | \frac{\bar{M}}{r_{ab}} | \nabla_r \Psi \rangle \tag{5.12}$$

Here, E and $\hat{V}$ are the non-relativistic energy and potential operator, and m_{ab} is the reduced mass for particles a, b. Writing the second integral in this way, the action of the $\nabla_{\mathbf{r}}$ operators in both the bra and ket leads to an integral involving an operator of the form $\mathbf{r}'\bar{X}\mathbf{r}/r_{ab}$, which has been derived in Eq. D18 in [59].

5.3 Results

All the data presented in Section 5.3 is given in atomic units. In Table 5.1 the nuclear masses $\{m_N\}$ and the bound state energies are collected. The nuclear masses have been determined using the atomic masses from the 2020 Atomic Mass Evaluation [99]. To find the nuclear masses we subtract Z electron masses and add the total electron binding energies which we have taken from the NIST Atomic Spectra Database [61]. The conversion factors employed for this purpose are taken from CODATA [134]. We used 0.000548579909065 u for the electron mass, and 9.3149410242×10^8 to convert from eV to u. We have reported both finite nuclear mass $E(m_\mu, m_N)$ and infinite nuclear mass $E(m_N \to \infty)$ energies. In calculating the infinite nuclear mass wavefunctions, we have used the same nonlinear parameters as for the finite mass wavefunctions, hence only the linear coefficients change. Only one optimization is performed for each ion, and for the finite nuclear mass Hamiltonian only.

As the bound state energies depend on these mass parameters, comparison with other variational energies is only possible by recalculating the energies using the appropriate m_μ and m_N. Using the results from [4, 5], it is possible to estimate the errors for our bound state energies for $Z = 2, 3$. Adopting the mass parameters from [4], our ^{4}He and $^\infty$He energies are -402.637 263 023 and -414.036 536 934, which are $\approx 1 \times 10^{-8}$ higher than those from [4]. Adopting the mass parameters from [5], our ^{7}Li energy is -917.650 220 002, which is $\approx 5 \times 10^{-8}$ a.u. higher than the result from [5]. The difference between the results in Table 5.1 with those from [4] and [5] is mostly due to the different muon mass parameters that have been used. The energies for $Z > 3$ are likely within 1×10^{-6} a.u. of their true values for the mass parameters used herein.

Table 5.1. Nuclear Masses and Bound State Energies

Isotope	m_N	$-E(m_\mu, m_N)$	$-E(m_N \to \infty)$
^{4}He	7294.29954142	-402.637 302 650	-414.036 578 934
^{7}Li	12786.3922777	-917.650 216 034	-932.457 317 687
^{9}Be	16424.2055204	-1638.080 534 553	-1658.646 346 288
^{11}B	20063.7369413	-2566.239 146 596	-2592.603 660 946
^{12}C	21868.6638503	-3699.468 393 419	-3734.329 260 198
^{14}N	25519.0452820	-5043.106 472 181	-5083.823 143 450
^{16}O	29148.9496970	-6594.480 270 224	-6641.085 310 275
^{19}F	34622.9756953	-8356.401 543 476	-8406.115 760 561
^{20}Ne	36433.9958789	-10320.572 462 50	-10378.914 493 99

In Table 5.2, the kinetic energies for each particle are collected, where it is seen that the muon and nucleus kinetic energies are very similar for all ions, with the latter being slightly larger. The electron kinetic energies for each ion are much smaller by comparison, while from $Z = 2$ to $Z = 10$, the ratio ∇_μ^2/∇_e^2 is reduced by a factor of three. We have also collected, in Table 5.3, the values for the related quantity:

$$v_i^{1/2} \equiv -(\langle \Psi | \nabla_i^2 / m_i^2 | \Psi \rangle)^{1/2} \tag{5.13}$$

For the electrons, $\sqrt{v_e}$ scales as $(Z-1)$, while for the muons, $\sqrt{v_\mu}$ is very nearly Z. In Table 5.4, the radial integrals are reported for each ion. One can verify that the $r_{\mu N}$ integrals are nearly identical to $3/(2Zm_{\mu N})$, where $M_{\mu N}$ is the muon-nucleus reduced mass for nucleus N. Between the $r_{e\mu}$ and r_{eN} integrals, the former is slightly larger, as expected. The ratio $\langle r_{eN} \rangle / \langle r_{\mu N} \rangle$ is meanwhile an interesting parameter to observe. For $Z = 2$, this ratio is ≈ 402, while with

Table 5.2. $-\nabla_i^2/2$ Integrals

Z	$-\nabla_e^2/2$	$-\nabla_\mu^2/2$	$-\nabla_N^2/2$
2	0.499 906 575	80 857.221	80 857.698
3	1.999 826 679	186 314.541	186 316.493
4	4.499 707 873	333 573.213	333 577.629
5	7.999 583 281	523 567.062	523 574.942
6	12.499 368 705	755 207.647	755 219.970
7	17.999 232 652	1 030 681.545	1 030 699.328
8	24.499 095 845	1 348 895.157	1 348 919.400
9	31.999 061 244	1 711 004.108	1 711 035.831
10	40.498 822 719	2 113 597.968	2 113 638.130

Table 5.3. $\sqrt{v_i}$ Integrals

Z	$\sqrt{v_e}$	$\sqrt{v_\mu}$	$\sqrt{v_N}$
2	0.999 906 570	1.944 869 578	0.055 130 520
3	1.999 913 337	2.952 258 983	0.047 741 122
4	2.999 902 622	3.950 268 910	0.049 731 216
5	3.999 895 818	4.948 997 509	0.051 002 633
6	4.999 873 739	5.943 801 073	0.056 199 115
7	5.999 872 107	6.943 738 011	0.056 262 182
8	6.999 870 833	7.943 651 343	0.056 348 853
9	7.999 882 654	8.946 570 789	0.053 429 383
10	8.999 869 190	9.943 568 453	0.056 431 748

Table 5.4. Radial Integrals

Z	$\langle r_{\mu N} \rangle$	$\langle r_{e\mu} \rangle$	$\langle r_{eN} \rangle$
2	0.003 730 068 97	1.500 166 320	1.500 160 416
3	0.002 457 270 10	0.750 046 245	0.750 041 003
4	0.001 836 456 68	0.500 025 295	0.500 020 878
5	0.001 465 851 96	0.375 016 456	0.375 012 692
6	0.001 220 514 88	0.300 012 849	0.300 009 584
7	0.001 044 753 94	0.250 009 670	0.250 006 793
8	0.000 913 244 72	0.214 293 350	0.214 290 781
9	0.000 810 869 08	0.187 505 945	0.187 503 626
10	0.000 729 566 82	0.166 671 908	0.166 669 796

increasing Z, the ratio tends toward the muon mass. Already then for $Z = 4$, the relative shell structure is closer to $Z = \infty$ than to $Z = 2$. The integrals with the squares of these distances are reported in Table 5.5. One can verify that the $r^2_{\mu N}$ integrals are nearly identical to $3/(Zm_{\mu N})^2$.

In Table 5.6 we collect the $\delta(r_{ab})$ integrals. In Table 5.7, we compare our results from Tables 5.2-5.6 for the ^{4}He and ^{7}Li muonic heliumlike ions, with those from [4, 5], which have used very accurate exponential wavefunctions to calculate the various integrals. Our integrals in Table 5.7 have been recalculated using the masses from [4, 5] to provide the best comparison.

For the interparticle delta functions, the first observation is that the absolute errors are much smaller for ^{4}He than for ^{7}Li. One reason these errors grow is simply because the magnitudes of the integrals grow with Z. In general, we expect that the absolute errors grow larger with increasing Z. However, the relative errors for $\delta(r_{e\mu})$ and $\delta(r_{\mu N})$ are quite similar. For $\delta(r_{eN})$, the relative agreement for ^{4}He is about one order of magnitude better than for ^{7}Li, which we regard as coincidental, as the ^{4}He wavefunction is not that well converged. Based on these considerations,

Table 5.5. Squared Radial Integrals

Z	$\langle r^2_{\mu N}\rangle$	$\langle r^2_{e\mu}\rangle$	$\langle r^2_{eN}\rangle$
2	1.855 121 981 $\times 10^{-5}$	3.000 671 360	3.000 653 760
3	8.050 902 031 $\times 10^{-6}$	0.750 092 593	0.750 084 771
4	4.496 764 326 $\times 10^{-6}$	0.333 366 585	0.333 362 187
5	2.864 962 725 $\times 10^{-6}$	0.187 515 988	0.187 513 175
6	1.986 208 846 $\times 10^{-6}$	0.120 009 886	0.120 007 932
7	1.455 347 782 $\times 10^{-6}$	0.083 339 458	0.083 338 024
8	1.112 021 261 $\times 10^{-6}$	0.061 228 588	0.061 227 490
9	8.766 782 494 $\times 10^{-7}$	0.046 877 753	0.046 876 886
10	7.096 903 493 $\times 10^{-7}$	0.037 039 182	0.037 038 480

Table 5.6. Delta Function Integrals

Z	$\langle \delta(r_{\mu N})\rangle$	$\langle \delta(r_{e\mu})\rangle$	$\langle \delta(r_{eN})\rangle$
2	20700142	0.313 758	0.320 631
3	72404447	2.510 203	2.558 819
4	173453018	8.471 593	8.625 443
5	341077909	20.080 370	20.430 560
6	590873705	39.218 150	39.883 762
7	942067159	67.768 698	68.895 507
8	1410465312	107.613 888	109.375 400
9	2014984411	160.637 613	163.234 006
10	2766487275	228.717 770	232.379 053

Table 5.7. Comparison of Expectation Values $\langle\Psi|\mathscr{O}|\Psi\rangle$ with Literature

$\mathscr{O}$	^{4}He	^{4}He [4]	^{7}Li	^{7}Li [5]
r_{eN}	1.50016060	1.500160720184	0.750041038	0.7500410435208
$r_{\mu N}$	0.0037300693440	0.003730069344784	0.00245727008994	0.002457270091
$r_{e\mu}$	1.50016650	1.500166624663	0.750046280	0.750046285521800
r_{eN}^2	3.00065453	3.000655963785	0.750084843	0.750084862932138
$r_{\mu N}^2$	$1.85512234569 \times 10^{-5}$	$1.85512234665 \times 10^{-5}$	$8.050901959 \times 10^{-6}$	$8.050901973 \times 10^{-6}$
$r_{e\mu}^2$	3.00067212	3.000673562997	0.750092665	0.750092684570279
$\delta(r_{eN})$	0.32063113	0.320631162	2.5588197	2.558823441
$\delta(r_{\mu N})$	20700136.25	20700137.343	72404448.86	72404453.27
$\delta(r_{e\mu})$	0.31375795	0.313760812	2.5102038	2.510223118
$\mathbf{p}_e^2/2$	0.499906457	0.4999065033469	1.9998265	1.9998266011528
$\mathbf{p}_\mu^2/2$	80857.20559	80857.2055843	186314.5433	186314.54326378
$\mathbf{p}_N^2/2$	80857.68243	80857.6824240	186316.4948	186316.49471713

we will assume a relative error model where the errors for the delta function integrals, for all ions, are calculated using the relative errors for ^{7}Li. These relative errors are $\approx 1.5 \times 10^{-6}$, 6.0×10^{-8}, and 7.7×10^{-6} for $\delta(r_{eN})$, $\delta(r_{\mu N})$, and $\delta(r_{e\mu})$, respectively. Hence, the errors in Table 5.6 for $Z > 3$ are assumed to be $I/(1-\varepsilon_i)$, where I is the magnitude of each integral, and ε_i is the relative error for the three different integrals, which are the relative errors stated above. This model suggests ≈ 5 significant figures for $\delta(r_{e\mu})$, ≈ 6 significant figures for $\delta(r_{eN})$, and ≈ 7 significant figures for $\delta(r_{\mu N})$. Obviously, this is only a very rough estimate of the errors. For the radial integrals, our results compare favorably with those from [4, 5]. The $r_{\mu N}$ values are in agreement to ≈ 12 decimals in both cases, while for $r_{e\mu}$ and r_{eN}, agreement is observed for $\approx$ 7-8 decimals. Excellent agreement for the kinetic energy integrals is noted, as well.

Now, let us show how the calculated delta function integrals can be used to determine the hyperfine splittings. For this purpose, the physical constants we have used [134, 136] are:

$$g_N(^7\mathrm{Li}) = 2.170951$$

$$g_N(^9\mathrm{Be}) = -0.784955$$

$$g_N(^{11}\mathrm{B}) = 1.792433$$

$$g_N(^{14}\mathrm{N}) = 0.403761$$

$$g_N(^{19}\mathrm{F}) = 5.257736$$

$$g_e = -2.002\ 319\ 304\ 362\ 56$$

$$g_\mu = -2.002\ 331\ 841\ 8$$

$$m_p = 1836.152\ 673\ 43$$

$$\alpha = 0.007\ 297\ 352\ 569\ 3$$

$$6.579\ 683\ 920\ 502 \times 10^9 \text{ MHz/a.u.}$$

Let us first consider $^4\mathrm{He}\mu e$. For the ^{4}He nucleus, the nuclear spin vanishes, and therefore only the b coefficient is non-zero, which determines $\Delta\nu_1$, while the experimental result from [125] is denoted $\Delta\nu_1^{exp}$:

$$\Delta\nu_1(^4\mathrm{He}\mu e) = 4464.52\mathrm{MHz}$$

$$\Delta\nu_1^{exp}(^4\mathrm{He}\mu e) = 4465.004(29)\mathrm{MHz}$$

One difference between these splittings is due to b missing various correction terms, such as those calculated in [129]. Meanwhile, if we use a more accurate value of $\delta(r_{e\mu})$, b becomes larger by ≈ 0.03 MHz. So at least for $Z = 2$, the primary difference with experiment appears to be on the physical side, and not resulting from numerical inaccuracies associated with our computational methodology. Now let us consider how our result changes if, instead of solving the non-adiabatic

Schrödinger equation, we assume an infinite nuclear mass. Calculating $\delta(r_{e\mu}) \approx 0.314002$ for the infinite nuclear mass, we find:

$$\Delta\nu_1(^{\infty}\mathrm{He}\mu e) = 4467.98\mathrm{MHz}$$

This analysis shows that it is essential to consider the full three-body problem, as has been done herein. For ^{7}Li, the nuclear spin is $3/2$, hence a, b, c are each non-zero. We find:

$$a(^7\mathrm{Li}\mu\mathrm{e}) = \text{-608349161 MHz}$$

$$b(^7\mathrm{Li}\mu\mathrm{e}) = 35718.13\ \mathrm{MHz}$$

$$c(^7\mathrm{Li}\mu\mathrm{e}) = \text{-4445.38 MHz}$$

Here, we use the relations $|a| >> |b|$ and $|a| >> |c|$ to calculate the hyperfine splitting, following [131]:

$$\Delta\nu_1(^7\mathrm{Li}\mu e) = (5/8)(b-3c) = 13988.75\ \mathrm{MHz}$$

$$\Delta\nu_2(^7\mathrm{Li}\mu e) = (3/8)(b+5c) = 21729.38\ \mathrm{MHz}$$

The corresponding results from [5] are $\Delta\nu_1 = 13989.19$ MHz and $\Delta\nu_2 = 21729.22$ MHz. Since more accurately calculated delta function integrals were reported in [5], we can use those to assess the errors in our $\Delta\nu_1, \Delta\nu_2$, that result from the errors in $\langle\delta(r_{e\mu}\rangle)$ and $\langle\delta(r_{eN})\rangle$. Doing so, we find that both $\Delta\nu_1, \Delta\nu_2$ increase by ≈ 0.17 MHz and ≈ 0.10 MHz, respectively. Using these results and comparing to [5], $\Delta\nu_1$ would be ≈ 0.3 MHz too small, while $\Delta\nu_2$ is ≈ 0.3 MHz too large. These 0.3 MHz differences reflect the differences between the exact diagonalization of Eq. 5.8 and the approximation formulas. In [3], the corresponding splittings, calculated using perturbation theory, have taken into account a number of different correction terms which we have not considered, leading to the results $\Delta\nu_1 = 13994.345$ MHz and $\Delta\nu_2 = 21731.04$ MHz. Hence, our computational model accounts for the large part of the hyperfine splitting for $Z = 3$. For $(^9\mathrm{Be}\mu e)$ and $(^{11}\mathrm{B}\mu e)$, we can attempt similar comparisons. The b, c and $\Delta\nu_1, \Delta\nu_2$ values are then:

$$(^9\mathrm{Be}\mu e) : b = 120543.79\mathrm{MHz}; c = -5418.07\mathrm{MHz}$$

$$(^{11}\mathrm{B}\mu e) : b = 285727.09\mathrm{MHz}; c = 29305.01\mathrm{MHz}$$

$$\Delta\nu_1(^9\mathrm{Be}\mu e) = 85498.75\mathrm{MHz}$$

$$[3] : 85539.16\mathrm{MHz}$$

$$\Delta\nu_2(^9\mathrm{Be}\mu e) = 35045.03\mathrm{MHz}$$

$$[3] : 35067.07\mathrm{MHz}$$

$$\Delta\nu_1(^{11}\mathrm{B}\mu e) = 123632.54\mathrm{MHz}$$

$$[3] : 123767.56\mathrm{MHz}$$

$$\Delta\nu_2(^{11}\mathrm{B}\mu e) = 162094.56\mathrm{MHz}$$

$$[3] : 162228.31\mathrm{MHz}$$

It is observed that our $\Delta\nu_1$, $\Delta\nu_2$ are much smaller in all cases compared to the results from [3], which is primarily due to the corrections that have not been considered herein. These corrections are listed in Table 1 in [3]. We would like to make a comparison with those results, by considering only the α^4 contributions, but also the α^5 electron vertex correction in 1γ interaction (rows 1, 2, and 12 from Table 1 in [3]). Using the sum of those values to calculate b, c, we will denote the splittings $\Delta\tilde{\nu}_1, \Delta\tilde{\nu}_2$ in order to avoid confusing the splittings from this sub-contribution with the final values in [3]:

$$[3] : \Delta\tilde{\nu}_1(^9\mathrm{Be}\mu e) = 85494.13\mathrm{MHz}$$

$$[3] : \Delta\tilde{\nu}_2(^9\mathrm{Be}\mu e) = 35042.69\mathrm{MHz}$$

$$[3] : \Delta\tilde{\nu}_1(^{11}\mathrm{B}\mu e) = 123622.51\mathrm{MHz}$$

$$[3] : \Delta\tilde{\nu}_2(^{11}\mathrm{B}\mu e) = 162087.07\mathrm{MHz}$$

These values are seen to agree well with our reported $\Delta\nu_1, \Delta\nu_2$. Hence, it can be concluded that our variational calculations are consistent with the perturbation theory results, but it should be emphasized that the corrections calculated in [3] are apparently very important with increasing Z.

While we have not calculated $\Delta\nu_1, \Delta\nu_2$ for the remaining ions, we will provide our calculated b, c. For the ^{12}C, ^{16}O, and ^{20}Ne muonic ions, one only needs to compute the b coefficient, while for ^{9}Be, ^{11}B, ^{14}N, and ^{19}F, the a and c coefficients are each non-vanishing. The remaining a coefficients can be calculated similarly using the integrals in Table 5.6.

$$(^{12}\mathrm{C}\mu e) : b = 558041.90\mathrm{MHz}$$

$$(^{14}\mathrm{N}\mu e) : b = 964292.63\mathrm{MHz}; c = 22260.46\mathrm{MHz}$$

$$(^{16}\mathrm{O}\mu e) : b = 1531256.79\mathrm{MHz}$$

$$(^{19}\mathrm{F}\mu e) : b = 2285740.62\mathrm{MHz}; c = 686796.70\mathrm{MHz}$$

$$(^{20}\mathrm{Ne}\mu e) : b = 3254465.05\mathrm{MHz}$$

CHAPTER 6

CONCLUSIONS

The big picture of this work was to consider select few-body problems that had not been addressed in the peer-review literature, either recently, or at all. We have focused on two systems: 1) lithiumlike ions; 2) muonic heliumlike ions. Each project represents a new contribution to the scientific literature. The most challenging part of this work was to construct the basis sets required to calculate accurate wavefunctions and first-order perturbed functions. For this task, we have relied on the use of explicitly correlated Gaussians and a stochastic optimization of nonlinear parameters. The next step for this research direction would be to implement a more powerful wavefunction optimization routine, or to consider exponential and/or Hylleraas functions as the basis functions used to expand the different objective functions. As stated, we would like to also improve the numerical performance of the solution to the generalized eigenvalue problem. Having an operational inverse iteration algorithm will be helpful to this end. The author hopes to pursue some of these ideas in the future.

BIBLIOGRAPHY

[1] H. A. Bethe and E. E. Salpeter. *Quantum Mechanics of One- and Two-Electron Atoms*. Dover Publications, 1957. ISBN 0-486-46667-1.

[2] L.-Y. Tang, Z.-C. Yan, T.-Y. Shi, and J. Mitroy. *Phys. Rev. A*, 81:042521, 2010. doi: https://doi.org/10.1103/PhysRevA.81.042521.

[3] R. N. Faustov, V. I. Korobov, A. P. Martynenko, and F. A. Martynenko. *arXiv preprint:2203.03599*, 2022.

[4] A. M. Frolov. *Phys. Rev. A*, 61:022509, 2000. doi: https://doi.org/10.1103/PhysRevA.61.022509.

[5] A. M. Frolov. *Phys. Lett. A*, 353:60, 2006. doi: https://doi.org/10.1016/j.physleta.2005.12.056.

[6] D. R. Bowler and T. Miyazaki. *J. Phys.: Condens. Matter*, 22:074207, 2010. doi: https://doi.org/10.1088/0953-8984/22/7/074207.

[7] G. D. Fletcher, D. G. Fedorov, S. R. Pruitt, T. L. Windus, and M. S. Gordon. *J. Chem. Theory Comput.*, 8:75, 2012. doi: https://doi.org/10.1021/ct200548v.

[8] T. Hirano and F. Sato. *Phys. Chem. Chem. Phys.*, 16:14496, 2014. doi: https://doi.org/10.1039/C3CP55514C.

[9] M.Bogojeski, L. Vogt-Maranto, M. E. Tuckerman, K.-R. Müller, and K. Burke. *Nat. Commun.*, 11:5223, 2020. doi: https://doi.org/10.1038/s41467-020-19093-1.

[10] A. Szabo and N. S. Ostlund. *Modern quantum chemistry: Introduction to advanced electronic structure theory*. Mcgraw-Hill, 1989. ISBN 0-07-062739-8.

[11] R. J. Bartlett and M. Musiał. *Rev. Mod. Phys.*, 79:291, 2007. doi: https://doi.org/10.1103/RevModPhys.79.291.

[12] M. O. Sinnokrot and C. D. Sherrill. *J. Phys. Chem. A*, 108:10200, 2004. doi: https://doi.org/10.1021/jp0469517.

[13] J. J. Eriksen et al. *J. Phys. Chem. Lett.*, 11:8922, 2020. doi: https://doi.org/10.1021/acs.jpclett.0c02621.

[14] B. S. Fales et al. *J. Chem. Theory Comput.*, 14:4139, 2018. doi: https://doi.org/10.1021/acs.jctc.8b00382.

[15] J. Mitroy et al. *Rev. Mod. Phys.*, 85:693, 2013. doi: https://doi.org/10.1103/RevModPhys.85.693.

[16] V. I. Korobov. *Phys. Rev. A*, 61:064503, 2000. doi: https://doi.org/10.1103/PhysRevA.61.064503.

[17] Z.-C. Yan, M. Tambasco, and G. W. F. Drake. *Phys. Rev. A*, 57:1652, 1998. doi: https://doi.org/10.1103/PhysRevA.57.1652.

[18] S. Nasiri, T. Shomenov, S. Bubin, and L. Adamowicz. *J. Phys. B*, 54:085003, 2021. doi: https://doi.org/10.1063/5.0065282.

[19] N. Dattani, G. LiManni, D. Feller, and J. Koput. *arXiv:2006.13453*, 2018. doi: https://doi.org/10.48550/arXiv.2006.13453.

[20] Y. Yang et al. *J. Chem. Phys.*, 143:124308, 2015. doi: https://doi.org/10.1063/1.4931667.

[21] S. Bubin, M. Pavanello, W.-C. Tung, K. Sharkey, and L. Adamowicz. *Chem. Rev.*, 113:36, 2013. doi: https://doi.org/10.1021/cr200419d.

[22] K. L. Sharkey and L. Adamowicz. *J. Chem. Phys.*, 140:174112, 2014. doi: https://doi.org/10.1063/1.4873916.

[23] E. Mátyus. *J. Chem. Phys.*, 149:194112, 2018. doi: https://doi.org/10.1063/1.5050403.

[24] A. Muolo, E. Mátyus, and M. Reiher. *J. Chem. Phys.*, 151:154110, 2019. doi: https://doi.org/10.1063/1.5121318.

[25] S. Bubin and L. Adamowicz. *J. Chem. Phys.*, 126:214305, 2007. doi: https://doi.org/10.1063/1.2736699.

[26] S. Bubin, M. Stanke, and L. Adamowicz. *J. Chem. Phys.*, 131:044128, 2009. doi: https://doi.org/10.1063/1.3195061.

[27] S. Bubin and L. Adamowicz. *J. Chem. Phys.*, 152:204102, 2020. doi: https://doi.org/10.1063/1.5144268.

[28] S. Bubin, L. Adamowicz, and M. Molski. *J. Chem. Phys.*, 123:134310, 2005. doi: https://doi.org/10.1063/1.2047487.

[29] I. Hornyák, S. Nasiri, S. Bubin, and L. Adamowicz. *Phys. Rev. A*, 104:032809, 2021. doi: https://doi.org/10.1103/PhysRevA.104.032809.

[30] M. Puchalski, J. Komasa, and K. Pachucki. *Phys. Rev. A*, 92:062501, 2015. doi: https://doi.org/10.1103/PhysRevA.92.062501.

[31] I. Hornyák, L. Adamowicz, and S. Bubin. *Phys. Rev. A*, 102:062825, 2020. doi: https://doi.org/10.1103/PhysRevA.102.062825.

[32] S. Nasiri, L. Adamowicz, and S. Bubin. *J. Phys. Chem. Ref. Data*, 50:043107, 2021. doi: https://doi.org/10.1063/5.0065282.

[33] L. M. Wang, C. Li, Z.-C. Yan, and G. W. F. Drake. *Phys. Rev. A*, 95:032504, 2017. doi: https://doi.org/10.1103/PhysRevA.95.032504.

[34] C. Schwartz. *Int. J. Mod. Phys. E*, 15:877, 2006. doi: https://doi.org/10.1142/S0218301306004648.

[35] D. T. Aznabaev, A. K. Bekbaev, and V. I. Korobov. *Phys. Rev. A*, 98:012510, 2018. doi: https://doi.org/10.1103/PhysRevA.98.012510.

[36] K. Singer. *Proc. R. Soc. Lond. A*, 258:412, 1960. doi: https://doi.org/10.1098/rspa.1960.0196.

[37] D. B. Kinghorn. *Int. J. Quant. Chem.*, 57:141, 1996.

[38] J. Komasa. *Phys. Rev. A*, 65:012506, 2001. doi: https://doi.org/10.1103/PhysRevA.65.012506.

[39] M. D. Girardeau. *Phys. Rev.*, 139:B500, 1965. doi: https://doi.org/10.1103/PhysRev.139.B500.

[40] S. Bubin, M. Cafiero, and L. Adamowicz. *Adv. Chem. Phys.*, 131:377, 2005.

[41] S. Bubin and L. Adamowicz. *J. Chem. Phys.*, 128:114107, 2008. doi: https://doi.org/10.1063/1.2894866.

[42] Y. Suzuki and K. Varga. *Stochastic Variational Approach to Quantum Mechanical Few-Body Problems*. Springer-Verlag, 1998. ISBN 3-540-65152-7.

[43] J. Mitroy, M. S. Safronova, and C. W. Clark. *J. Phys. B*, 43:202001, 2010. doi: https://doi.org/10.1088/0953-4075/43/20/202001.

[44] A. J. Sadlej. *Int. J. Quant. Chem.*, 23:147, 1983. doi: https://doi.org/10.1002/qua.560230116.

[45] J. Sapirstein and K. T. Cheng. *Phys. Rev. A*, 63:032506, 2001. doi: https://doi.org/10.1103/PhysRevA.63.032506.

[46] Z.-C. Yan, W. Nörteshäuser, and G. W. F. Drake. *Phys. Rev. Lett.*, 100:243002, 2008. doi: https://doi.org/10.1103/PhysRevLett.100.243002.

[47] P. K. Kabir and E. E. Salpeter. *Phys. Rev.*, 108:1256, 1957. doi: https://doi.org/10.1103/PhysRev.108.1256.

[48] H. Araki. *Prog. Theor. Phys.*, 17:619, 1957. doi: https://doi.org/10.1143/PTP.17.619.

[49] J. Sucher. *Phys. Rev.*, 109:1010, 1958. doi: https://doi.org/10.1103/PhysRev.109.1010.

[50] P. Labelle. *Phys. Rev. D*, 58:093013, 1998. doi: https://doi.org/10.1103/PhysRevD.58.093013.

[51] M. Haidar, Z-X Zhong, V. I. Korobov, and J.-Ph. Karr. *Phys. Rev. A*, 101:022501, 2020. doi: https://doi.org/10.1103/PhysRevA.101.022501.

[52] K. Pachucki. *Phys. Rev. A*, 71:012503, 2005. doi: https://doi.org/10.1103/PhysRevA.71.012503.

[53] W. E. Caswell and G. P. Lepage. *Phys. Lett. B*, 167:437, 1986. doi: https://doi.org/10.1016/0370-2693(86)91297-9.

[54] V. Patkóš, V. A. Yerokhin, and K. Pachucki. *Phys. Rev. A*, 100:042510, 2019. doi: https://doi.org/10.1103/PhysRevA.100.042510.

[55] K. Pachucki. *Phys. Rev. A*, 74:022512, 2006. doi: https://doi.org/10.1103/PhysRevA.74.022512.

[56] L. M. Wang and Z.-C. Yan. *Phys. Rev. A*, 100:032505, 2019. doi: https://doi.org/10.1103/PhysRevA.100.032505.

[57] M. Stanke, D. Kędziera, S. Bubin, M. Molski, and L. Adamowicz. *J. Chem. Phys.*, 128:114313, 2008. doi: https://doi.org/10.1063/1.2834926.

[58] S. Bubin, M. Stanke, D. Kędziera, and L. Adamowicz. *Phys. Rev. A*, 75:062504, 2007. doi: https://doi.org/10.1103/PhysRevA.75.062504.

[59] D. Kędziera, M. Stanke, S. Bubin, M. Barysz, and L. Adamowicz. *J. Chem. Phys.*, 125:084303, 2006. doi: https://doi.org/10.1063/1.2236113.

[60] B. A. Bushaw, W. Nörtershäuser, G. W. F. Drake, and H.-J. Kluge. *Phys. Rev. A*, 75:052503, 2007. doi: https://doi.org/10.1103/PhysRevA.75.052503.

[61] A. Kramida, Yu. Ralchenko, J. Reader, and NIST ASD Team. NIST Atomic Spectra Database (ver. 5.8), Available: `https://physics.nist.gov/asd`. National Institute of Standards and Technology, Gaithersburg, MD., 2020.

[62] A. E. Kramida, A. N. Ryabtsev, J. O. Ekberg, I. Kink, S. Mannervik, and I. Martinson. *Phys. Scr.*, 78:025301, 2008. doi: 10.1088/0031-8949/78/02/025301.

[63] V. A. Yerokhin, M. Puchalski, and K. Pachucki. *Phys. Rev. A*, 102:042816, 2020. doi: https://doi.org/10.1103/PhysRevA.102.042816.

[64] K. Chung. *Phys. Rev. A*, 44:5421, 1991. doi: https://doi.org/10.1103/PhysRevA.44.5421.

[65] D. McKenzie and G. W. F. Drake. *Phys. Rev. A*, 44:R6973(R), 1991. doi: https://doi.org/10.1103/PhysRevA.44.R6973.

[66] J. Sapirstein and K. Cheng. *Phys. Rev. A*, 83:012504, 2011. doi: https://doi.org/10.1103/PhysRevA.83.012504.

[67] V. A. Yerokhin, A. Surzhykov, and A. Müller. *Phys. Rev. A*, 96:042505, 2017. doi: https://doi.org/10.1103/PhysRevA.96.042505.

[68] M. Puchalski and K. Pachucki. *Phys. Rev. A*, 78:052511, 2008. doi: https://doi.org/10.1103/PhysRevA.78.052511.

[69] Z.-C. Yan and G. W. F. Drake. *Phys. Rev. A*, 66:425041, 2002. doi: https://doi.org/10.1103/PhysRevA.66.042504.

[70] A. E. Kramida. *Phys. Scr.*, 72:309, 2005. doi: https://doi.org/10.1238/Physica.Regular.072a00309.

[71] M. Tunklev, L. Engström, C. Jupén, and I. Kink. *Phys. Scr.*, 55:707, 1997. doi: https://doi.org/10.1088/0031-8949/55/6/010.

[72] V. M. Shabaev, I. I. Tupitsyn, and V. A. Yerokhin. *Phys. Rev. A*, 88:012513, 2013. doi: https://doi.org/10.1103/PhysRevA.88.012513.

[73] L. Engström. *Phys. Scr.*, 29:113, 1984. doi: https://doi.org/10.1088/0031-8949/29/2/004.

[74] B. Edlén. *Phys. Scr.*, 19:255, 1979. doi: https://doi.org/10.1088/0031-8949/19/3/007.

[75] A. E. Kramida and M.-C. Buchet-Poulizac. *Eur. Phys. J. D*, 39:173, 2006. doi: https://doi.org/10.1140/epjd/e2006-00122-3.

[76] R. Hallin. *Ark. Fys.*, 31:511, 1966.

[77] K. Pachucki, W. Cencek, and J. Komasa. *J. Chem. Phys.*, 122:184101, 2005. doi: https://doi.org/10.1063/1.1888572.

[78] R. J. Drachman. *J. Phys. B*, 14:2733, 1981. doi: https://doi.org/10.1088/0022-3700/14/16/003.

[79] V. A. Yerokhin, V. Patkóš, and K. Pachucki. *Symmetry*, 13:1246, 2021. doi: https://doi.org/10.3390/sym13071246.

[80] Z-.C. Yan. *J. Phys. B*, 33:2437, 2000. doi: https://doi.org/10.1088/0953-4075/33/13/305.

[81] M. Stanke, J. Jurkowski, and L. Adamowicz. *J. Phys. B*, 50:065101, 2017. doi: https://doi.org/10.1088/1361-6455/aa56ad.

[82] G. W. F. Drake and S. P. Goldman. *Can. J. Phys.*, 77:835, 1999. doi: https://doi.org/10.1139/p00-010.

[83] Z.-C. Yan and G. W. F. Drake. *Phys. Rev. Lett.*, 91:113004, 2003. doi: https://doi.org/10.1103/PhysRevLett.91.113004.

[84] K. Pachucki and J. Komasa. *Phys. Rev. Lett.*, 92:213001, 2004. doi: https://doi.org/10.1103/PhysRevLett.92.213001.

[85] C. Schwartz. *Phys. Rev.*, 123:1700, 1961. doi: https://doi.org/10.1103/PhysRev.123.1700.

[86] V. I. Korobov. *Phys. Rev. A*, 85:042514, 2013. doi: https://doi.org/10.1103/PhysRevA.85.042514.

[87] S. Bubin, J. Komasa, M. Stanke, and L. Adamowicz. *Phys. Rev. A*, 81:052504, 2010. doi: https://doi.org/10.1103/PhysRevA.81.052504.

[88] S. Bubin, J. Komasa, M. Stanke, and L. Adamowicz. *J. Chem. Phys.*, 132:114109, 2010. doi: https://doi.org/10.1063/1.3358999.

[89] G. W. F. Drake and R. A. Swainson. *Phys. Rev. A*, 41:1243, 1990. doi: https://doi.org/10.1103/PhysRevA.41.1243.

[90] S. P. Goldman and G. W. F. Drake. *J. Phys. B*, 17:L197, 1984. doi: https://doi.org/10.1088/0022-3700/17/7/001.

[91] V. A. Yerokhin and K. Pachucki. *Phys. Rev. A*, 81:022507, 2010. doi: https://doi.org/10.1103/PhysRevA.81.022507.

[92] K. Pachucki and J. Komasa. *Phys. Rev. A*, 68:042507, 2003. doi: https://doi.org/10.1103/PhysRevA.68.042507.

[93] K. Pachucki. *Phys. Rev. A*, 74:062510, 2006. doi: https://doi.org/10.1103/PhysRevA.74.062510.

[94] A. J. Thakkar and T. Koga. *Theor. Chem. Acc.*, 109:36, 2003. doi: https://doi.org/10.1007/s00214-002-0407-1.

[95] F. W. King. *Phys. Rev. A*, 40:1735, 1989. doi: https://doi.org/10.1103/PhysRevA.40.1735.

[96] C. L. Pekeris. *Phys. Rev.*, 112:1649, 1958. doi: https://doi.org/10.1103/PhysRev.112.1649.

[97] M. Puchalski and K. Pachucki. *Phys. Rev. A*, 92:012513, 2015. doi: https://doi.org/10.1103/PhysRevA.92.012513.

[98] M. Puchalski, J. Komasa, P. Czachorowski, and K. Pachucki. *Phys. Rev. Lett.*, 117: 263002, 2016. doi: https://doi.org/10.1103/PhysRevLett.117.263002.

[99] M. Wang, W. J. Huang, F. G. Kondev, G. Audi, and S. Naimi. *Chin. Phys. C*, 45: 030003, 2021. doi: https://doi.org/10.1088/1674-1137/abddaf.

[100] D. Lunney, J. M. Pearson, and C. Thibault. *Rev. Mod. Phys.*, 75:1021, 2003. doi: https://doi.org/10.1103/RevModPhys.75.1021.

[101] G. W. F. Drake. *J. Phys. B*, 53:223001, 2020. doi: https://doi.org/10.1088/1361-6455/abb832.

[102] P. Jeszenszki, D. Ferenc, and E. Mátyus. *J. Chem. Phys.*, 154:224110, 2021. doi: https://doi.org/10.1063/5.0051237.

[103] K. Pachucki and J. Komasa. *Phys. Rev. A*, 70:022513, 2004. doi: https://doi.org/10.1103/PhysRevA.70.022513.

[104] Y.-H. Zhang, L.-Y. Tang, J.-Y. Zhang, and T.-Y. Shi. *Phys. Rev. A*, 103:032810, 2021. doi: https://doi.org/10.1103/PhysRevA.103.032810.

[105] D. Spelsberg, T. Lorenz, and W. Meyer. *J. Chem. Phys.*, 99:7845, 1993. doi: https://doi.org/10.1063/1.465663.

[106] Z.-W. Wang and K. T. Chung. *J. Phys. B*, 27:855, 1994. doi: https://doi.org/10.1088/0953-4075/27/5/005.

[107] M. Puchalski, D. Kędziera, and K. Pachucki. *Phys. Rev. A*, 84:052518, 2011. doi: https://doi.org/10.1103/PhysRevA.84.052518.

[108] J. Pipin and D. M. Bishop. *Phys. Rev. A*, 45:2736, 1992. doi: https://doi.org/10.1103/PhysRevA.45.2736.

[109] M. Mérawa and M. Rérat. *J. Chem. Phys.*, 108:7060, 1998. doi: https://doi.org/10.1063/1.476124.

[110] J. Muszyńska, D. Papierowska, and W. Woźnicki J. Pipin. *Int. J. Quantum Chem.*, 22:1153, 1982. doi: https://doi.org/10.1002/qua.560220603.

[111] G. D. Zeiss, W. J. Meath, J. C. F. MacDonald, and D. J. Dawson. *Can. J. Phys.*, 55: 2080, 1977. doi: https://doi.org/10.1139/p77-252.

[112] Z.-W. Wang, X.-W. Zhu, and K. T. Chung. *Phys. Scr.*, 47:65, 1993. doi: https://doi.org/10.1088/0031-8949/47/1/011.

[113] J. Pipin and W. Woźnicki. *Chem. Phys. Lett*, 95:392, 1983. doi: https://doi.org/10.1016/0009-2614(83)80580-6.

[114] M. B. Ruiz, J. T. Margraf, and A. M. Frolov. *Phys. Rev. A*, 88:012505, 2013. doi: https://doi.org/10.1103/PhysRevA.88.012505.

[115] M. Puchalski, K. Szalewicz, M. Lesiuk, and B. Jeziorski. *Phys. Rev. A*, 101: 022505, 2020. doi: https://doi.org/10.1103/PhysRevA.101.022505.

[116] R. Pohl et al. *Nature*, 466:213, 2010. doi: https://doi.org/10.1038/nature09250.

[117] A. Antognini et al. *Science*, 339:417, 2013. doi: 10.1126/science.1230016.

[118] R. Pohl, R. Gilman, G. A. Miller, and K. Pachucki. *Annu. Rev. Nucl.*, 63:175, 2013. doi: https://doi.org/10.1146/annurev-nucl-102212-170627.

[119] J. J. Krauth et al. *Nature*, 589:527, 2021. doi: https://doi.org/10.1038/s41586-021-03183-1.

[120] A. A. Krutov, A. P. Martynenko, F. A. Martynenko, and O. S. Sukhorukova. *Phys. Rev. A*, 94:062505, 2016. doi: https://doi.org/10.1103/PhysRevA.94.062505.

[121] A. E. Dorokhov, A. P. Martynenko, F. A. Martynenko, and O. S. Sukhorukova. *Phys. Rev. A*, 100:062513, 2019. doi: https://doi.org/10.1103/PhysRevA.100.062513.

[122] A. E. Dorokhov, A. A. Krutov, A. P. Martynenko, F. A. Martynenko, and O. S. Sukhorukova. *Phys. Rev. A*, 98:042501, 2018. doi: https://doi.org/10.1103/PhysRevA.98.042501.

[123] K.-N. Huang and V. W. Hughes. *Phys. Rev. A*, 20:706, 1979. doi: https://doi.org/10.1103/PhysRevA.20.706.

[124] S. D. Lakdawala and P. J. Mohr. *Phys. Rev. A*, 24:2224, 1981. doi: https://doi.org/10.1103/PhysRevA.24.2224.

[125] C. J. Gardner et al. *Phys. Rev. Lett.*, 48:1168, 1982. doi: https://doi.org/10.1103/PhysRevLett.48.1168.

[126] K. Pachucki. *Phys. Rev. A*, 63:032508, 2001. doi: https://doi.org/10.1103/PhysRevA.63.032508.

[127] D. T. Aznabayev, A. K. Bekbaev, and V. I. Korobov. *Phys. Part. Nucl. Lett.*, 15: 236, 2018. doi: https://doi.org/10.1134/S1547477118030032.

[128] A. M. Frolov. *Phys. Lett. A*, 357:334, 2006. doi: https://doi.org/10.1016/j.physleta.2006.04.059.

[129] A. P. Martynenko and A. A. Ulybin. *J. Phys. B*, 48:195003, 2015. doi: https://doi.org/10.1088/0953-4075/48/19/195003.

[130] A. E. Dorokhov, V. I. Korobov, A. P. Martynenko, and F. A. Martynenko. *Phys. Rev. A*, 103:052806, 2021. doi: https://doi.org/10.1103/PhysRevA.103.052806.

[131] A. P. Martynenko and A. A. Ulybin. *Phys. At. Nucl.*, 79:247, 2016. doi: https://doi.org/10.1134/S1063778816010142.

[132] F. Moncada, D. Cruz, and A. Reyes. *Chem. Phys. Lett.*, 570:16, 2013. doi: https://doi.org/10.1016/j.cplett.2013.03.004.

[133] E. Posada, F. Moncada, and A. Reyes. *J. Phys. Chem. A*, 118:9491, 2014. doi: https://doi.org/10.1021/jp501289s.

[134] E. Tiesinga, P. J. Mohr, D. B. Newell, and B. N. Taylor. *Rev. Mod. Phys.*, 93: 025010, 2021. doi: https://doi.org/10.1103/RevModPhys.93.025010.

[135] I. Hornyák, L. Adamowicz, and S. Bubin. *Phys. Rev. A*, 102:062825, 2020. doi: https://doi.org/10.1103/PhysRevA.102.062825.

[136] N. J. Stone. *At. Data Nucl. Data Tables*, 90:75, 2005. doi: 10.1016/j.adt.2005.04.001.

VITA

William P. Earwood

2017 - M.S. Engineering Science, University of Mississippi

2015 - B.S. Mechanical Engineering, University of Mississippi

ACADEMIC EMPLOYMENT

2017-2022 - Undergraduate Chemistry Laboratory Teaching Assistant

2015-2017 - Materials Science Laboratory Teaching Assistant